공학박사학위논문

Dispersion Engineering in Elastic Guided Waves by Phononic Crystals and Metamaterials

포노닉 크리스털과 메타물질을 이용한 탄성 유도 초음파의 분산 특성 엔지니어링

2014년 2월

서울대학교 대학원

기계항공공학부

마 평 식

Dispersion Engineering in Elastic Guided Waves by Phononic Crystals and Metamaterials

포노닉 크리스털과 메타물질을 이용한 탄성 유도 초음파의 분산 특성 엔지니어링

지도교수 김 윤 영

이 논문을 공학박사 학위논문으로 제출함

2013년 11월

서울대학교 대학원

기계항공공학부

마 평 식

마평식의 공학박사 학위논문을 인준함

2013년 12월

위 원 장 : 조 맹 효

부위원장 : 김 윤 영

위 원 : 이 정 훈

위 원 : 엄 원 석

위 원 : 김 도 년

ABSTRACT

Dispersion Engineering in Elastic Guided Waves by Phononic Crystals and Metamaterials

Pyung Sik Ma

School of Mechanical and Aerospace Engineering

The Graduate School

Seoul National University

This dissertation presents manipulation of elastic guided waves by artificial structured materials: phononic crystals and metamaterials. Recently, due to their ability to control waves, artificial materials for electromagnetic waves have been extensively studied, leading to interesting results such as sub-diffraction lenses and cloaking devices. This study demonstrates that phononic crystals and elastic metamaterials can provide the promising functionalities in elastic guided waves. The main focus of this investigation is on tailoring multiple guided modes in an elastic waveguide. In a waveguide, multiple guided waves exhibit complex behavior which causes problematic issues in practical applications; an inputted wave is distorted due to an excitation of multiple modes and their strongly dispersive nature. Here, a method to control the dispersion relations of multiple guided modes by phononic crystals and elastic metamaterials is developed.

In this thesis, dispersion relations of guided waves are engineered in frequency and wavenumber domains. The main contributions are to separate multiple guided

modes, to suppress an undesired mode, and to reduce group velocity dispersion. Multiple shear-horizontal waves in a plate are separated by engineered phononic crystal plates. The dispersion relation of each guided mode is manipulated in the wavenumber domain to obtain different propagation directions. Also, the excitation of undesired wave modes is suppressed by opening the forbidden band gap of phononic crystals over a target frequency range. A wave distortion due to the dispersion effect is prevented by employing phononic crystals and anisotropic metamaterials; the dispersion relation in the frequency domain is tailored to exhibit a constant group velocity. Realization of phononic crystals and elastic metamaterials is a challenging task to achieve the desired wave properties for multiple wave modes. Here, systematic engineering methods including size, shape, and topology optimization methods are proposed to obtain proper structures. The lattice parameters of phononic crystals and a topology of a unit structure in anisotropic metamaterials can be designed through the suggested methods. To confirm wave properties in the engineered waveguides, numerical simulations and ultrasonic wave experiments are conducted. In experiments, ultrasonic transducers are properly designed to selectively excite a target wave mode and adjust its beam pattern in an elastic waveguide. Through this research, it is demonstrated that phononic crystals and elastic metamaterials can be effectively exploited to engineer wave properties in elastic waveguides.

Keywords: Ultrasonic guided waves, Dispersion relation, Phononic crystals, Elastic metamaterials, and Optimization method

Student Number: 2010-30187

TABLE OF CONTENTS

LIST OF TABLES

Page

LIST OF FIGURES

Page

CHAPTER 1

INTRODUCTION

1.1 Introductory remarks

In recent decades, phononic crystals [1-5] and acoustic metamaterials [6-10] have been intensively studied because of their ability to control phonons (mechanical vibrations). These artificial structures exhibit abnormal wave properties which cannot found in nature over a wide range of scales and frequencies: from seismic waves (Hz) [11, 12] to heat conduction (THz) [13, 14]. As these abnormal properties arise from their unit structures, one can tailor the wave properties by changing unit structures in subwavelength scale compared to conventional approaches which modify configuration of materials in the atomic or molecular level. From this fact, phononic crystals and acoustic metamaterials have been focused on by researchers in many areas of science and technology. In this thesis, artificial structures are applied to control *ultrasonic waves in elastic waveguides*. Controlling guided waves is challenging because they exhibit complex behavior in propagation: an elastic waveguide can support an infinite number of wave modes which cause problematic issues in practical application such as non-destructive evaluation; an inputted elastic wave is distorted due to multiple wave mode excitations and dispersion effect [15, 16]. Recently, it has been demonstrated that the phononic crystal and elastic metamaterials exhibit a forbidden band gap and

negative refraction for guided waves [17-19]. In spite of their fruitful wave phenomena, however, a little effort is paid to apply these artificial structures to resolve practical issues in ultrasonic guided waves. *In this thesis, we present that phononic crystals and elastic metamaterials can be effectively employed to control the elastic waves in a waveguide. In particular, the main focus is on multiple wave modes in an elastic waveguide.* We exploit extraordinary wave phenomena of phononic crystals and metamaterials to control multiple guided modes. Since their wave properties arise from an interaction between waves and their artificial structures, the systematic engineering methods including size, shape, and topology optimization methods are proposed for the unit structures of phononic crystals and elastic metamaterials.

Before presenting detailed investigations of this study, the extraordinary wave propagation in the artificial structures will be discussed. Phononic crystals and acoustic metamaterial have been investigated with successful demonstration of photonic crystals and electromagnetic metamaterials. Although the detailed physics of acoustic or elastic waves are different from that of electromagnetic waves, they share the same physical origin of the extraordinary wave properties in artificial structures. Photonic crystals and electromagnetic metamaterials were independently studied in the beginning. A dominant mechanism, which is attributed to their abnormal wave properties, was different: multiple scattering for photonic crystals and resonance for electromagnetic metamaterials. But, nowadays, these two research subjects, photonic crystals and electromagnetic metamaterials, are studied in the same category; they are considered as artificial structures which are proposed to control material properties. In the followings, the origin of artificial structures for

electromagnetic waves and their applications are discussed. After then, investigations of phononic crystals and metamaterials for acoustic and elastic waves will be addressed.

1.2 Photonic crystals and electromagnetic metamaterials

The first photonic crystals are proposed independently by John and Yablonovitch in 1987; John found the forbidden band gap of photonic crystals while studying localization of light in a disordered medium [20] and Yablonovitch utilized photonic crystal to suppress the spontaneous light emission of lasers for a better efficiency [21]. They reported that electromagnetic waves cannot propagate through a periodic structure of photonic crystals like electrons in semiconductors. Based on the background of solid-state physics for electrons, the Bloch theorem was applied to Maxwell's equation for photonic crystals and band structures of photons in periodic dielectric materials can be analyzed in 1990 [22, 23]. In photonic crystals, reflected waves from periodic inclusions interfere constructively at the specific wavelength, resulting the forbidden band gap which suppresses light propagating through photonic crystals. Since the band gap for light was introduced, photonic crystals have been extensively studied to control electromagnetic waves. It was presented that electromagnetic waves are confined along a line-defect or localized a point-defect in photonic crystals [24, 25]. The photonic crystal-based circuits were proposed in hope of replacing the silicon-based devices.[26] The waveguiding effect of photonic crystals was utilized for photonic crystal lasers [27, 28], slow light [29], and enhancement of nonlinear effect [30].

Besides the localization of light in defects of photonic crystals, abnormal light propagation through photonic crystals was studied. At band edges of the photonic band gap, extraordinary light propagation was observed. In 1998, Kosaka reported that inputted lights of $\pm 12^{\circ}$ onto Si and SiO_2 photonic crystals are refracted from -90° to 90°. They called these unusual wave propagation superprism phenomena in [31]. They also showed that photonic crystals can manipulate the diffraction properties of light [32]. Depending on the incident angle of light, light was broadened over photonic crystals or collimated with a constant beam width. At the band edge, the band gap of photonic crystals is partially developed for the particular directions not fully for all directions; this is called the partial band gap where the Bragg scattering condition is fulfilled for some particular directions. At this situation, despite there are no external waveguides in photonic crystals, light are confined in some directions of photonic crystals, leading to the anisotropic wave propagation in photonic crystals as shown in the superprism and the self-collimating phenomena. In this thesis, the anisotropic behavior of waves in periodic medium will be applied to elastic guided waves and details of investigation will fully discussed in Chapter 3.

Next, Let us discuss about electromagnetic metamaterials. In 2000, Pendry proposed that lens made of negative index materials can defeat the sub-diffraction limit [33]. Although negative value of material property seems counter-intuitive, it was proved that electromagnetic waves can propagate in the negative index material without violating physical principles by Veselago in 1968 [34]. After then, the negative index material were realized by split-ring resonators in microwave frequencies [35, 36], pairs of metal nanorods [37], and fishnet structures in optical

frequencies [38]. Because this type of metamaterials exploited resonances to obtain negative refractive index for electromagnetic waves, they have inherent drawbacks: material loss and narrow bandwidth. To overcome these limitations, another type of metamaterial, anisotropic metamaterials, was proposed. In 2006 and 2007, anisotropic metamaterial lens were suggested for far-field sub-diffraction imaging [39, 40]. It composed of alternating layers of different materials, whose properties exhibits an extremely large anisotropy. Besides, photonic crystals have been investigated as alternatives of negative index metamaterials. The negative refraction of electromagnetic waves was demonstrated in photonic crystals [41, 42]. From the negative index due to the Bragg scattering, photonic crystal-based flat-lens were suggested for sub-wavelength imaging by excitation of surface modes [43, 44].

1.3 Phononic crystals and acoustic metamaterials

With advances in electromagnetic metamaterials for controlling light in microwave and optical frequencies, manipulation of acoustic and elastic waves by phononic crystals and acoustic metamaterials has been also investigated. From the analogy to photonic crystals, the band gap for acoustic and elastic waves in periodic medium was theoretically predicted by Sigalas in 1992 [1]. To demonstrate the band gap of phononic crystals, transmission experiments were carried out in an aluminum plate having array of mercury cylinder [2] and in periodic steel cylinders in an epoxy resin [3]. It was experimentally observed that elastic waves cannot propagate through phononic crystals at the forbidden gap predicted from band structures. Negative refractions of acoustic and elastic waves in phononic crystals were also demonstrated; Sukhovich reported that acoustic waves were refracted at a negative

angle in two-dimensional phononic crystals made of steel rods in water [4]. In 2010, Morvan showed the negative refraction of elastic waves in prism-shape phononic crystals consisting of square arrays of holes in aluminum matrix [5]. By employing negative refraction of phononic crystals, wave focusing and sub-diffraction imaging were demonstrated. It was observed that a sound beam in ultrasonic regime can be focused into a focal spot that is close to the diffraction limit by phononic crystals [45]; subwavelength imaging can be also achieved by phononic crystals in 2009 [46]. In their phononic crystal lens, evanescent components of the waves, which contains the high-resolution information, can be propagated by the so-called bound slab mode of the phononic crystals.

On the other hand, acoustic metamaterials that differ from phononic crystals in the mechanisms have been widely proposed. In 2000, due to the resonance of unit structures, a material consisting of a hard material coated by soft material was proven to exhibit the negative material properties [6]. At the resonant frequency, an inputted wave is localized within microstructures of the materials, then, the forbidden band gap can be formed. This type of acoustic metamaterial was theoretically analyzed by Li in 2004. According to their explanation, the Mie resonance of the structures attributed to negative density and negative bulk modulus of the resonant metamaterials [7]. And double negativity, negative density and bulk modulus, makes negative refraction property. As another type of a resonant mechanism, the Helmholtz resonator was considered for negative modulus [8, 9] and arrays of membranes and holes, for the double negativity [10, 47].

To overcome the narrow operating bandwidth of the resonant-metamaterials,

broadband acoustic metamaterials have been proposed. First, the subwavelength imaging were demonstrate with anisotropic metamaterials consisting of alternating layers for acoustic [48] and elastic waves [49]. The anisotropy of acoustic metamaterial was applied to bend elastic waves for cloaking devices in thin plates [50]. In 2012, demonstration of an elastic cloaking was achieved in a thin polymer plate for 200 to 400 Hz [51]. Next, acoustic metamaterials made of a winding channel, the so-called space-coiling metamaterials, was proposed in 2012 [52]. It allows us to make not only a high-index materials but also negative index materials due to the Bragg scattering. Recently, its effective property of negative and zero indexes was experimentally observed by two different groups [53, 54]. Lastly, pentamode metamaterials were also realized by elastic metamaterials in 2012. To mimic anisotropic metafluids by an elastic medium, in 1995, Milton proposed theoretically configurations of pentamode metamaterial to exhibit the required stiffness tensor [55]; it can be fabricated more recently [56].

1.4 Motivation and research objectives

The main concern of this thesis is to control ultrasonic waves in an elastic waveguide. For about 50 years, guided waves have been investigated for a non-destructive evaluation of pipes and plates and developed into commercial products; see Refs. [16, 57] and references therein. The main advantage of a use of guided waves in the inspection is that a large area of test structures can be evaluated by a single transducer, which is attributed to the fact that the guided waves can propagate over a long distance through the waveguide. The same fact, however, causes difficulties in evaluation procedures; guided waves are likely to be distorted after

propagating through a waveguide due to excitations of multiple modes and their dispersive nature. Since scattered waves contain information about defects in a test structure, numerous efforts were made to overcome the distortion of the guided waves. To avoid multiple wave excitations, undesired waves were mechanically filtered with a comb transducer [58] or phased array of transducers [59]. The dispersion effect of the guided waves was compensated by a numerical processing technique [60]. Also, signals measured at different points are numerically synthesized to obtain a clear signal of a desired wave mode [61].

To make guided waves be more effective in the non-destructive evaluation, the ability to control their complex behavior is essential. In this regard, phononic crystals and acoustic metamaterials can be a good candidate; they allow us to manipulate the wave propagation by exploiting their extraordinary properties. For example, a selective wave excitation can be realized by the phononic band gap and multiple guided modes can be measured separately by the anisotropic properties of phononic crystals. However, although there have been many studies to show abnormal wave phenomena of phononic crystals and elastic metamaterials for ultrasonic guided waves [17-19], the work concerning problematic issues in practical applications of guided elastic wave have not been proposed so far.

In this thesis, we employ phononic crystals and elasitc metamaterials to resolve the wave distortion due to multiple wave excitation and group velocity dispersion in a waveguide. Detailed objectives of this study are summarized as follows:

1. To apply phononic crystals and acoustic metamaterials for resolving practical issues in non-destructive evaluaion:

Phononic crystals and acoustic metamaterials provide the extraordinary phenomena, resulting from an interaction between waves and their unit structures. Among the numerous mechanisms, the band gap from the Bragg scattering and a highly anisotropic property are considered for ultrasonic guided waves. By exploiting these properties, an undesired wave mode is prevented from propagating by opening the band gap or spatially separated by using anisotropic wave property. Also, the dispersion effect of a desired wave mode can be reduced by manipulating group velocities over a target frequency bandwidth.

2. To develop systematic engineering methods to tailor phononic crystals and acoustic metamaterials

Although it was investigated how the abnormal wave properties can be achieved by phononic crystals and anisotropic metamaterials, however, realization of microstructures satisfying multiple requirements at a single frequency is challenging problem. To systematically design structures of phononic crystals and acoustic metamaterials, we employ the engineering optimization methods. The design formulations are proposed to engineer size and shape of phononic crystals and topology of a unit cell in non-resonant elastic metamaterials.

3. To experimentally verify wave propagation in the engineered waveguide

In this thesis, an effectiveness of the engineered structure is confirmed by ultrasonic experiments. As mentioned above, there are considerably many wave modes to be considered in a waveguide. Moreover, wave properties of phononic crystals are

sensitive to the frequency and propagating direction. In this regard, a selective excitation and measurement of guided waves are crucial for successful demonstration. Here, we will experimentally demonstrate the engineered structures by using magnetostrictive transducers which are capable of tuning excited wave modes and beam patterns.

1.5 Outline of this thesis

The main effort of this thesis is to manipulate the dispersion relation of elastic guided waves by employing artificial structured materials including phononic crystals and elastic metamaterials. By carefully tailoring structural parameters of their unit structures, the dispersion relation can be engineered. In this sense, we call design process of artificial structures *dispersion engineering* throughout this thesis. This thesis is divided into two parts: dispersion engineering by phononic crystals (Chapters 3 and 4) and by elastic metamaterials (Chapter 5). Depending on the scale of the unit structure, phononic crystals are comparable to the operating wavelength while elastic metamaterials are composed of sub-wavelength unit structures, the proper engineering method will be investigated in each chapter. In particular, the main focus is on the wavenumber domain of the dispersion relation in Chapter 3 and the frequency domain in Chapter 4.

In Chapter 2, the fundamental physics of elastic wave propagation in a periodic medium are given before we discuss the dispersion engineering by the structured materials. Since we consider phononic crystals and elastic metamaterials which are made of periodic structures, a clear understanding of wave propagation in that

medium is crucial. In this chapter, the fundamental concepts including the Bloch's theorem, the Christoffel equation, the dispersion relation and the slowness curve will be discussed. Also, we present numerical schemes to calculate the dispersion relation of a periodic elastic medium. Detailed derivations for the plane wave expansion and the finite element method will be given for an infinite case and a waveguide case with numerical examples.

In Chapter 3, the guided waves in a waveguide are spatially separated by using a phononic crystal plate. To do this, propagation directions of multiple waves are properly tailored to separate them into each wave mode. To investigate an effect of phononic crystals on the propagation direction, *the dispersion relation in the wavenumber domain* is studied. Also, a design method to make an elastic wave propagate along a given direction is proposed for two-dimensional phononic crystals. From an investigation of a two-dimensional case, we can obtain proper lattice parameters for the mode separation in a waveguide case. It will be presented that the shear-horizontal guided waves in an aluminum plate are successfully separated by the phononic crystal plate. Also, results of an experimental demonstration will be given.

In Chapter 4, *the dispersion relation in the frequency domain* is engineered to suppress an undesired wave and to minimize the dispersion effect of a target wave mode in a waveguide. The phononic crystal structure is tailored to have a constant group velocity for a target mode, while to open the forbidden band gap for an undesired mode. In order to find a proper phononic crystal structure, size optimization method is proposed. Detailed optimization procedure and an

engineered dispersion relation will be presented. For demonstration, numerical simulations and ultrasonic experiments are carried out in the engineered phononic crystal waveguide.

In Chapter 5, the group velocity dispersion of a guided wave is aimed to be suppressed by elastic anisotropic metamaterials. Compared to phononic crystals whose periodicity comparable to wavelength in Chapter 4, metamaterials allow us to tailor the dispersion relation of an elastic waveguide in the subwavelength-scale. The main challenge in this approach is *to realize anisotropic metamaterials* which exhibit a desired material property. In this chapter, to design microstructure of elastic metamaterials, we employ topology optimization method. The microstructures of anisotropic metamaterials which is designed through a proposed optimization method will be presented. Also, we will show results of numerical study for wave propagation in the waveguide consisting of the realized anisotropic metamaterial.

CHAPTER 2

ANALYSIS OF ELASTIC WAVE PROPAGATION IN PERIODIC MEDIUM

2.1 Elastic wave propagation in a homogeneous infinite medium

In this section, fundamental wave properties and governing equations will be given for understanding wave propagation in an elastic medium. For an infinite elastic medium, the wave equations are given by

$$\rho \frac{\partial^2 \mathbf{u}}{\partial t^2} = \nabla \cdot \boldsymbol{\sigma} \tag{2.1}$$

where ρ, $\mathbf{u}$, and $\boldsymbol{\sigma}$ represent density, displacement, and stress, respectively [15]. In general, wave solutions to (2.1) have the following form as a function of time t and space $\mathbf{x}$:

$$\mathbf{u}(\mathbf{x},t) = \tilde{\mathbf{u}} e^{j(\mathbf{k}\mathbf{x}-\omega t)} \tag{2.2}$$

where $\tilde{\mathbf{u}}$ is an amplitude of displacement, $\mathbf{k}$ is the wavenumber, ω is the angular frequency. This solutions is called plane waves, which propagate along the direction $\mathbf{k} = k_x \hat{\mathbf{x}} + k_x \hat{\mathbf{y}} + k_z \hat{\mathbf{z}}$ where $\hat{\mathbf{x}}$, $\hat{\mathbf{y}}$, $\hat{\mathbf{z}}$ are the unit vectors in rectangular Cartesian coordinates. In the region of linear deformation, the stress is expressed as a linear function of all the components of strain $\boldsymbol{\varepsilon}$ as follows:

$$\boldsymbol{\sigma} = \mathbb{C}\boldsymbol{\varepsilon} \tag{2.3}$$

where $\mathbb{C}$ is elastic stiffness constants; this equation is called the constitutive relation of an elastic medium. The strain $\boldsymbol{\varepsilon}$ is defined by the gradient of displacement $\mathbf{u}$ as follows:

$$\boldsymbol{\varepsilon} = \frac{\partial \mathbf{u}}{\partial \mathbf{x}}. \tag{2.4}$$

One can deduce the wave equations in terms of material properties and displacement fields by substituting (2.3) and (2.4) into (2.1). From the symmetries of the strain and stiffness constants, the equations of motion can be briefly expressed in the abbreviated subscript notation as in (2.5).

$$\rho\omega^2 u_i = \nabla_{iK}\mathbb{C}_{KL}\nabla_{Lj}u_j, \quad i,j = x,y,z \tag{2.5}$$

For the plane wave of the given wavenumber $\mathbf{k}$, operators ∇_{iK}, ∇_{Lj} and the elastic stiffness constant $\mathbb{C}_{KL}$ in the right-hand side of (2.5) is given by

$$\nabla_{iK} = \begin{bmatrix} jk_x & 0 & 0 & 0 & jk_z & jk_y \\ 0 & jk_y & 0 & jk_z & 0 & jk_x \\ 0 & 0 & jk_z & jk_y & jk_x & 0 \end{bmatrix}, \tag{2.6}$$

$$\nabla_{Lj} = \begin{bmatrix} jk_x & 0 & 0 \\ 0 & jk_y & 0 \\ 0 & 0 & jk_z \\ 0 & jk_z & jk_y \\ jk_z & 0 & jk_x \\ jk_y & jk_x & 0 \end{bmatrix}, \tag{2.7}$$

and

$$\mathbb{C}_{KL} = \begin{bmatrix} c_{11} & c_{12} & c_{13} & c_{14} & c_{15} & c_{16} \\ c_{21} & c_{22} & c_{23} & c_{24} & c_{25} & c_{26} \\ c_{31} & c_{32} & c_{33} & c_{34} & c_{35} & c_{36} \\ c_{41} & c_{42} & c_{43} & c_{44} & c_{45} & c_{46} \\ c_{51} & c_{52} & c_{53} & c_{54} & c_{55} & c_{56} \\ c_{61} & c_{62} & c_{63} & c_{64} & c_{65} & c_{66} \end{bmatrix}. \tag{2.8}$$

The equation (2.5) is referred as the Christoffel equation in the literature [15]. By solving this equation, one can obtain the angular frequencies ω as the eigenvalues for the given wavenumber $\mathbf{k}$ of the plane wave. For a three-dimensional elastic medium, there are three wave solutions corresponding to two quasi-transverse modes and one quasi-longitudinal mode at the particular wavenumber $\mathbf{k}$. As an example, the dispersion relation of in-plane wave modes for Gallium arsenide (GaAs) is calculated by using (2.5). Because the material property of GaAs has a cubic symmetry, the wave equations (2.1) can be decomposed into two subsets for in-plane wave modes and out-of-plane wave, respectively. As shown in Figure 2.1(a), two straight lines indicate the dispersion relation for the in-plane wave modes: quasi-longitudinal and quasi-transverse mode. Also, *x*- and *y*-displacement distributions of wave modes denoted by Points A and B are presented in Figure 2.1(b) and (c), respectively; one can check their dominant wave motions depending on wave mode.

From dispersion relations, the phase velocity and the group velocity can be calculated. As a simple case, let us consider an wave packet which contains two one-dimensional waves having slightly different k and ω as follows:

$$\cos(kx-\omega t)+\cos\{(k+\delta k)x-(\omega+\delta\omega)t\}$$
$$=2\cos\left\{\left(k+\frac{\delta k}{2}\right)x-\left(\omega+\frac{\delta\omega}{2}\right)t\right\}\cos\left(\frac{\delta kx}{2}-\frac{\delta\omega t}{2}\right). \tag{2.9}$$

From the right hand side of (2.9), the phase velocity $\mathbf{V}_p$ and the group velocity $\mathbf{V}_g$ are defined by

$$V_p=\frac{\omega+\delta\omega/2}{k+\delta k/2}\rightarrow\frac{\omega}{k} \tag{2.10}$$

and

$$V_g=\frac{\delta\omega}{\delta k}\rightarrow\frac{\partial\omega}{\partial k}. \tag{2.11}$$

This equation can be extended for a three-dimensional wave as follows:

$$\mathbf{V}_g=\frac{\partial\omega}{\partial k_x}\hat{\mathbf{x}}+\frac{\partial\omega}{\partial k_y}\hat{\mathbf{y}}+\frac{\partial\omega}{\partial k_z}\hat{\mathbf{z}}. \tag{2.12}$$

In a lossless medium, the group velocity $\mathbf{V}_g$ is identical to the energy velocity $\mathbf{V}_e$, which have to be normal to the slowness curve; see Ref. [15] for a detailed proof. The slowness curve is a diagram that represents the inverse of the phase velocity, $1/V_p=k/\omega$. It can be drawn by wavenumbers $\mathbf{k}$ of different propagating directions at the given frequency ω. In Figure 2.2, the slowness curve of GaAs is presented as an example. The directions of the phase and group velocity of a particular point on the quasi-transverse wave mode are denoted by the dashed and solid black arrows. One can check that directions of the phase velocity and the group velocity are not identical due to the anisotropy of GaAs.

2.2 Elastic wave propagation in two-dimensional periodic medium

When elastic waves propagate through a periodically modulated medium, it has been proved [62] that the wave has the following form:

$$\mathbf{u}(\mathbf{x},t) = \bar{\mathbf{u}} e^{j(\mathbf{kx}-\omega t)} \tag{2.13}$$

where $\bar{u}$ is a periodic function having the same periodicity as the medium. This periodic wave form is called a Bloch wave named after Felix Bloch who had proved the theorem describing electrons in a crystal. Based on the Bloch theorem, various analysis schemes have been developed for electromagnetic, acoustic, and elastic waves in a periodic medium. In this section, two analysis schemes, the plane wave expansion method [1, 63, 64] and the finite element method [65, 66], are introduced for design formulations in the following chapter. In the Plane Wave Expansion method (PWE), the periodic Bloch function $\bar{u}$ is expanded by its Fourier components which are treated as plane waves. Because one can access an each component of the particular plane wave, it is easy to grasp the physical insight of wave propagation in a periodic medium. Since the PWE is based on the Fourier transform, an inclusion of the periodic medium is restricted to a particular phase and the limited shape [67]. In this regard, the Finite Element Method (FEM) can be infinitely extended to various structures; this fact is an advantage to design periodic structures in a variety of situations.

In the following subsection, detailed derivations of the plane wave expansion method (Subsection 2.2.1) and the finite element method (Subsection 2.2.2) will be presented with numerical examples for two-dimensional phononic crystals.

2.2.1 Plane wave expansion method

In this subsection, the detailed formulation of the plane wave expansion method is addressed [1, 63, 64]. In a periodic elastic medium, a material property α, can be expanded in a sum of infinite plane waves:

$$\alpha(\mathbf{x}) = \sum_{\mathbf{G}} \mathrm{A}_{\mathbf{G}} e^{-j\mathbf{G}\mathbf{x}} \tag{2.14}$$

where $\mathrm{A}_{\mathbf{G}}$ is a Fourier component of α, $\mathbf{G}$ is reciprocal lattice vectors of the medium. If lattice vectors that describe a periodicity of the medium are $\mathbf{d}$, the reciprocal lattice vectors $\mathbf{G}$ are given by

$$\begin{aligned} \mathbf{G}_1 &= 2\pi \frac{\mathbf{d}_2 \times \mathbf{d}_3}{\mathbf{d}_1 \cdot (\mathbf{d}_2 \times \mathbf{d}_3)} \\ \mathbf{G}_2 &= 2\pi \frac{\mathbf{d}_3 \times \mathbf{d}_1}{\mathbf{d}_2 \cdot (\mathbf{d}_3 \times \mathbf{d}_1)} \\ \mathbf{G}_3 &= 2\pi \frac{\mathbf{d}_1 \times \mathbf{d}_2}{\mathbf{d}_3 \cdot (\mathbf{d}_1 \times \mathbf{d}_2)}. \end{aligned} \tag{2.15}$$

Since the Bloch function of a field variable β have the same periodicity with the medium, it can be also expanded by Fourier series as follows:

$$\beta(\mathbf{x}) = \sum_{\mathbf{G}} \mathrm{B}_{\mathbf{k}+\mathbf{G}} e^{j\{\omega t - (\mathbf{k}+\mathbf{G})\mathbf{x}\}} \tag{2.16}$$

where $\mathrm{B}_{\mathbf{k}+\mathbf{G}}$ is a Fourier component of β, $\mathbf{k}$ is the wavenumber, and ω is the angular frequency. The material properties (density and elastic stiffness constant) and the field variable (displacement, strain, stress) in the wave equations and the constitutive equation can be expanded by (2.14) and (2.16), then (2.1) becomes

$$\text{L.H.S. of } (2.1) = \sum_{\mathbf{G}'} \rho_{\mathbf{G}'} e^{-jG_i' x_i} \sum_{\mathbf{G}} -\omega^2 u_{i_{\mathbf{k}+\mathbf{G}}} e^{j(\omega t - G_i x_i - k_i x_i)}$$

$$= (\sum_{\mathbf{G}'} \sum_{\mathbf{G}} -\rho_{\mathbf{G}'} \omega^2 u_{i_{\mathbf{k}+\mathbf{G}}} e^{-j(G_i' + G_i)x_i}) e^{j(\omega t - k_i x_i)} \tag{2.17}$$

$$\text{R.H.S. of } (2.1) = (\sum_{\mathbf{G}} -j(k_j + G_j)\sigma_{ij_{\mathbf{k}+\mathbf{G}}} e^{-jG_i x_i}) e^{j(\omega t - k_i x_i)}.$$

By multiplying $e^{j\mathbf{G}^*\mathbf{x}}$ and integrating both sides over a primitive unit cell of a periodic medium, (2.17) can be written as

$$\omega^2 \sum_{\mathbf{G}} \rho_{\mathbf{G}^*-\mathbf{G}} u_{i_{\mathbf{k}+\mathbf{G}}} = j(k_j + G_j)\sigma_{ij_{\mathbf{k}+\mathbf{G}^*}}. \tag{2.18}$$

The constitutive equation (2.3) can be expanded into infinite plane waves and be expressed as

$$\text{L.H.S. of } (2.3) = \sum_{\mathbf{G}} \sigma_{ij_{\mathbf{k}+\mathbf{G}}} e^{j(\omega t - G_i x_i - K_i x_i)}$$

$$\text{R.H.S. of } (2.3) = \sum_{\mathbf{G}'} \mathbf{C}_{ijkl_{\mathbf{G}'}} e^{-jG_i' x_i} \sum_{\mathbf{G}} -j(k_l + G_l) u_{k_{\mathbf{k}+\mathbf{G}}} e^{j(\omega t - G_i r_i - k_i x_i)} \tag{2.19}$$

$$= (\sum_{\mathbf{G}'} \sum_{\mathbf{G}} -j(k_l + G_l)\mathbb{C}_{ijkl_{\mathbf{G}'}} e^{-j(G_i' + G_i)x_i}) e^{j(\omega t - k_i x_i)}.$$

After integration over a unit cell, it becomes

$$\sigma_{ij_{\mathbf{k}+\mathbf{G}^*}} = \sum_{G} -j(k_l + G_l)\mathbb{C}_{ijkl_{\mathbf{G}^*-\mathbf{G}}} u_{k_{\mathbf{k}+\mathbf{G}}}. \tag{2.20}$$

Substituting stress components of (2.20) into (2.18) yields

$$\omega^2 \sum_{\mathbf{G}} \rho_{\mathbf{G}^*-\mathbf{G}} u_{i_{K+G}} = (k_j + G_j) \sum_{\mathbf{G}'} (k_l + G_l')\mathbb{C}_{ijkl_{\mathbf{G}^*-\mathbf{G}'}} u_{k_{\mathbf{k}+\mathbf{G}'}}. \tag{2.21}$$

To obtain the dispersion relation numerically, the Fourier expansion are truncated with *N* plane waves. In this case, (2.21) can be expressed in the following matrix form:

$$\omega^2 \mathbf{M}\mathbf{U} = \mathbf{\Gamma}_i \mathbf{C}_{ij} \mathbf{\Gamma}_i \mathbf{U} \tag{2.22}$$

with

$$\mathbf{M} = \begin{bmatrix} \rho_{\mathbf{0}}\mathbf{I} & \cdots & \rho_{\mathbf{G}^1-\mathbf{G}^N}\mathbf{I} \\ \vdots & \ddots & \vdots \\ \rho_{\mathbf{G}^N-\mathbf{G}^1}\mathbf{I} & \cdots & \rho_{\mathbf{0}}\mathbf{I} \end{bmatrix}, \tag{2.23}$$

$$\mathbf{C}_{ij} = \begin{bmatrix} \mathbb{C}_{ijkl\mathbf{0}} & \cdots & \mathbb{C}_{ijkl\mathbf{G}^1-\mathbf{G}^N} \\ \vdots & \ddots & \vdots \\ \mathbb{C}_{ijkl\mathbf{G}^N-\mathbf{G}^1} & \cdots & \mathbb{C}_{ijkl\mathbf{0}} \end{bmatrix}, \tag{2.24}$$

and

$$\mathbf{\Gamma}_i = \begin{bmatrix} \mathbf{k}+\mathbf{G}^1 & & 0 \\ & \ddots & \\ 0 & \cdots & \mathbf{k}+\mathbf{G}^N \end{bmatrix}. \tag{2.25}$$

One can find the frequency ω at the given wavenumber $\mathbf{k}$ ($\omega(\mathbf{k})$ formulation) or the wavenumber $\mathbf{k}$ at the given frequency ω ($\mathbf{k}(\omega)$ formulation) with (2-22)-(2.25). As an example, the numerical results for a two-dimensional phononic crystal will be presented in Subsection 2.2.3.

2.2.2 Finite element method

In this subsection, the detailed formulation of the finite element method is addressed for a periodic elastic medium [65, 66]. By the finite element method, an analysis domain is discretized into finite elements in which the fields are interpolated using the shape functions. Then, the global field is expressed as a function of nodal values of finite elements. The weak form of the elastic wave equations are given by

$$\begin{aligned} \int_\Omega \delta\mathbf{u}\rho\frac{\partial^2\mathbf{u}}{\partial t^2}dV &= \int_\Omega \delta\mathbf{u}\nabla\cdot\boldsymbol{\sigma}\,dV \\ &= \int_\Omega \delta\mathbf{u}\mathbb{C}\frac{\partial}{\partial\mathbf{x}}\left(\frac{\partial\mathbf{u}}{\partial\mathbf{x}}\right)dV. \end{aligned} \tag{2.26}$$

Applying the divergence theorem yields

$$\int_{\Omega} \delta \mathbf{u} \rho \frac{\partial^2 \mathbf{u}}{\partial t^2} dV = \int_{\partial\Omega} \delta \mathbf{u} \boldsymbol{\sigma} \mathbf{n} \, dS - \int_{\Omega} \frac{\partial \delta \mathbf{u}}{\partial \mathbf{x}} \mathbb{C} \frac{\partial \mathbf{u}}{\partial \mathbf{x}} dV. \tag{2.27}$$

The first term on the right side of (2.27) equals to zero because there is no external force. The displacement fields $\mathbf{u}(\mathbf{x})$ and the strain $\boldsymbol{\varepsilon}(\mathbf{x})$ in an element are interpolated with the shape function $\mathbf{N}(\mathbf{x})$ as follows:

$$\mathbf{u}(\mathbf{x}) = \mathbf{N}(\mathbf{x}) \mathbf{U}_e \tag{2.28}$$

$$\boldsymbol{\varepsilon}(\mathbf{x}) = \frac{\partial \mathbf{u}(\mathbf{x})}{\partial \mathbf{x}} = \frac{\partial \mathbf{N}(\mathbf{x})}{\partial \mathbf{x}} \mathbf{U}_e = \mathbf{B}(\mathbf{x}) \mathbf{U}_e \tag{2.29}$$

where $\mathbf{U}_e$ is the nodal displacements of an element. Substituting (2.28) and (2.29) into (2.27) yields

$$\omega^2 \mathbf{M}_e \mathbf{U}_e = \mathbf{K}_e \mathbf{U}_e \tag{2.30}$$

where $\mathbf{M}_e$ and $\mathbf{K}_e$ are the element mass matrix and element stiffness matrix,

$$\mathbf{M}_e = \rho_e \int_{\Omega} \mathbf{N}^T \mathbf{N} dV \tag{2.31}$$

$$\mathbf{K}_e = \int_{\Omega} \mathbf{B}^T \mathbb{C}_e \mathbf{B} dV. \tag{2.32}$$

The global mass and stiffness matrices of the primitive unit cell of a periodic medium can be assembled with element matrices derived in (2.31) and (2.32). After the assembly of the global matrices, the Bloch theorem (2.13) has to be applied to obtain the dispersion relation of the periodic medium. To do this, the periodic boundary conditions that describe a phase shift between two boundaries of the unit cell are applied. For example, if there are two points apart from d on the boundary, then the phase of the second point is shifted e^{jkd} compared to the first point. By applying these periodic boundary conditions with different wavenumbers, one can calculate the dispersion relation of a periodic medium.

There is an alternative formulation of the finite element method, which begins with the Bloch theorem. Before interpolating the displacement in the weak form of elastic wave equations (2.27), it can be assumed that the displacement fields have the form in the Bloch theorem. Then, (2.27) becomes

$$\omega^2 \int_\Omega \delta\bar{\mathbf{u}}^* \rho \bar{\mathbf{u}}\, dV = -\int_\Omega \left(\frac{\partial \delta\bar{\mathbf{u}}}{\partial \mathbf{x}} + j\mathbf{k}\bar{\mathbf{u}} \right)^* \mathbb{C} \left(\frac{\partial \bar{\mathbf{u}}}{\partial \mathbf{x}} + j\mathbf{k}\bar{\mathbf{u}} \right) dV \tag{2.33}$$

where $\bar{u}$ is the Bloch function and the superscript * denotes the Hermitian operator, and $e^{j(\mathbf{kx}-\omega t)}$ is omitted on both sides. After the displacements of the Bloch function is interpolated with the shape function, then, (2.33) can be written as

$$\omega^2 \mathbf{M}_e \bar{\mathbf{U}}_e = \bar{\mathbf{K}}_e \bar{\mathbf{U}}_e \tag{2.34}$$

where $\bar{\mathbf{K}}_e$ are the element stiffness of the following form

$$\bar{\mathbf{K}}_e = \int_\Omega (\mathbf{B} + j\mathbf{kN})^* \mathbb{C}_e (\mathbf{B} + j\mathbf{kN})\, dV. \tag{2.35}$$

In this case, equations are expressed for the Bloch function so that it is not needed to employ the explicit phase shift between the boundaries. This fact has an advantage to analysis the dispersion relation at the given frequency at which the wavenumber component is unknown; see Ref. [68] for detailed derivation of the analysis at the given frequency.

2.2.3 Numerical examples

Up to now, detailed derivation of the PWE and the FEM were given. In this subsection, they are applied to calculate the dispersion relation of a two-dimensional phononic crystal. Phononic crystals are an artificial material which is composed of inclusions regularly distributed in a matrix. As an example, the

phononic crystals consisting of circular epoxy inclusions arranged with the rectangular and the triangular lattices in the aluminum matrix are considered; see Figure 2.3(a) and (b) for configurations of square-lattice and triangular-lattice phononic crystals, respectively. The lattice parameter is $d_1 = d_2 = 5\text{mm}$ and the diameter of circular inclusion is 2.5mm. In a formulation by the plane wave expansion method, 441 plane waves are used for the expansion of the displacements. In the finite element method, the unit cell of the considered phononic crystal is discretized by 10000 finite elements.

Numerical results of the dispersion relation of the considered square-lattice phononic crystals are presented in Figure 2.4. The angular frequency is calculated along the two directions of wavenumber: $\Gamma - \text{X}$ and $\Gamma - \text{M}$, where Γ, X, and M are the symmetric points of the 1st (irreducible) Brillouin zone of the rectangular phononic crystals; see the Brillouin zone shown in the right panel of Figure 2.3(a). In Figure 2.4, Black dots are presented the result by the plane wave expansion while red dots, by the finite element method. In phononic crystals, waves are scattered by the periodic inclusions, leading to destructive or constructive interferences depending on the wavelength. Due to the wave scattering, there are multiple propagating modes in the phononic crystal while two kinds of wave modes, the quasi-longitudinal and the quasi-transverse modes, only exist in a homogeneous elastic medium. Between branches of propagating modes, it is shown that the band gap of a quasi-transverse wave is opened as denoted by the gray shading in Figure 2.4. At this frequency range ($220.6 < f < 319.7\,\text{kHz}$), elastic wave of the quasi-transverse mode cannot propagate through the phononic crystals. Also, one can find that the dispersion relation is the symmetric in the wavenumber domain as be

proved by the Bloch theorem. Its irreducible unit in the wavenumber domain is called 1st Brillouin zone which is represented by the shading in the right panel of Figure 2.3.

In Figure 2.5, the Equi-Frequency Contours (EFC's) at different frequencies are given for phononic crystals arranged in the rectangular and the triangular lattices, respectively. In each panel of Figure 2.5, the outer contour represents the EFC of the quasi-transverse wave mode and the inner contour, the quasi-longitudinal mode. The EFC is a diagram of the wavenumbers that satisfy the wave equations at the given frequency. It is similar to the slowness curve of a homogeneous medium that is discussed in Section 2.1. From the Christoffel equations of a homogeneous medium, the wavenumber is always proportional to the frequency so that the shape of EFC is always the same regardless of the frequency. But the EFC's of the phononic crystal shown in Figure 2.5 exhibit different shapes depending on the frequency: At 100 kHz, EFC's of the quasi-longitudinal and the quasi-transverse modes are almost circular. As the frequency increased, they become a non-circular shape. In EFC's 250 kHz, the quasi-transverse wave cannot propagate in $\Gamma - X$ direction while propagates with the zero-diffraction in some directions. This finding can be interpreted as an anisotropy induced by the phononic crystals. As mentioned earlier, the effect of the phononic crystals on the wave scattering is different depending on the periodicity of the inclusions; compare EFC's of two different lattice type shown in Figure 2.5.

2.3 Elastic wave propagation in a waveguide

Here, wave propagation in a periodic waveguide will be discussed. In previous sections of Chapter 2, elastic waves in an infinite medium were addressed. Unlike the infinite medium in which there is no boundary to be considered, elastic waves in a waveguide are confined within free boundaries; successive reflections from free boundaries lead to develop the guided modes in a waveguide. In this section, after the dispersion relation of an elastic waveguide is briefly addressed, analysis schemes of the dispersion relation for a periodic waveguide will be introduced.

2.3.1 Elastic wave propagation in a homogeneous waveguide

When elastic waves propagate along a waveguide, such as pipes and plates, the longitudinal and the transverse wave modes are coupled due to reflections at free boundaries. By applying the transverse resonance condition to the reflection coefficient of each wave mode at the free boundary, the dispersion relation of the guided waves can be derived [15]. The dispersion relation for the symmetric and the antisymmetric wave modes in an isotropic waveguide are given by

$$\frac{\tan k_{yT} h/2}{\tan k_{yL} h/2} = -\frac{4k_x^2 k_{yL} k_{yT}}{\left(k_{yT}^2 - k_x^2\right)^2} \tag{2.36}$$

and

$$\frac{\tan k_{yT} h/2}{\tan k_{yL} h/2} = -\frac{\left(k_{yT}^2 - k_x^2\right)^2}{4k_x^2 k_{yL} k_{yT}} \tag{2.37}$$

where k_{yL}, k_{yT} is the y components of wavenumber for the longitudinal and the

transverse wave modes, k_x is the wavenumber in the propagating direction, h is the thickness of the waveguide [15, 16]. The relations between the wavenumbers are

$$k_{yL}{}^2 = \left(\frac{\omega}{V_L}\right)^2 - k_x^2 \tag{2.38}$$

and

$$k_{yT}{}^2 = \left(\frac{\omega}{V_T}\right)^2 - k_x^2 \tag{2.39}$$

where V_L, V_T are the phase velocities of the longitudinal and the transverse waves in an infinite isotropic medium. The dispersion relations of the waveguides can be analyzed by searching the $\omega - k_x$ pair which satisfies (2.36) – (2.39).

As an example, the dispersion relation of an aluminum plate of 30 mm in thickness is analyzed numerically. As shown in Figure 2.6(a), an aluminum plate supports infinite wave modes. Their modal distributions of displacements are given in Figure 2.6(b). Note that wave modes at the fixed wavenumber of 400 rad/m are evaluated. It is found that wave modes of higher branches have more nodal points in the thickness direction. Moreover, their wave properties exhibit complex behavior compared to those for the bulk wave; see the dispersion relations of an infinite medium given in Figure 2.1(a). For example, the group velocity of the guided wave mode is different depending on the frequency, leading to the dispersion of a wave packet. The dispersive nature of guided waves causes difficulties in their practical applications: multiple wave mode excitations and the group velocity dispersion. As the objective of this research is to overcome the problematic issues by employing periodic structures into waveguides, analysis schemes for the dispersion relation of

a periodic waveguides will be discussed in the following subsection.

2.3.2 Elastic wave propagation in a periodic waveguide

For an infinitely periodic medium, the plane wave expansion method and the finite element method were discussed in Section 2.2. In analysis of the dispersion relation of a periodic waveguides, the main idea to deal with the periodicity in a medium is the same: to expansion the Bloch function by the Fourier transform in the plane wave expansion method; to apply the periodic boundary condition in the finite element method [69-71]. The difference in the case of periodic waveguides is the traction free boundaries. In this subsection, it is introduced how the free boundaries are considered in the plane wave expansion method and the finite element method.

As an example, consider a waveguide in which the square inclusions are periodically arranged in the *x* direction shown in Figure 2.7(a). This periodic waveguide has the free boundaries at $y = \pm h/2$ while it is infinitely long in the *z* direction. To analysis the dispersion relation by the plane wave expansion method, the supercell in which waveguide are stacked in the *y* direction can be considered as shown in Figure 2.7(b). To mimic the free boundaries of the original waveguides, a Low Impedance Material (LIM) layer is inserted between the periodic waveguides [70, 71]. Because an impedance difference is quite big enough to confine elastic waves in the periodic waveguides, one can use the PWE method for an infinitely periodic medium to a finite periodic waveguide system. In the case for the periodic waveguides, additional efforts are needed in calculation of the Fourier components of the unit cell of the waveguide supercell which is represented in Figure 2.7(b).

Next, the analysis procedure by the FEM for the periodic waveguide is quite the same with the case for the infinite periodic medium. As mentioned in Subsection 2.2.2, a unit cell of the periodic medium is discretized by the finite element. Then, based on the Bloch theorem, the periodic boundary conditions are applied to boundaries of a unit cell. In the case of the periodic waveguide, it is enough to replace the periodic boundary condition at the free boundaries by the traction free boundary condition. It is the same when the formulation for the Bloch function in (2.34) is used. By using the finite element method, the dispersion relation of a 30 mm thick aluminum waveguide in which square epoxy inclusions arranged periodically ($d_x = 6\,\mathrm{mm}$) is analyzed. The calculated dispersion relation is given in Figure 2.8. As for an infinite periodic medium, it is shown that the band gap for the fundamental guided mode is opened and the small partial band gaps are also opened due to the mode coupling between wave modes. Detailed analysis of the dispersion relation for a periodic waveguide will be discussed in the following chapters.

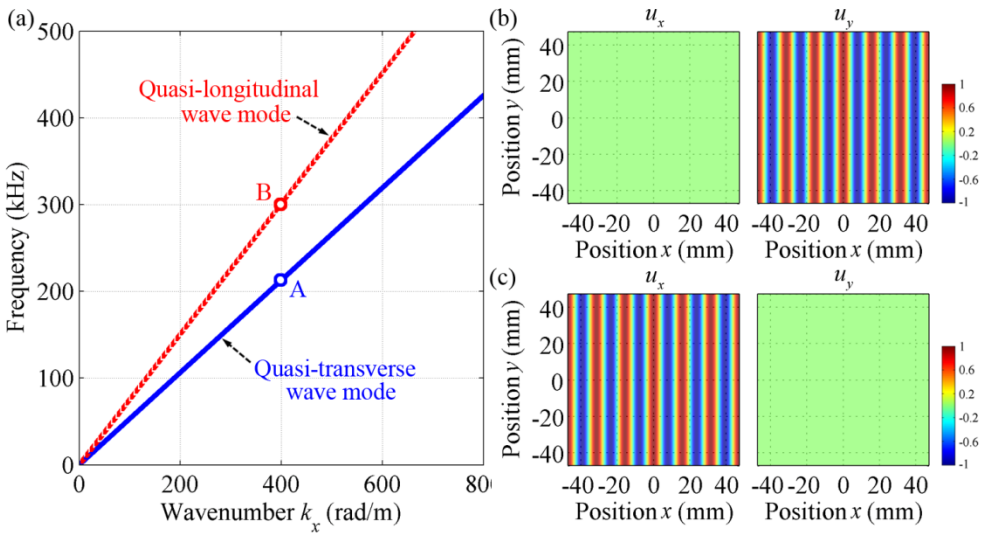

Figure 2.1 (a) Dispersion curves of quasi-longitudinal and quasi-transverse waves in an infinite Gallium arsenide. The distributions of *x*- and *y*-displacements of eigenmodes at (b) Point A and (c) Point B in Figure 2.1(a).

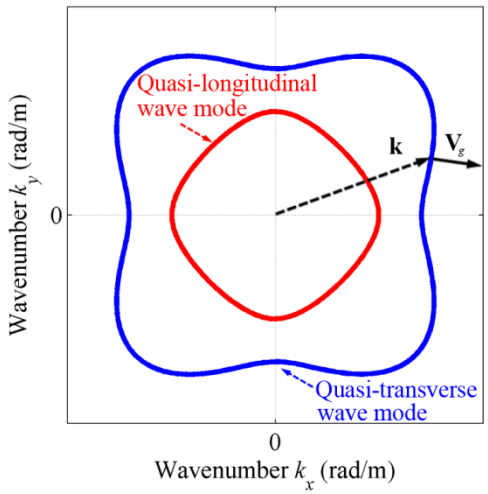

Figure 2.2 (a) Slowness curves of quasi-longitudinal and quasi-transverse waves in an infinite Gallium arsenide. The directions of phase velocity is denoted by dashed line while the group velocity, by solid line.

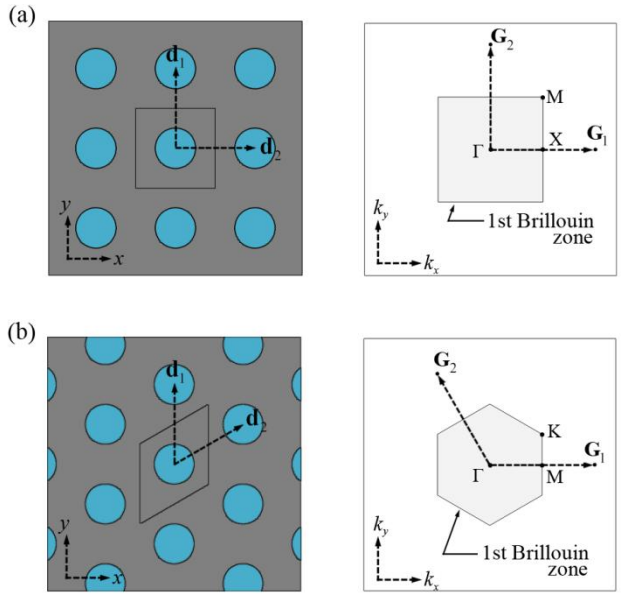

Figure 2.3 Schematics of phononic crystals (left) and the corresponding irreducible Brillouin zone (right) for (a) square lattice and (b) triangular lattice.

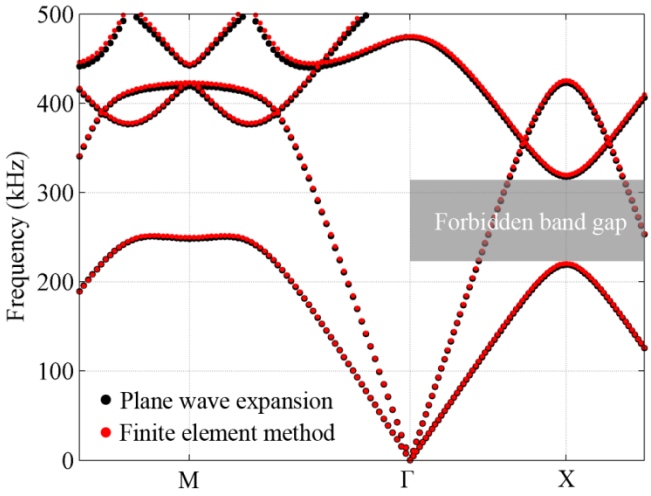

Figure 2.4 Dispersion relation of the phononic crystal consisting of epoxy inclusions with square lattice in aluminum matrix. Black dots represent the results by the plane wave expansion while red dots, by the finite element method.

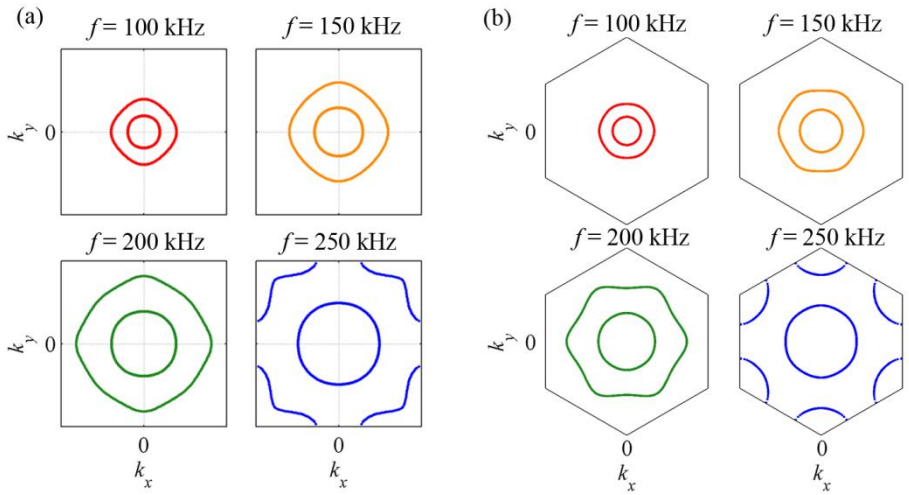

Figure 2.5 The equi-frequency contours (EFC's) at different frequencies for (a) the square-lattice and (b) the triangular-lattice phononic crystals

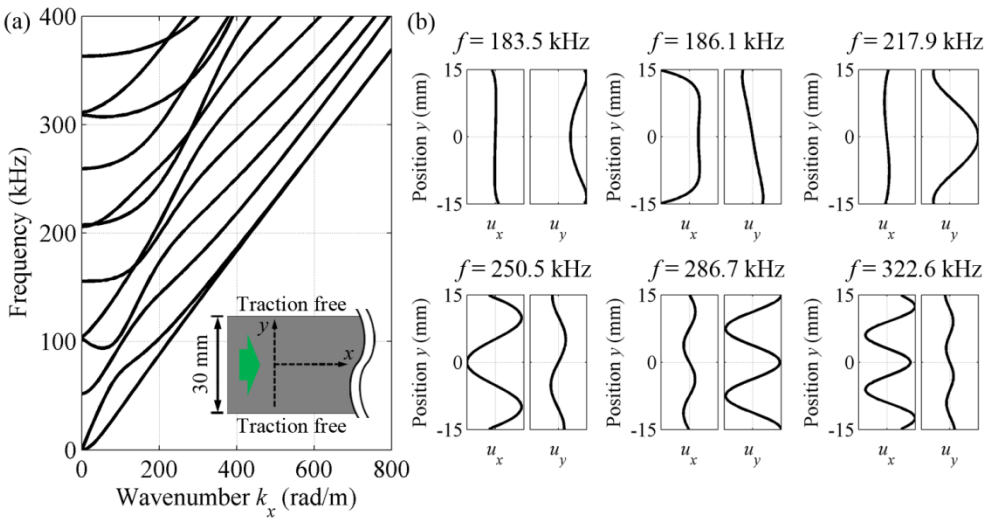

Figure 2.6 (b) The dispersion relations of elastic guided waves in a homogeneous waveguide of 30 mm in the width. (b) The distributions of the *x*- and *y*-displacement components of eigenmodes at $k_x = 400$ rad/m.

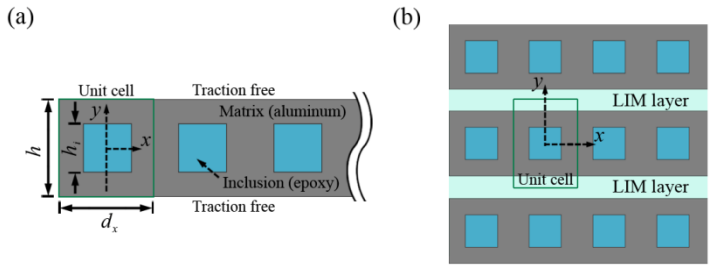

Figure 2.7 (a) Schematic of phononic crystal plate consisting the periodic inclusions in the middle of the plate. (b) Schematic of the supercell of phononic crystal plate. Between the phononic crystal plates, the low-impedance material (LIM) layers are used to suppress the transmission.

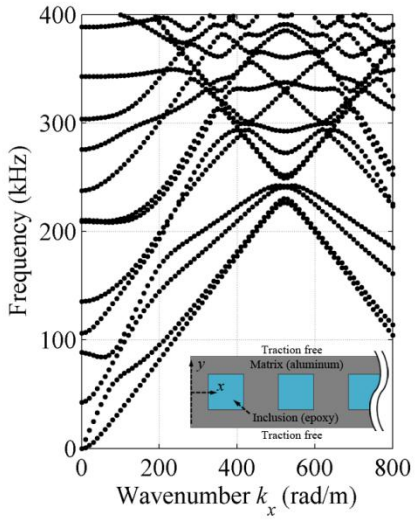

Figure 2.8 (a) Dispersion relation of the phononic crystal plate which is made of epoxy inclusions in an aluminum plate.

CHAPTER 3

DISPERSION ENGINEERING IN WAVENUMBER DOMAIN BY PHONONIC CRYSTALS

3.1 Overview

In the ultrasonic non-destructive evaluation by guided waves, multi-mode excitation should be resolved to improve the resolution of an evaluation. But, above the cutoff frequency, the other wave modes which have a longer wavelength are inevitably excited. These long-wavelength wave modes are undesired in the evaluation process and should be removed for a better resolution. From this motivation, multiple wave modes in a waveguide are aimed to separate by employing phononic crystals in this chapter. Here, the anisotropic property of phononic crystals is investigated to separate a multi-modal wave in a waveguide. As mentioned in Chapter 1, the photonic and phononic crystals exhibit strongly anisotropic properties at edges of the band gap; it has been demonstrated that waves are refracted at an extremely large angle, the superprism effect [31], or propagate maintaining their waveform unchanged, the self-collimation phenomena [32]. These anisotropic properties of phononic crystals are strongly dependent on the frequency and the wavenumber. Furthermore, elastic waves in a waveguide exhibit the complex behavior compared to in a bulk medium.

In earlier researches on wave separation of electromagnetic waves, the extraordinary wave phenomena of photonic crystals have been exploited: the band gap phenomenon [72-74], waveguide effect [75], and refractive property [32, 76, 77]. For acoustic waves, a little effort has been paid to separate the waves by phononic crystals. In 2004, acoustic waves of different frequencies were separated by employing waveguide effect of phononic crystals [78] and no investigation has been made for the separation of elastic waves. In the situation where the mode separation cannot be achieved by the alternative way, such as the frequency filtering or the signal processing, phononic crystals can be effectively applied to separate multi-modal waves. Here, we present that the anisotropic characteristics of phononic crystals [4, 45, 79, 80] can be used for complete mode separation. In the non-destructive evaluation by guided waves, the main efforts were devoted to single mode excitation and measurement by enhancing a target mode [58, 59] or suppressing an undesired mode [61]. For example, If only one mode is to be selected, a meander-like type transducer with the lines spaced by a target wavelength may be considered [81]. Compared to the presenting techniques, the proposed approach by phononic crystals can provide the possibility of multiple mode measurement, leading to the advance in non-destructive evaluation application.

In this study, the propagation direction was tailored to have a different value depending on a mode. Multiple wave modes, which are incident onto the same position of the phononic crystal, propagate along different propagating directions, then, they can be separated at the exit side of phononic crystals. For clear separation, the propagation directions are as different as possible and the spatial dispersion

effect should be considered. To control these wave properties, we focus on the dispersion relation in the wavenumber domain of phononic crystals. The aims of this chapter are (1) to manipulate the dispersion relation in the wavenumber domain by an optimization method for two-dimensional phononic crystals; (2) to select lattice parameters of a phononic crystal plate for mode separation of guided waves; (3) to confirm the mode separation in phononic crystal plate by numerical analysis and ultrasonic experiments.

Before investigating the mode separation for a waveguide, the dispersion relation of two-dimensional phononic crystals is investigated in the wavenumber domain as a simplified problem. Since wave properties of a transverse wave mode in a bulk elastic medium is identical to a fundamental shear-horizontal (SH) guided mode in a plate, the effect of phononic crystals on the spatial dispersion can be understood from this two-dimensional study. In particular, the self-collimating phononic crystal is focused as a preliminary study. Phononic crystal structures which allows the wave to propagate without diffraction broadening [32] are designed by employing an optimization method. We formulate the shape optimization by using the plane wave expansion method and select the periodicity of a lattice and the filling factor of circular air holes so that an elastic wave can propagate along a predetermined direction without the spatial dispersion.

In Section 3.3, a necessary requirement for mode separation of guided waves, the fundamental SH and the second order SH1 wave modes in a waveguide, is discussed. Then, the lattice parameters of a phononic crystal plate are determined based on the results of the two-dimensional case. By a selected phononic crystal

plate, the dispersion relation in the wavenumber domain at the target frequency, EFC, is analyzed; a direction of the group velocity and a degree of the spatial dispersion for each wave mode are examined. Finally, an effectiveness of the phononic crystal plate for the mode separation of SH waves is demonstrated by a numerical harmonic analysis and ultrasonic experiments.

3.2 Dispersion engineering of two-dimensional phononic crystals

In this section, the dispersion engineering for self-collimated waves in a two-dimensional phononic crystal is carried out by a numerical optimization. As be discussed earlier, where the dispersion relation of phononic crystals have the flat EFC's, elastic waves can propagate without the dispersion. At the flat region of EFC's, the group velocities are almost collinear and the self-collimation effect is observed. As shown Figure 2.5, the region where the self-collimation is observed depends on the frequency and the structure of phononic crystals. In this situation, it is important to select the proper phononic crystal to have a desired propagation direction at the given frequency. Here, a gradient-based shape optimization method is formulated by the plane wave expansion method to determine a lattice parameter and a filling factor of phononic crystal. After the design formulation by plane wave expansion method is given, the self-collimating phononic crystals are designed to have the prescribed propagation direction at the given frequency.

3.2.1 Design formulation for self-collimating phononic crystals

Here, a shape optimization method for self-collimating phononic crystals is formulated. The objective of an optimization problem is to exhibit the self-collimation effect for elastic waves in phononic crystals. The dispersion relation in the wavenumber domain is manipulated by tailoring the phononic crystal structures. To this end, we propose the shape optimization method to design the lattice parameters of phononic crystals. We consider two-dimensional phononic crystal consisting of air holes arranged with a parallelogram lattice. As design variables, the

lattice parameters of phononic crystals are considered; see a diagram of a phononic crystal shown in Figure 3.1(a). The objective function is defined by the square norm of differences in the group velocities as follows:

$$\min_{|\mathbf{d}_i|,\, f} \left\| \theta - \theta_{\text{ref}} \right\| \quad \text{, in} \quad \Delta k_y \tag{3.1}$$

where θ is the direction of a group velocity at the particular k_y, θ_{ref} is the predetermined propagation direction, $\| \ \|$ denotes the square norm, and Δk_y is the target wavenumber range. The design variables are as follows: the periods $|\mathbf{d}_i|$ of lattice vectors, the direction α of a lattice vector $\mathbf{d}_2$ (the direction of $\mathbf{d}_1$ is fixed at $\hat{y}$), and the filling fraction f of inclusion. By minimizing the objective function in (3.1), the EFC of the parallelogram lattice can have the self-collimation region in the target wavenumber range Δk_y at the given frequency.

Since the direction of a group velocity, θ, is normal to its EFC at the particular frequency, $k(\omega)$ formulation is helpful to reduce the numerical cost in the dispersion analysis compared to $\omega(k)$ formulation [82, 83]. When the plane wave expansion method is applied in calculation of EFC's, $\omega(k)$ formulation of dispersion analysis is expressed by matrix form as follows:

$$\omega^2 \mathbf{M}\mathbf{U} = \left(\mathbf{\Gamma}_i^k + \mathbf{\Gamma}_i^{\mathbf{G}} \right) \mathbf{C}_{ij} \left(\mathbf{\Gamma}_i^k + \mathbf{\Gamma}_i^{\mathbf{G}} \right) \mathbf{U} \tag{3.2}$$

where

$$\mathbf{\Gamma}_i^k = k \begin{bmatrix} \mathbf{l} & & 0 \\ & \ddots & \\ 0 & & \mathbf{l} \end{bmatrix}, \tag{3.3}$$

$$\mathbf{\Gamma}_i^G = \begin{bmatrix} \mathbf{G}^1 & & 0 \\ & \ddots & \\ 0 & & \mathbf{G}^N \end{bmatrix}, \tag{3.4}$$

and $\mathbf{l} = l_x\hat{\mathbf{x}} + l_x\hat{\mathbf{y}} + l_z\hat{\mathbf{z}}$ is a unit vector of $\mathbf{k}$. Then, (3.2) becomes the polynomial eigenvalue problem for a wavenumber *k* as follows:

$$\begin{aligned} \mathbf{\Gamma}_i^k \mathbf{C}_{ij} \mathbf{\Gamma}_i^k \mathbf{U} + \left(\mathbf{\Gamma}_i^k \mathbf{C}_{ij} \mathbf{\Gamma}_i^{\mathbf{G}} + \mathbf{\Gamma}_i^{\mathbf{G}} \mathbf{C}_{ij} \mathbf{\Gamma}_i^k \right) \mathbf{U} \\ + \left(\mathbf{\Gamma}_i^{\mathbf{G}} \mathbf{C}_{ij} \mathbf{\Gamma}_i^{\mathbf{G}} - \omega^2 \mathbf{M} \right) \mathbf{U} = 0. \end{aligned} \tag{3.5}$$

By solving (3.5) at the given frequency ω, EFC's of phononic crystals can be analyzed. And the direction of a group velocity is obtained by numerical derivation of calculated EFC's.

The dispersion engineering in (3.1), the design variables (lattice vectors, filling factor of inclusion) are updated by the Method of Moving Asymptotes (MMA) [84], the gradient-based optimizer, until convergence criteria is satisfied. We present an iteration history of an optimization example in Figure 3.2(a): As the proposed dispersion engineering is progressed, the objective function is minimized; phononic crystals of different iteration numbers and corresponding EFC's are also presented in Figure 3.2 (b) and (c), respectively. At an initial stage, phononic crystal has a circular shape of EFC's that is the same with those of an isotropic medium. But, as the optimization is progressed, the self-collimation effect appears in its EFC. In the following subsection, detailed information of various numerical examples will be presented.

3.2.2 Design examples

In this subsection, the formulated optimization method in (3.1) is applied to design the self-collimating phononic crystals to have different propagation direction. The structure of phononic crystals is engineered to exhibit the desired wave properties: the self-collimation effect and the predetermined direction of wave propagation. In this study, the transverse wave mode in a bulk aluminum is considered at the target frequency of 300 kHz. The following material properties of aluminum are used: density $\rho = 2631.4 \text{kg/m}^3$, Young's modulus E = 67.78 GPa, Poisson's ratio $\nu = 0.33$. The phononic crystal is designed to propagate along the prescribed direction $\theta_{\text{ref}}^* = 10^\circ$, 20°, 30°, and 40°, respectively. The target wavenumber region of $156.7 < k_y < 347.4 \text{rad/m}$ is controlled. The design variables, the periods of lattice, the angle of parallelogram lattice, and a filling factor of air holes, are constrained as follows: $0 < |\mathbf{d}_1|, |\mathbf{d}_2| < \lambda$, $0 < \alpha < 90^\circ$, and $0 < f < 1.0$, respectively. The wavelength λ of the transverse wave mode in a bulk aluminum is 10.37mm at 300 kHz. Initial values of the design variables are $|\mathbf{d}_1|, |\mathbf{d}_2| = \lambda/10$, $\alpha = 90^\circ$, and $f = 0.01$, respectively. From these values, they are so optimized to achieve the desired characteristics in the wavenumber domain.

Figure 3.3 shows results of the dispersion engineering by the proposed optimization method. Designed phononic crystals and their EFC's at 300 kHz are given for $\theta_{\text{ref}}^* = 10^\circ$, 20°, 30°, and 40°, respectively. Depending on the given propagation direction θ_{ref}^*, phononic crystals are designed through optimization procedures. The

converged value of design variables for self-collimating phononic crystals are summarized in Table 3.1. Note that the phononic crystals are presented in a region on $-\lambda/2 < x, y < \lambda/2$. The EFC's have the flat portion in the target wavenumber domain denoted by the gray shading; the direction of group velocity, which is normal to EFC, is almost the same with the target values, θ^*_{ref}. In Figure 3.4, we present the propagation direction as a function of an inputted angle of the transverse mode from a bulk aluminum. Note that the target wavenumber range corresponds to the incident angle of $15^\circ < \theta < 35^\circ$. As can be aniticipated from EFC's, the propagation direction is constant for designed phononic crystals compared with a bulk aluminum. From this profile where the propagation directions are almost constant in Δk_y, it is expected that the spatial dispersion of the elastic medium is successfully suppressed by the engineered phononic crystal.

To demonstrate this dispersion engineering, numerical harmonic analysis is conducted. The phononic crystal slabs of $100\,\text{mm}(\approx 10\lambda)$ are constructed into an aluminum with the design periodic structure. Around the analysis domain, the Perfectly Match Layer (PML) is made to suppress the edge reflection. The transverse wave is excited at a source located the left side of the phononic crystal slab with an incident angle of 25°. Figure 3.5 shows the distribution of shear stress $\sigma_{x'y'}$ calculated by time-harmonic analysis for phononic crystal slabs of $\theta^*_{\text{ref}} = 10^\circ$, 20°, 30°, and 40°, respectively. Note that the coordinate for an evaluation of the shear stress $\sigma_{x'y'}$ is rotated by 25 degrees. In each panel of Figure 3.5, inputted waves are refracted depend on the constructed phononic crystal structures shown in

Figure 3.3. And it is presented that the refracted wave propagates without spatial dispersion in the phononic crystals region. The interfaces between a bulk aluminum and the designed phononic crystal are remarked by black dashed lines.

In summary of this section, the dispersion relation of the elastic waves is controlled in the wavenumber domain by the properly designed phononic crystals. To find the lattice parameter of a phononic crystal which exhibits the desired wave properties, the optimization method is proposed. The shape optimization problem is formulated to make the phononic crystal have the self-collimation effect at the given frequency and the wavenumber range. Through the optimization problem, phononic crystal structures having different propagation directions can be obtained. The self-collimation in the engineered phononic crystal is confirmed by the numerical simulation.

3.3 Mode separation of guided waves in a phononic crystal plate

In this section, the ability of phononic crystals to manipulate the dispersion relation in the wavenumber domain is employed for the mode separation in an elastic waveguide. Above the first cutoff frequency of a waveguide, f_{cutoff} , high-frequency pulses generated from a transducer inevitably excite multiple wave modes having both large and short wavenumbers. To achieve high-resolution elastic wave based imaging or damage detection, one should use wave pulses of short wavelengths (i.e., large wavenumbers). Here, we apply phononic crystals in which the propagation direction of elastic waves can be controlled. The main challenge of this study is that the propagation directions of multiple wave modes are engineered at a single frequency. To examine the situation in which the mode separation is applied, let us consider a thin homogeneous aluminum plate as shown in Figure 3.6(a). When the center frequency of a wave pulse is higher than the cutoff frequency of 311 kHz, two wave modes corresponding to the circled points in the dispersion relation of Figure 3.6(b) are simultaneously excited. This fact is confirmed by ultrasonic experiments. In Figure 3.6(c), we measured the elastic wave signal at Point A in Figure 3.6(a), which shows the multiple guided modes are simultaneously excited at 357 kHz.

Here, the anisotropic wave property of phononic crystal is applied to make guided waves propagate in different directions. Figure 3.7(a) shows a schematic of this mode separation in waveguide. When a phononic crystal plate is inserted in a homogeneous plate, the propagation directions of two wave modes are manipulated and they can be separated. This can be confirmed by the experimentally measured

wave signal at A′ in Figure 3.7(b); the fundamental shear-horizontal (SH) wave only appears in the signal. In the following section, we present the related numerical analysis and experimental demonstration as well as the findings from this study.

3.3.1 Selection of phononic crystal plates for mode separation

The objective of this work is to separate two shear waves, SH0 and SH1 wave modes, in a homogeneous plate. To this end, the dispersion relations of guided SH waves are controlled to have different propagation directions by phononic crystal plate. As discussed in Section 3.2, we can manipulate the propagation direction of elastic waves by tailoring the unit structures of phononic crystals. Before the lattice parameter of phononic crystal plate is selected, it is helpful to review the dependency of the dispersion relation in the wavenumber domain on the frequency. At the low frequency when the wavelength is smaller than the periodicity of a phononic crystal, the dispersion relation of phononic crystal is almost the same as that of homogeneous medium. In other words, the effect of the phononic crystal on wave propagation is homogenized at the low frequency regime. As the frequency increased, the wavelength becomes comparable to the periodicity. Then, the destructive interference occurs in some directions; this leads to the partial band gaps in which waves cannot propagates; see EFC's at 250 kHz in Figure 2.5. At this frequency, the wave propagated without the spatial dispersion as in the waveguide, which is called the self-collimation. In the Section 3.2, we tailored the periodicity of the phononic crystal, leading to change in the direction where the partial band gap is opened.

For mode separation, the propagation directions of two SH waves should be as different as possible; in addition, the spatial dispersion effect should be minimized. From the previous studies, the formation of the partial band gap exhibits different behaviors depending on the branch of dispersion curves [41, 85]. Based on this condition, here, the lattice parameters of phononic crystal plate is so selected that the different branches are excited depending on the wave mode at the target frequency: the second branch (folded branch) for SH0 wave mode and the first branch for SH1 wave mode. In an aluminum plate of 5 mm, the wavelengths of SH0 wave and SH1 wave modes at 357 kHz are 8.71 mm and 17.78 mm, respectively. By considering these wavelengths, a lattice parameter a of the triangular phononic crystal and a diameter d of air holes are selected as $a = 8\,\text{mm}$ and $d = 2\,\text{mm}$, respectively. In the following subsection, the dispersion relation of the selected phononic crystal is examined for the mode separation.

3.3.2 Analysis of dispersion relations of phononic crystal plate

For mode separation of guided SH waves, the phononic crystal plate consists of the air-filled holes of triangular-lattice in a 5 mm thick aluminum plate (density $\rho = 2631.4\,\text{kg/m}^3$, Young's modulus $E = 67.78\,\text{GPa}$, and Poisson's ratio $\nu = 0.33$) is selected in this study. The phononic crystal plate has air holes of $d = 2\,\text{mm}$ with a lattice parameter of $a = 8\,\text{mm}$. Figure 3.8(a) shows the dispersion relation of the phononic crystal plate for a wave vector along symmetry directions of the irreducible and extended Brillouin zone [80, 86]. The dispersion curve was calculated by using the FEM. Because there are many coupled wave modes in

dispersion curves of a phononic crystal, it is difficult to select the wave modes that have shear dominant motions resembling the homogeneous plate. Note that displacements of two SH wave modes in the homogeneous plate are given in Figure 3.6(b). When SH guided elastic waves propagating in the *x* direction are considered, the dominant displacement component is u_y (the displacement in the *y* direction). From the band folding of phononic crystals and the displacement field distributions of mode shapes [18, 87, 88], the wave mode exhibits the dominant motions in the *y* direction can found. They are denoted by Point A ($k_x = 777.3\text{rad/m}$) and B ($k_x = 411.9\text{rad/m}$) in the dispersion curves. And their displacement field distributions of a unit cell of the phononic crystal are plotted in Figure 3.8(b). From the similarities between the displacement mode shapes of the homogeneous plate and those of the phononic crystal plate, it can be found that the incident SH0 and SH1 modes from the homogeneous plate can excite the selected modes of the wave in the phononic crystal located at Points A and B in Figure 3.8(a).

Next, directions of the group velocity and their spatial dispersion are examined for the selected modes in a phononic crystal plate. To do this, the EFC's for the SH0 and SH1 wave modes at the frequency of 357 kHz are analyzed. When the wave is incident upon the phononic crystal plate with an oblique angle, the refracted wave which has the same tangential component of the wavenumber, k_y in this situation, with an incident homogeneous medium is excited due to conservation of momentum [45, 80, 86]. Since the geometry of the EFC for the SH0 wave is quite different compared to that for the SH1 wave, the refraction angles of the two wave modes are correspondingly different; it is expected that the successful mode separation can be

achieved by the selected phononic crystal plate.

To separate the incident waves through the phononic crystal plate, the refraction angles should be as different as possible. To this end, one should consider possible incident angles using the EFC's of the homogeneous and phononic crystal plates shown in Figure 3.9(a). We evaluate the angles of refraction (θ_r) for the incident SH0 and SH1 mode waves of the uniform plate by using the EFC of the PC plate in the first (irreducible) Brillouin zone and that in the second zone, respectively. The refraction angles of refracted waves for varying angles of incidence, θ_i, are presented in Figure 3.9(b). As shown in the profiles of the refraction angles, the difference between the refraction angle (θ_r^0) for the incident SH0 wave and the refraction angle (θ_r^1) for the incident SH1 wave is increased as θ_i is increased. Instead, the spatial dispersion effect, which is related to the changes in the direction of the group velocity, becomes stronger at the large angle of incidence. From the consideration of the difference in the refraction angle and the spatial dispersion effect, we select an angle of incidence equal to 8.00° for which the refraction angles are $\theta_r^0 = 21.43^\circ$ and $\theta_r^1 = -0.67^\circ$ for SH0 and SH1 wave, respectively.

3.3.3 Numerical and experimental demonstration of mode separation

Here, the mode separation in the phononic crystal plate is demonstrated. To do this, the guided wave propagation in the phononic crystal plate is studied by numerical

harmonic simulations and ultrasonic experiments.

Let us discuss about numerical demonstration. We constructed the phononic crystal plate which has 20 air holes in the *x* (or ΓK) direction, and 10 air holes in the *y* direction in the middle of a homogeneous aluminum plate. Then, the SH wave are generated by the source which is placed 50 mm away from the origin of the coordinate system and 8° aligned from the normal to the interface. For a clear demonstration, the selective shear source is used to generate an each wave mode, SH0 and SH1 wave, respectively. Figure 3.10 shows the results of the harmonic analysis by three-dimensional finite element method. Amplitudes of the shear stress are plotted in Figure 3.10 (a) and (b) for incident SH0 and SH1 wave mode, respectively. For incident SH0 mode, guided wave is refracted with a large positive angle and exits the phononic crystal plate at a large *y* value. On the contrary, the refracted SH1 wave propagates along the same direction with the incident wave maintain its waveform. From the results of the numerical simulations, it is shown that the refraction angle strongly depends on the wave mode of incidence as expected by the dispersion relation.

Next, ultrasonic experiments are conducted as shown in Figure 3.11(a) for mode separation of guided waves. The phononic crystal having a air holes arrange in triangular lattice are fabricated in an aluminum plate: 20 air holes in the *x* (or ΓK) direction, and 15 air holes in the *y* direction. For shear wave generation in a plate, we employed the Planar Solenoid Array-type Orientation-Adjustable Patch type Magnetostrictive Transducer (PSA-OPMT) [19, 49], shown in Figure 3.11(b). PSA-OPMT consists of a rectangular magnetostrictive patch, permanent magnets, and a

Planar Solenoid Array (PSA). The patch is subjected to both the static bias field by the magnets and the dynamic field induced by a current flowing into the PSA. To generate guided SH waves, the applied dynamic magnetic field should be perpendicular to the static magnetic field [89]. If PSA is employed in composing a magnetostrictive patch transducer, one can adjust the distance between planar solenoids to improve the directivity and wavelength tuning of the generated guided wave. In this mode separation experiment, the distance between planar solenoids is adjusted to be half the sum of the wave wavelengths of the two modes in order to generate the two wave modes of equal power. For a wave measurement, we design a magnetostrictive transducer using a single-line meander coil shown in the lower panel of Figure 3.11(b).

A Gaussian wave pulse of 357 kHz was inputted to the PSA-OPMT, resulting both the SH0 and SH1 waves were generated in the PC plate. After propagating through the phononic crystals, the guided SH0 and SH1 wave modes exit to the homogeneous aluminum plate. The shear wave is measured along line $1-1'$ and $2-2'$, respectively. The inputted Gaussian pulse was amplified by a RAM-5000 power amplifier (Ritex Inc., Warwich, RI) and measured signals, by SR560 low-noise pre-amplifier (Stanford Research Systems, Sunnyvale, CA). Measurements are made at 25 points for each measurement line. Figure 3.12 shows the spatiotemporal distributions of the squared magnitudes of the 357 kHz components of the processed signals. As shown in Figure 3.12, experimental results show that guided SH waves are separated by the phononic crystal plate. This is confirmed by calculating the group velocities of peaks: The calculated group velocities of each peak in Figure 3.12 were 2847.72 m/s and 1411.83 m/s respectively. From the

theoretical dispersion relation of an aluminum plate with thickness of 5 mm, the group velocities of SH0 and SH1 wave modes are equal to 3111.73 m/s and 1524.72 m/s at 357 kHz respectively. Despite the discrepancy in group velocities, it is shown that the faster peak for the larger *y* value corresponds to the SH0 wave mode; the other peak is the SH1 wave mode. Also, the experimental traveling times (τ_{ex}) from the transmitter to the line $1-1'$ are compared with the theoretical values (τ_{th}): $\tau_{th}=104.60\,\mu$s and $\tau_{ex}=96.23\,\mu$s for the SH0 mode and $\tau_{th}=160.77\,\mu$s and $\tau_{ex}=164.83\,\mu$s for the SH1 mode, which are in good agreement. Finally, the experimental separation distance between two SH waves, 7.79*a*, is also agreed well with the estimated distance, 8.09*a*. (*a*: the triangular lattice parameter)

For weak peaks follows the SH0 and SH1 wave mode marked by circles in Figure 3.12, the following anlaysis is made. It is shown that the peaks A and C can be attributed to reflections between the phononic crystal slab. It appears about $150\,\mu$s later than the SH0 waves and this time delay agrees with the predicted time $146.7\,\mu$s, which is calculated with the size of the PC slab equal to 20*a* and the wave propagating speed of the SH0 mode in the PC plate equal to 2181.3 m/s. The peaks B and D are the waves reflected from the side edge of a homogeneous plate since the wave measured along $2-2'$ was measured at the earlier time than that along $1-1'$ with the relatively strong magnitude.

3.4 Concluding remarks

In this chapter, the dispersion engineering in the wavenumber domain was studied. To manipulate the propagation direction of elastic waves for the self-collimation in two-dimensional phononic crystals, the lattice parameters of phononic crystal are engineered through the proposed dispersion engineering method. Based on results of the dispersion engineering in two-dimensional case, the proper lattice parameters of phononic crystals can be selected for mode separation of multiple wave modes in an elastic waveguide. The phononic crystal plate was determined by considering the propagation direction and the spatial dispersion effect. The ability of phononic crystals to control the propagation direction of multiple guided modes was confirmed by numerical simulations and ultrasonic experiments. The investigation presented in this chapter was published in the international journal in 2011 [90].

Table 3.1 The lattice parameters of designed phononic crystals for different self-collimation angle θ_{ref}^{*}.

θ_{ref}^{*} (degrees)	$\lvert\mathbf{d}_1\rvert$ (mm)	$\lvert\mathbf{d}_2\rvert$ (mm)	α (degrees)	r (mm)
10	2.314	1.927	21.293	0.283
20	2.134	1.892	24.506	0.273
30	3.373	3.891	80.583	0.680
40	1.315	3.643	90.000	0.399

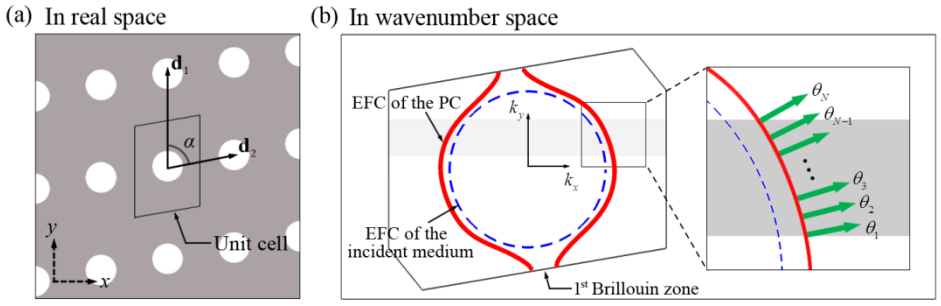

Figure 3.1 (a) Schematic of a two-dimensional phononic crystal consisting of air holes arranged with a parallelogram lattice in an aluminum matrix. (b) Equi-Frequency Contour (EFC) at the target frequency in the irreducible Brilluin zone. Solid line denotes EFC of the phononic crystal and dashed line, of the homogeneous medium. In dispersion engineering for the self-collimation effect, a direction of group velocity which is normal to EFC's is considered.

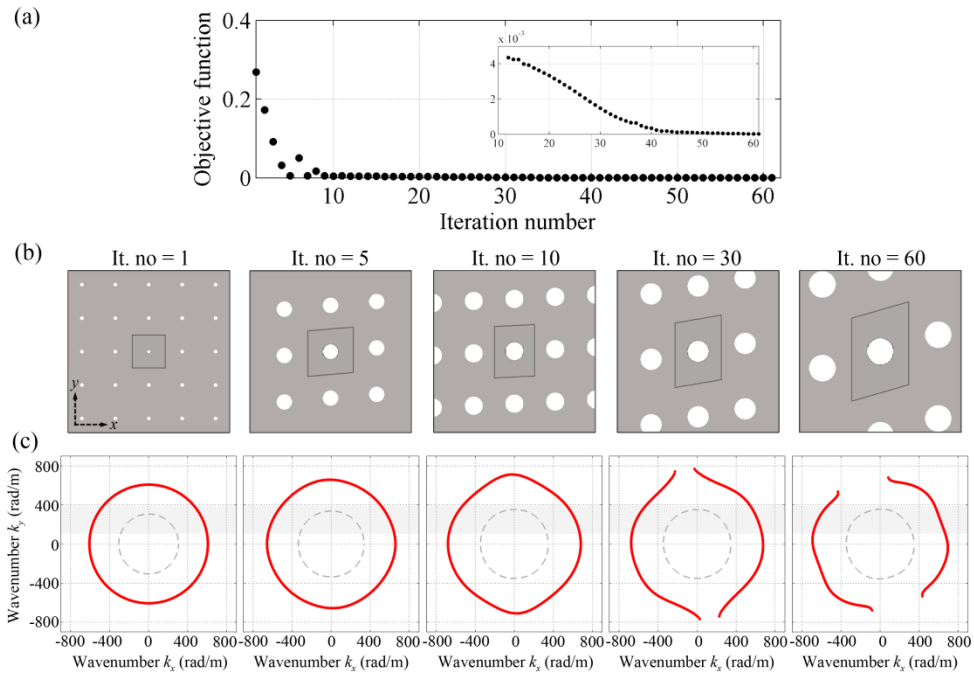

Figure 3.2 (a) Iteration history of the objective function in dispersion engineering. (b) Schematics of parallelogram phononic crystals for iteration number of 1, 5, 10, 30, and 60. (c) The corresponding EFC's at the target frequency. Solid red lines denote the EFC for the transverse wave mode.

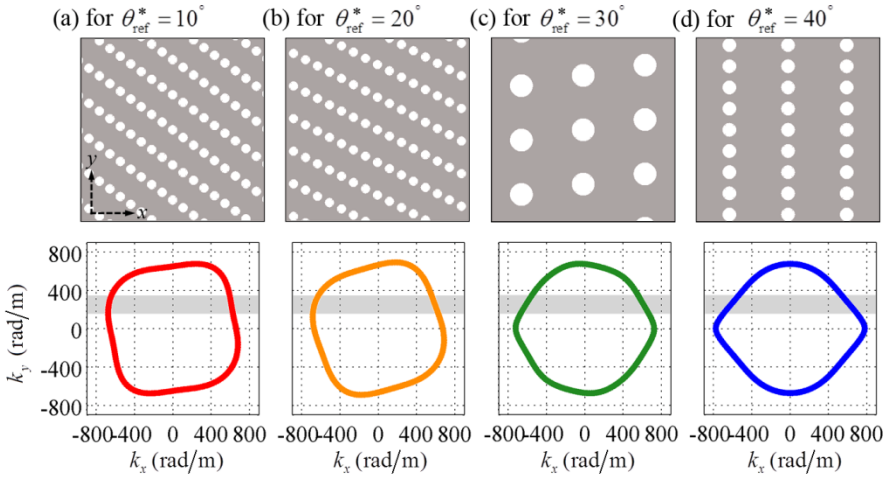

Figure 3.3 The engineered phononic crystals and the corresponding EFC's for (a) the given propagation direction θ_{ref}^{*} of 10°, (b) 20°, (c) 30°, and (d) 40°.

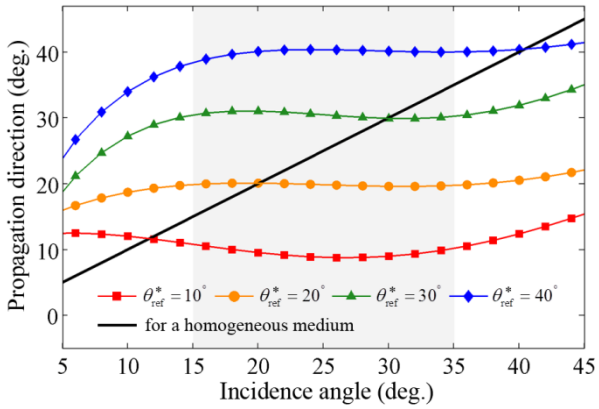

Figure 3.4 The variations of the propagation direction in the engineered phononic crystals as a function of incident angle from a homogeneous medium.

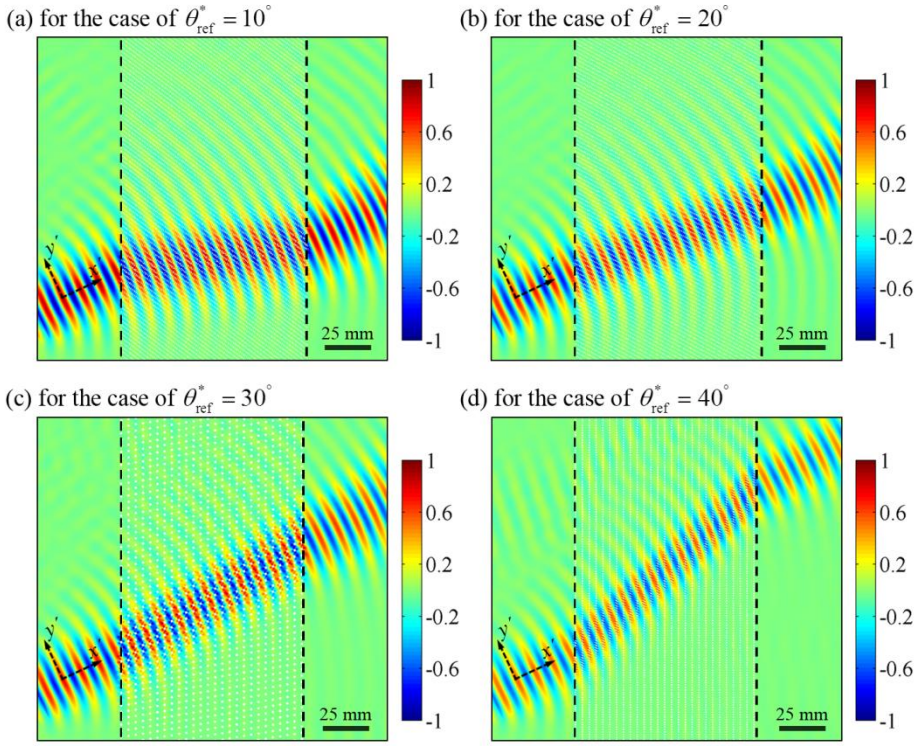

Figure 3.5 The distributions of a shear stress calculated by harmonic simulations of 300 kHz. The transverse wave is inputted to the different phononic crystal structures of (a) $\theta^*_{ref} = 10^\circ$, (b) 20°, (c) 30°, and (d) 40°, respectively.

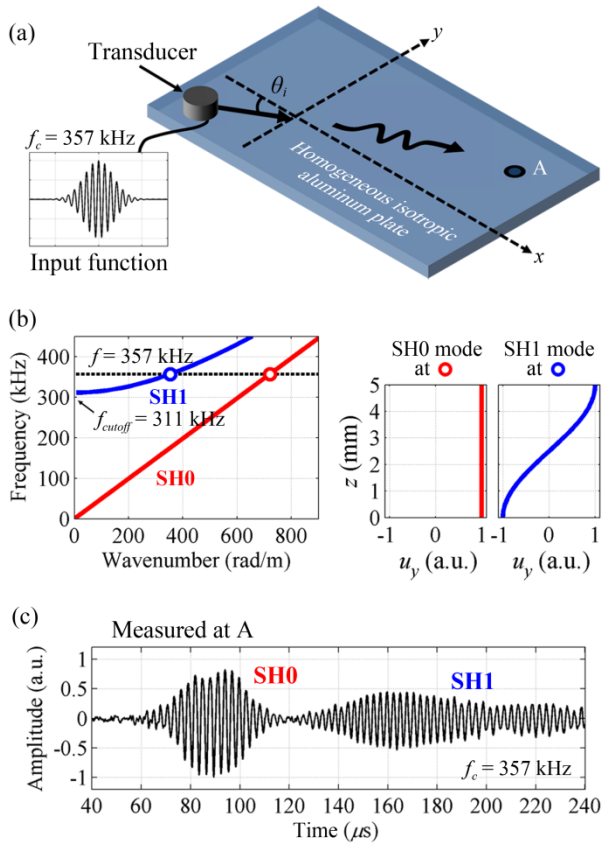

Figure 3.6 (a) Illustration of a guided-wave experiment in an isotropic homogenous uniform plate. A Garbor pulse (a modulated Gaussian pulse) centered at 357 kHz is inputted from the transducer. (b) The dispersion relation of the shear-horizontal guided wave in an aluminum plate of 5mm in thickness. The distributions of the *y*-displacements along the plate thickness direction are also shown. (c) The measured signal at Point A showing that two wave modes corresponding to two circles in the dispersion curves are generated upon the single-frequency excitation.

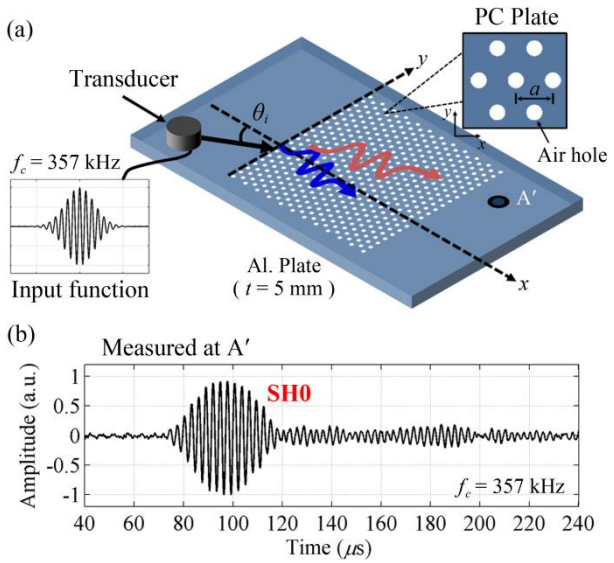

Figure 3.7 (a) Illustration of the same experiment as in Figure 3.6 on an aluminum plate of 5 mm in thickness with a PC inserted in the middle. (b) The measured signal at Point A′ upon the same pulse input as used in the experiment for Figure 3.6, showing the propagation of a single mode. The inserted PC serves to separate two propagating modes.

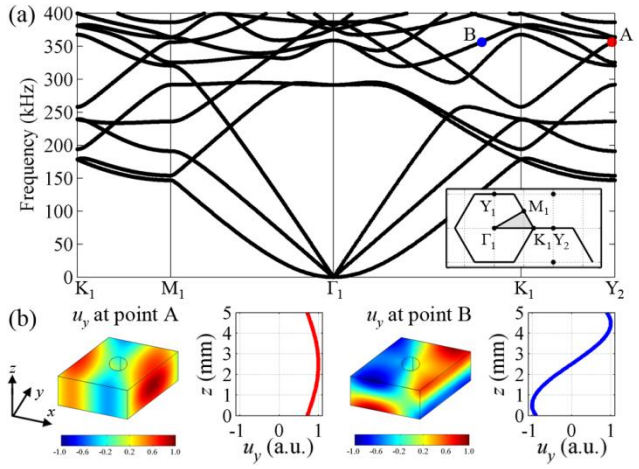

Figure 3.8 (a) Dispersion relation of the aluminum phononic crystal plate of 5 mm in thickness with air holes. It is plotted mainly on the irreducible and extended Brillouin zone of the triangular lattice. (b) The distribution of the *y*-displacement component of the eigenmode at Point A and B in Figure 3.8(a). (the wave is assumed to propagate in the *x* direction)

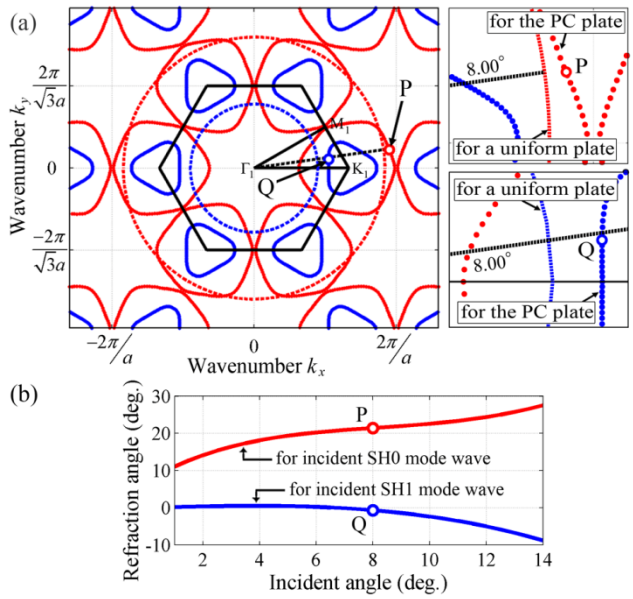

Figure 3.9 (a) EFC's for the SH0 (red) and SH1 mode (blue) in the first and second Brillouin zone of the triangular phononic crystal palte where the pentagon enclosed by the black lines represents the first irreducible Brillouin zone. The dotted circles represent the EFC's of the uniform plate, where the red and blue lines correspond to the SH0 and SH1 mode, respectively. (b) The variations of the refraction angles in the phononic crystal for incident SH0 (red) and SH1 (blue) waves from the uniform plate.

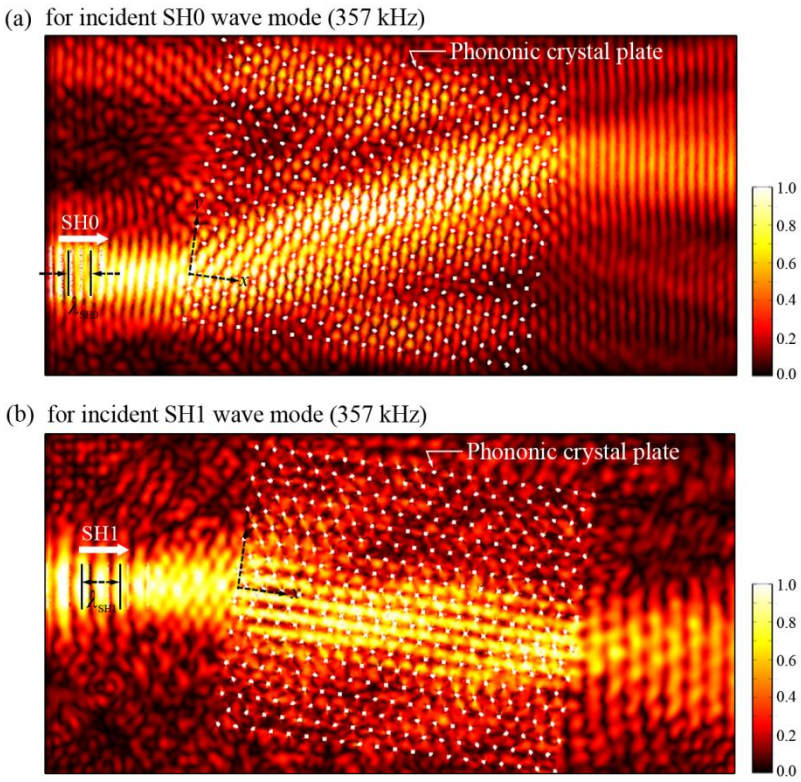

Figure 3.10 Results of numerical wave simulations for (a) incident SH0 and (b) incident SH1 waves, respectively. The in-plane SH wave is refracted in the phononic crystal plate depending on the incident wave mode.

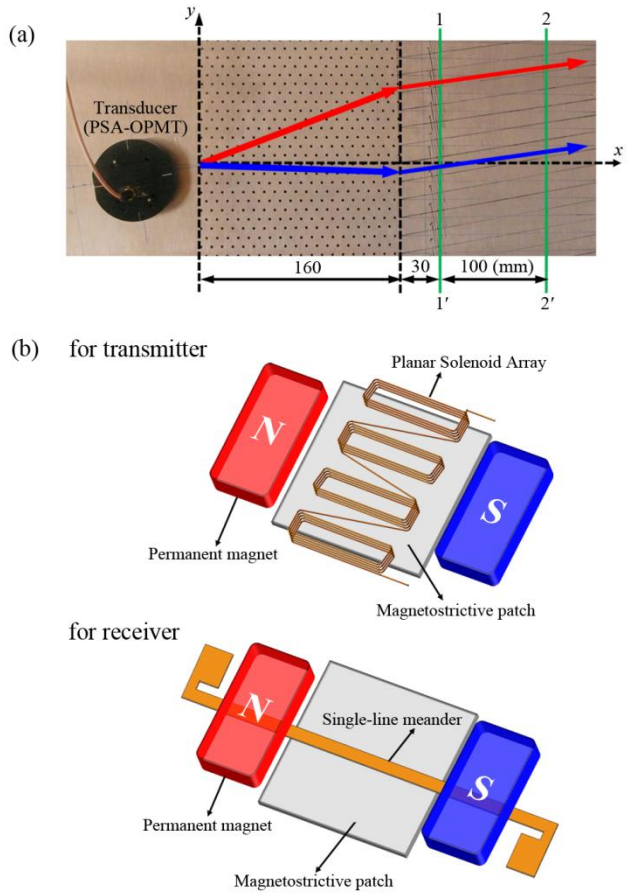

Figure 3.11 (a) Photo of the experimental setup for the mode separation of a single-frequency bi-modal SH wave into two modes by using a phononic crystal plate. (b) Illustration of the Planar Solenoid Array-type Orientation-Adjustable Patch type Magnetostrictive Transducer (PSA-OPMT) for transmitter (upper) and a magnetostrictive patch transducer having a single-line meander for receiver (lower).

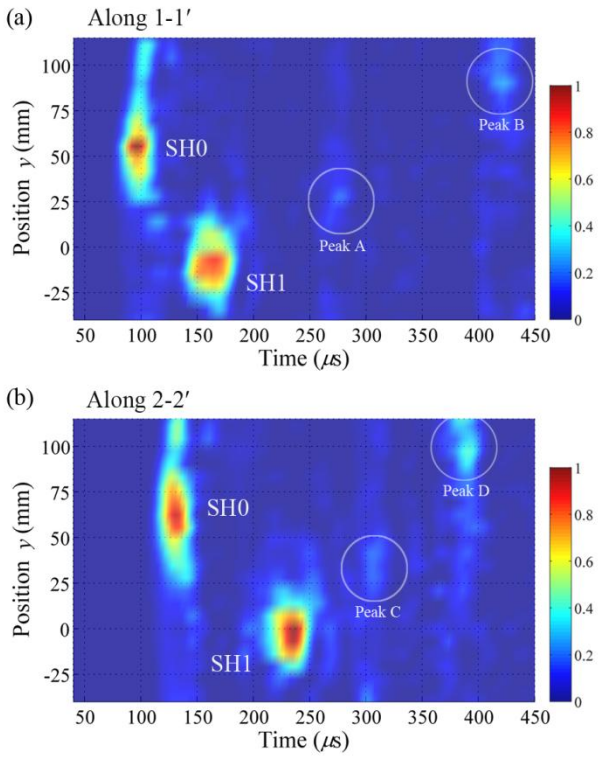

Figure 3.12 The spatiotemporal distributions of the squared magnitudes of the 357 kHz frequency component of the signals measured (a) along the $1-1'$ and (b) $2-2'$ lines.

CHAPTER 4

DISPERSION ENGINEERING IN FREQUENCY DOMAIN BY PHONONINC CRYSTALS

4.1 Overview

In the preceding chapter, we employed phononic crystals to spatially separate multiple wave modes in an elastic waveguide. The dispersion relation in the wavenumber domain was focused on and the propagation direction was manipulated by phononic crystals. In this chapter, we use phononic crystals to suppress an excitation of an undesired wave mode and the group velocity dispersion of a target guided mode. In particular, the forbidden band gap and dispersion engineering in the frequency domain are investigated. As a target application in this chapter, an ultrasonic waveguide transducer [91-96] is considered; see schemataic of waveguide transducer in Figure 4.1(a). This type of transducer has been developed to evaluate a test structure where the active transducer element, piezoelectric or magnetostrictive materials, cannot be directly installed. For example, when a temperature of a test structure is higher than the Curie temperature, the poling direction of piezoelectric material is broken. For this reason, the transducers consist of piezoelectric materials cannot work at high temperature environments. Also, the structure under the opaque fluids cannot be evaluated with the typical transducers. In this situation, the waveguide has been used as the buffer.

As mentioned earlier, however, multi-mode waves are inevitable generated in a waveguide and they are distorted by the dispersive nature as shown in Figure 4.1(c). To overcome the signal distortion through a waveguide, we aim to tailor the dispersion relation of a waveguide by employing phononic crystals in this chapter.

As we use the band gap phenomena and dispersion tailoring of the phononic crystals, earlier works applying photonic or phononic crystals to the problems similar to the present one is reviewed. First, it was reported that the forbidden band gap for the guided Lamb waves can be opened by the periodic structures in a waveguide. In Refs. [97-99], the acoustic waveguides have been investigated to study the effect of the periodic free boundaries on band gap phenomena. Also, it was presented that the band gap of guided waves were affected by the scatterers in waveguides [100-102]. Next, regarding the dispersion tailoring, the guided mode in a line-defect of photonic/phononic crystals was also tailored in Refs. [88, 103, 104, 105]. As mentioned in Chapter 1, electromagnetic waves can confined within a line-defect of the photonic band gap, which shows the strong dispersive behavior. To reduce the dispersion effect of this type of guided mode, inclusions nearby the line-defect was tailored [103-105]. As a result of the change in the structure, the band structures of the waveguide modes in photonic band gap have been adjusted, leading to suppression of the dispersion effect. Based on these earlier researches, we propose waveguide transducers that have phononic crystals in the middle of the waveguide and present the engineering method for unit structure of phononic crystals.

The objectives of this chapter are different for each wave mode: (1) to minimize the

transmission of an undesired wave mode and (2) to suppress the dispersion effect of a target wave mode. To achieve this, the dispersion relation of a target wave mode is adjusted to minimize its dispersion effect, while an undesired wave mode is suppressed by opening the band gap of a phononic crystal. To find the proper phononic crystal structures satisfying the design objectives, we employ a size optimization method which is formulated by the dispersion relation in the frequency domain. Through the proposed optimization method, phononic crystals which satisfy multiple objectives can be realized and a validity of the proposed waveguide structure is confirmed by time-transient numerical simulation and ultrasonic experiments.

In Section 4.2, we will discuss about the group velocity dispersion in a homogeneous elastic waveguide. We experimentally measure transmitted signals at different frequencies. By analyzing the signals with the dispersion relation, the wave distortion issues in a waveguide can be clarified. Then, an effect of two-dimensional phononic crystal on the dispersion effect is also studied. It will be presented that the group velocity dispersion is clearly appeared as the frequency approaches the band gap of phononic crystals. Because we apply the phononic crystal to a waveguide, these preliminary studies are helpful to understand propagation behavior in phononic crystals. Next, in Section 4.3, we design the phononic crystal waveguide to resolve the wave distortion in a waveguide. A size optimization method for sizes of inclusions and the periodicity of phononic crystal structures is proposed. After detailed design procedure is described, the validity of the designed phononic crystal structure is confirmed by the numerical analysis. Finally, results of ultrasonic experiments in a proposed waveguide will be discussed.

4.2 Group velocity dispersion in an elastic waveguide

To give a motivation of this study, the signal distortion of a guided wave will be described with results of ultrasonic experiments in a waveguide. We show measured signals of different frequencies and analyze them by using the dispersion relation. It is shown that the guided wave is distorted due to the multi-mode generation and the group velocity dispersion. The distortion of the guided wave is a main issue in this study, which is suppressed by employing phononic crystals. For this reason, the wave propagation in two-dimensional phononic crystal is also investigated to show the effect of its periodic structure on the group velocity dispersion. Phononic crystals of different structures are considered and their dispersion relations in the wavenumber and the frequency domains will be investigated. Then, we present the elastic waves are broadened in time and space depending on the structure of a phononic crystal.

4.2.1 Group velocity dispersion of ultrasonic waves in a waveguide

To show the distortion of the guided waves, we conduct ultrasonic experiments in an aluminum strip of 40 mm in thickness. The pitch-catch experiments using two magnetostrictive patch transducers are carried out. Figure 4.2(a) shows the dispersion curves for in-plane wave modes of the aluminum strip. Among the various guided wave modes, the wave modes having a dominant motion in the *y* direction are considered in this experiment; the wave modes of interest are denoted by Mode A and B in Figure 4.2(a). Note that detailed information of the wave modes is given in Section 4.3.

In Figure 4.2(b), the measured signals are given for the different frequencies: the center frequencies of an inputted Gaussian pulse are 100, 150, 200, and 300 kHz, respectively. In each signal, wave pulses are identified by comparing its traveling time from the transmitter with theoretical values. For example, at 150 kHz, the group velocity of Mode A and B are 2899.97 and 2498.85 m/s calculated from the dispersion curve. As the distance between the transmitter and receiver is 800 mm, the corresponding traveling times are 275.87 and 320.15 μs for Mode A and B, respectively. The experimental values of a traveling time are 286.5 and 350.9 μs, which is obtained by the Hilbert transform of the measured signal. As can be seen in Figure 4.2(b), at 150 and 200 kHz, two wave modes are simultaneously excited and Mode B is broadened due to the group velocity dispersion at 150 kHz. Since the group velocity is defined as the gradient of frequency with respect to the wavenumber, this fact can be checked by the dispersion curve of Mode B; a slope of the dispersion curve of Mode B is changed as the frequency is changed, while that of Mode A is almost linear over the frequency band of interest.

To avoid this distortion, many studies are focused on the frequency ranges where a single non-dispersive wave can be excited; when a pulse is excited at low or high frequency range, the wave distortion can be avoided because the dispersion curves approache that of the bulk waves at these frequency ranges [93, 95]. In these frequencies, the wavelengths are considerably long or short compared to the thickness of waveguide. However, depending on the thickness of a waveguide, there are the additional issues in the ultrasonic waveguide transducer application. First, the waveguides having a wide thickness require longer buffer length to satisfy the necessary temperature level [95]. It restricts the overall size of the waveguide

transducers in the situation where the compact waveguide transducers are needed. Inversely, though the waveguides having an extremely small thickness exhibit the dispersion-free propagation, they cannot support the sufficient power to test structures with only one waveguide [93]. Here, we employ the phononic crystal to overcome the wave distortion in the waveguides. In the following subsection, the an effect of phononic crystals on the group velocity dispersion is discussed by considering elastic waves in two-dimensional phononic crystals.

4.2.2 Dispersion effect in two-dimensional phononic crystals

In Section 3.2, we discussed that wave in phononic crystals can propagate without the dispersion in space, which is called the self-collimation effect. To analyze and manipulate this phenomenon, the dispersion relation in the wavenumber domain, EFC, is considered. In this subsection, we address the dispersion relation in the frequency domain and discuss the group velocity dispersion of two-dimensional phononic crystals. We consider a homogeneous medium and three different phononic crystals as shown in Figure 4.3(a). The phononic crystals consist of air holes arranged with a rectangular lattice in an aluminum: a lattice parameter and a diameter of air holes are $1.813\,\mathrm{mm}$ and $0.895\,\mathrm{mm}$ for PC1; $2.305\,\mathrm{mm}$ and $1.334\,\mathrm{mm}$ for PC2; $2.918\,\mathrm{mm}$ and $1.783\,\mathrm{mm}$ for PC3, respectively. The $\Gamma\mathrm{M}$ direction of the rectangular lattice is aligned along the x direction.

Figure 4.3(b) show the dispersion relation in the frequency domain for the quasi-transverse wave mode. The dispersion curve of a homogeneous aluminum,

presented by solid black line, is straight line, which means the group velocity is constant regardless of the frequency. For phononic crystals, as the lattice parameter and the diameter of air holes are increased ($\mathrm{PC1} \rightarrow \mathrm{PC3}$), the band gap frequency is decreased; this leads to the strong dispersion effect at the target frequency of 300 kHz. One can find that the curvature of dispersion curve of PC3 has the maximum value. On the contrary, PC3 exhibits the smallest spatial dispersion as can be seen in an EFC of Figure 4.3(c). This fact can be checked by the refraction angles shown in Figure 4.3(d).

To show propagation behavior of elastic waves in phononic crystals, we conduct time-transient analysis with phononic crystal samples of 15λ in the *x* direction and 10λ in the *y* direction ($\lambda = 10.37\,\mathrm{mm}$: the wavelength of transverse wave at 300 kHz). A 2λ -wide shear source is located apart from the left side of the phononic crystal sample. The Gaussian pulse $\exp(-t^2 / 2\sigma^2)\cos(2\pi f_c t)$ as a function of time *t* was inputted to the source, where σ of 1.0 and f_c of 300 kHz are used as the standard deviation of the Gaussian pulse and the center frequency, respectively. The spatiotemporal distributions of *y* displacements measured along the exit side of phononic crystal samples are presented in Figure 4.3(a). The inputted Gaussian wave pulse undergoes the dispersion in time and space as propagates through the phononic crystal structure. As the lattice parameter and the diameter of air holes are increased ($\mathrm{PC1} \rightarrow \mathrm{PC3}$), the spatial dispersion is reduced while the temporal dispersion is increased; see Figure 4.4(b) and (c) for their dispersion relation in the frequency and the wavenumber domains. From these results, it is shown that phononic crystals can affect the dispersion of elastic waves in time as well as in

space. In the following section, phononic crystal structures are applied to manipulate the dispersion in time domain for the waveguide transducer application.

4.3 Dispersion engineering for ultrasonic waveguide transducer

In this section, we present the dispersion engineering of the waveguide by employing phononic crystals. For the ultrasonic waveguide transducer application shown in Figure 4.1(a), the single-mode dispersion-free wave excitation would be preferred for their practical uses. As mentioned earlier, however, multi-mode waves are inevitable generated and they are distorted by their dispersive nature. This fact can be seen in Figure 4.1(c) which presents time signals inputted to the elastic waveguide and measured after propagating through the waveguide; the inputted Gaussian pulse is separated into multiple wave modes and broadened because of the group velocity dispersion. The goal of this section is to solve two issues in the elastic wave propagation through ultrasonic waveguide transducers: (1) multiple wave mode excitations, (2) group velocity dispersion. To this end, the dispersion relation of phononic crystal waveguide is tailored to open the band gap of an undesired wave mode and to minimize a difference in group velocities of a desired wave mode in a target frequency range.

We suggest a size optimization method to design the phononic crystal structures in a waveguide transducer. By properly tuning the phononic crystal unit, the periodicity of the unit, a number of inclusions, and their sizes, we can realize the desired phononic crystal waveguide. The effectiveness of phononic crystals in elastic waveguides was confirmed by numerical time-transient analysis and ultrasonic experiments with the magnetostrictive patch transducers. It is shown that the transmission of an unwanted mode was successfully suppressed and also a target mode propagates with relatively small dispersion effect in the engineered phononic

crystal based waveguide.

4.3.1 Design of phononic crystal-based waveguide structures

The chosen waveguide is an aluminum strip (density $\rho = 2631.4\,\mathrm{kg/m^3}$, Young's modulus $E = 67.78\,\mathrm{GPa}$, and Poisson's ratio $\nu = 0.33$) having a rectangular profile in the *y*-*z* plane, the width in the *y*-direction is 30 mm and the thickness in the *z*-direction is 3.15 mm (the wave propagation direction is the *x*-direction). The dispersion curves of the considered waveguide are plotted in Figure 4.1(b). Among various guided wave modes, the shear dominant wave modes are focused in this work; the fundamental and second order shear dominant wave modes are highlighted. In the dispersion curve, gray solid lines represent the results by the three-dimensional waveguide while dashed lines, by the two-dimensional waveguide with the plane-stress condition. They are agreed well with each other because the thickness in the *z*-direction is relatively thin. When the center frequency of the excitation pulse f_c is 200 kHz, two wave modes of interest are simultaneously excited as shown in the right panel of Figure 4.1(c). Each peak is identified with its traveling time, dispersive nature; the first arrived peak corresponds to the fundamental shear dominant wave mode while the following peak, to the second order shear dominant mode. The second order shear dominant mode is preferred for ultrasonic waveguide transducers application [106] since most shear energy is concentrated on the center of the waveguides; see the mode shapes of these wave modes in the inset of Figure 4.1(b). The second order shear dominant mode is considered as a target mode that is adjusted to minimize its dispersion

effect. On the contrary, the fundamental shear dominant mode is suppressed as an unwanted mode by opening the band gap of the phononic crystal.

The phononic crystal to be considered in this study is presented in Figure 4.5(a). In the waveguide unit, the circular air holes are equally placed in the *y*-direction, and this unit is arranged in the *x*-direction with a lattice parameter p_x. A number of air holes *N* is varied from 2 to 10 in this study. For each *N*, the air holes are symmetrically distributed about the plane of $y = 0$ to consider the symmetries of the wave modes of interest. To find the waveguide unit exhibiting the desired band structure, diameters d_i of air holes, and the periodicity p_x in the *x*-direction, are carefully tuned with an optimization procedure. The optimization problem is formulated with an objective function and constraints that are defined with the dispersion relation of the phononic crystal based waveguides. First, to reduce the transmission of the unwanted mode, the band gap of the phononic crystal based waveguide is so tuned that can be larger than the target frequency range, Δf. To do this, the 1st and 3rd frequencies at the edge of the first Brillouin zone, f_{X}^1 and f_{X}^3, are constrained to move out of the target frequency range denoted by the gray shading in Figure 4.5(b). Second, to minimize the dispersion effect of the target mode, the square norm of the group velocity dispersion parameter, $\|\beta\|$, in the target frequency range is considered as the objective function to be minimized; see Refs. [103-105] for use of β in dispersion engineering. The group velocity dispersion parameter $\beta \equiv \partial^2 k_x / \partial \omega^2$ is the second derivative of the wavenumber k_x with respect to the angular frequency ω. Note that the curvature of the

dispersion curve β was evaluated at every 1 kHz for a frequency range Δf. A square norm of β values was minimized to reduce dispersion effect. The shape optimization problem of phononic crystal waveguide can be summarized by

$$\begin{aligned} &\min_{d_i,\, p_x} \|\beta\| \\ &\text{subject to } f_X^1 < \underline{f},\ f_X^3 > \overline{f}, \end{aligned} \tag{4.1}$$

where $\underline{f}$ and $\overline{f}$ are the lower and upper bound of Δf. As the dispersion parameter $\|\beta\|$ is minimized, one can make the band structure flat in the target frequency range resulting the group velocities are almost constant, i.e. non-dispersive.

Figure 4.5(b) shows the band structure of the nominal phononic crystal based waveguide. The dispersion curve is calculated by using finite element analysis software COMSOL multiphysics. The shading in the frequency range from 175 to 225 kHz is represented the target frequency range, Δf, which is considered with the spectral width of the Gaussian pulse which is centered at 200 kHz and has $21.459\,\mu$s as the time spread. The phononic crystal based waveguide units having different numbers *N* of air holes, from 2 to 10, are designed in this work. Depending on *N* in the waveguide unit, the periodicity in the *y*-direction, p_y, and an allowable diameter of air holes are determined. Figure 4.6(a) shows the designed phononic crystal based waveguide units. Their group velocity dispersion parameters $\|\beta\|$ of the target mode and frequencies at the edge of the first Brillouin zone are presented in Figure 4.6(b) and (c), respectively. Phononic crystal based waveguide units for $N \geq 7$ exhibit the considerably reduced the dispersion effect of the target mode and

a sufficient frequency range of the band gap compared with the target frequency range. The periodicities and diameters for the designed phononic crystal waveguide for different numbers of inclusions are summarized in Table 4.1.

4.3.2 Numerical analysis of phononic crystal-based waveguides

For demonstration, the waveguide unit of $N=8$ is selected by considering the performance in terms of $\|\beta\|$ and $f_{\mathrm{X}}^{3}-f_{\mathrm{X}}^{1}$ among the designed waveguides. Figure 4.7 shows the dispersion curves of the selected waveguide unit of $N=8$. It is shown that the value of $\|\beta\|$ is converged to 0.186 from its initial value of 1.0, that for a homogeneous waveguide, and the frequencies at the edge of the first Brillouin zone are 170.61 kHz and 225.09 kHz corresponding to the 1st and 3rd wave modes. Note that the frequencies for the nominal phononic crystal waveguide were $f_{\mathrm{X}}^{1}=177.76\,\mathrm{kHz}$ and $f_{\mathrm{X}}^{3}=191.45\,\mathrm{kHz}$ as shown in Figure 4.5(b).

Before numerical and experimental demonstrations are carried out, we examine mode shapes of the target wave mode in the phononic crystal waveguide. First, the modal distributions calculated by a two-dimensional model are compared with those by a three-dimensional model for the target mode and the undesired wave mode. Figure 4.8(a) shows the dispersion curves of elastic waves were calculated by a three-dimensional waveguide (3.15-mm thick, black) and by a two-dimensional waveguide (plane-stress condition, yellow). As shown in Figure 4.8(a), the dispersion curves by a two-dimensional waveguide with plane-stress condition agreed well with those by a three-dimensional waveguide. Also, the mode shapes

for the wave modes of interest, denoted by Points A and B in dispersion curves, were plotted in Figure 4.8(b) and (c), respectively. It is found that the displacement fields of the two dimensional waveguide in *x*-*y* plane have the same distribution with those of the three-dimensional waveguide and the displacement fields along the *z* direction were almost constant. And their mode shapes have similar distributions with the homogeneous waveguide which is depicted in the inset of Figure 4.1(b). This is why the target mode and the undesired wave mode are presented by blue and red circles in Figure 4.7. Also, it is checked that the wave mode between the undesired mode and the target mode are not the shear-dominant wave mode.

In addition, the mode shapes of higher branches are examined. Figure 4.9 shows the modal distributions at k_x = 400, 450, and 500 (rad/m). Since the branches at a high frequency are coupled with the folded branches above the first band gap, it is hard to characterize these wave modes. This fact can be confirmed by the modal distributions shown in Figure 4.9. Compared with the fundamental branch of the undesired wave mode (at the 1st frequency), its folded branch cannot be clearly found due to mode coupling at higher frequencies.

4.3.3 Demonstration of wave propagations in the engineered waveguide

For demonstrations, the elastic wave propagation in the engineered phononic crystal based waveguide is investigated by the full wave simulation and ultrasonic experiments. A schematic of the demonstration model is presented in Figure 4.10(a)

with the photography of the fabricated waveguide in Figure 4.10(b). The 123 engineered phononic crystal based waveguide unit ($N = 8$ case) are constructed over 750 mm in the *x* direction and a 15-mm-wide source generates the in-plane shear dominant wave. The modulated Gaussian pulse of the form $\exp(-t^2 / 2\sigma^2)\cos(2\pi f_c t)$, where σ is standard deviation of the Gaussian pulse and f_c is the center frequency of 200 kHz, was inputted to the source lines. In order to enhance the target wave mode the shear source consists of five elements with half wavelength spacing. In numerical simulations, a two-dimensional finite element model with the plane-stress condition is used and time-transient analysis is carried out in COMSOL multiphysics. The selected maximum element size and time step in the simulations are 0.879 mm and $0.2\,\mu$s, respectively, which satisfy the convergence criterion. In ultrasonic experiments, the patch-type magnetostrictive transducer [19, 49, 81] is employed to generate and detect the in-plane shear waves in the phononic crystal based waveguide. To delay the waves reflected at the left side, a buffer of sufficient length was made on the left side of a phononic crystal-based waveguide. We can focus on the transmitted waves in the numerical and experimental simulations.

Figure 4.11(a) show results of the time-transient analysis (the *y*-displacement fields in the engineered phononic crystal based waveguides). It is demonstrated that the wave distortion, transmission of the unwanted mode and the wave broadening due to the dispersion effect, are successfully suppressed in the engineered phononic crystal based waveguide. For comparison, the wave propagation in a homogeneous waveguide with the same excitation conditions as the phononic crystal-based

waveguide is examined. As shown in Figure 4.11(b), one can find the input signal undergoes the distortion as propagating through the homogeneous waveguide. Figure 4.11(c) shows the *y* displacement distributions at initial time steps. After the shear wave is generated by the source, wave pulses propagate in two opposite directions along the waveguide. One can find that the target wave mode propagating in positive *x* direction is transmitted to the phononic crystal waveguide while the undesired wave mode is totally reflected at the interface of the phononic crystal.

Next, ultrasonic experiments are conducted with the fabricated waveguide shown in Figure. 4.10(b). In experiments, before the Gaussian pulse is inputted to the transmitter, the pulse was amplified by a AG-1017L power amplifier (T&C Power Conversion Inc. Rochester, NY). The measured signal is also amplified by a SR 560 low-noise pre-amplifier (Stanford Research Systems, Sunnyvale, CA). The signals measured at the exit side of phononic crystal, $x = 785.18\,\mathrm{mm}$ are given in the upper panel of Figure 4.12(a). It is shown that the inputted shear wave is mainly transmitted through a single wave mode with the minimized dispersion effect. In the lower panel of Figure 4.12(a), the signal in a homogeneous waveguide is given. It shows that the target wave mode is broadened and the undesired wave is simultaneously generated. To identify the wave mode, the traveling time, τ, from the source to the measurement point were compared with the numerical results shown in Figure 4.12(b), the spatiotemporal distributions of *y*-displacements calculated in numerical simulations. They are in good agreement; $\tau_{num} = 396.40\,\mu\mathrm{s}$ and $\tau_{ex} = 383.14\,\mu\mathrm{s}$ are numerical, and experimental values of traveling time, respectively. Also, the temporal Full Width at Half Maximum (FWHM) of the target

wave pulse is calculated to compare the dispersion effect; FWHM is $22.20\,\mu s$ for the engineered phononic crystal based waveguide as indicated with arrows in the upper panel of Figure 4.12(b) while, $52.00\,\mu s$ in the homogeneous waveguide (the lower panel of Figure 4.12(b)).

The minor signals for the phononic crystal waveguide shown in the Figure 4.12(a) can be explained by excitations of the other wave modes. At the excitation frequency of 200 kHz, there are six wave modes in the dispersion relation shown in Figure 4.7. In consideration of their group velocities, the wave modes at $k_x = 162.91$ and $k_x = 169.85\,\mathrm{rad/m}$ may arrive after the target wave mode. The group velocities and traveling times which are calculated from the dispersion curves are summarized in Table 4.2. It is expected to reduce the excitation of these wave modes in future works.

4.4 Concluding remarks

Up to now, we presented that phononic crystals can be employed to manipulate the elastic waves in waveguides for ultrasonic waveguide transducer applications. To overcome multiple mode excitations and the wave broadening due to the group velocity dispersion, the dispersion relation in the frequency domain is tailored by employing phononic crystals. By properly tuning the phononic crystal unit, inclusion sizes and the periodicity of the unit, we can realize the phononic crystal waveguide that exhibits the desired wave properties. The effectiveness of phononic crystals in elastic waveguides was confirmed by numerical time-transient analysis and ultrasonic experiments with the magnetostrictive patch transducers. In the engineered phononic crystal-based waveguide, it was shown that the transmission of the unwanted mode was successfully suppressed and also the dispersion effect of the target mode was considerably reduced. Although the temperature gradient of the waveguide transducers was not considered in this work, the effect of the temperature on the dispersion relation of phononic crystal based waveguides [107, 108] can be further investigated to reflect realistic evaluation situations in the near future. The investigation presented in this chapter was published in the international journal in 2013 [109].

Table 4.1 The periodicities and diameters of the designed phononic crystal waveguide for different number *N* of inclusions. (Unit: mm)

N	p_x	p_y	d_1	d_2	d_3	d_4	d_5
2	6.391	14.700	1.675	N/A	N/A	N/A	N/A
3	6.168	9.600	1.644	2.784	N/A	N/A	N/A
4	6.040	7.100	1.860	2.444	N/A	N/A	N/A
5	5.917	5.700	2.060	2.750	2.037	N/A	N/A
6	5.677	4.700	2.081	2.816	2.230	N/A	N/A
7	5.968	4.000	1.554	2.226	2.496	1.679	N/A
8	6.053	3.500	1.529	1.572	2.446	1.744	N/A
9	5.958	3.100	1.397	1.268	2.351	1.839	1.238
10	5.119	2.800	2.035	1.681	2.359	1.523	0.025

Table 4.2 The group velocity v_g and traveling time τ_{th} from the source of the different guided modes at 200 kHz. (Highlight: the target wave mode)

k_x (rad/m)	162.91	169.85	260.12	265.09	305.05	436.69
v_g (m/s)	1727.01	1909.17	3067.62	4171.68	2191.81	1989.92
τ_{th} (μs)	454.65	411.22	255.96	188.22	358.23	394.58

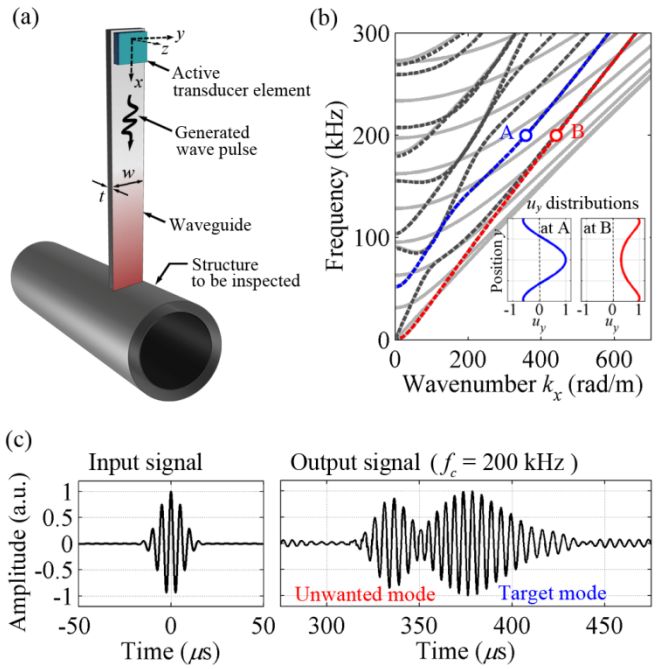

Figure 4.1 (a) Illustration of an ultrasonic waveguide transducer used to inspect high-temperature structures. (b) The dispersion relations of the elastic guided waves in a homogeneous waveguide of 30 mm in the width. The distributions of the *y*-displacement components of eigenmodes are also shown in the inset. (c) The input signal of a Gaussian pulse centered at 200 kHz (left panel) and measured signal of after propagating through the waveguide (right panel).

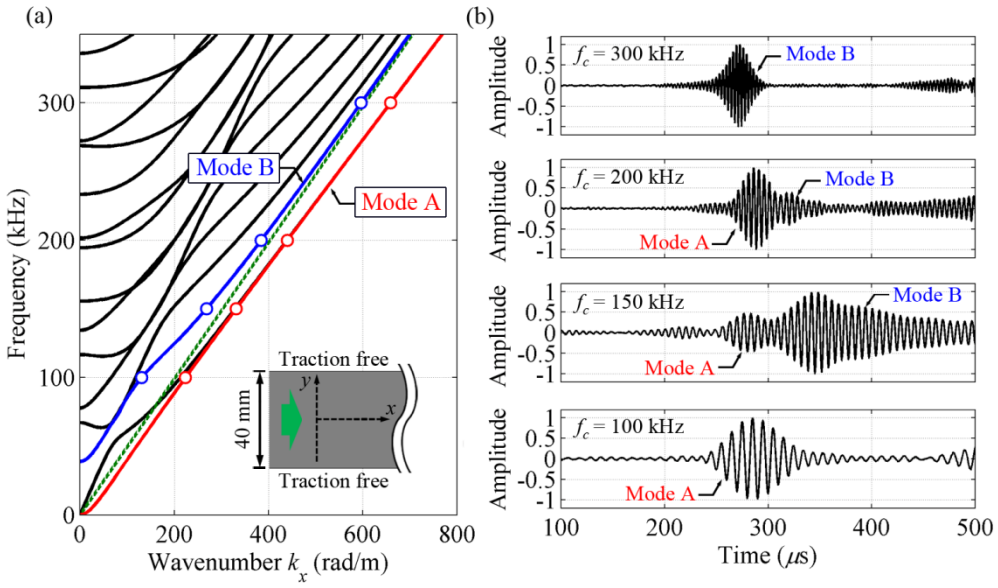

Figure 4.2 (a) Dispersion relation of an aluminum waveguide of 40 mm in the width. The fundamental and second order shear-dominant waves are denoted by Modes A and B, respectively. A dashed line represents a dispersion curve of shear-dominant waves in an infinite aluminum. (b) The measured signals in a waveguide which is excited with Gabor pulses centered at 100, 150, 200, and 300 kHz, respectively.

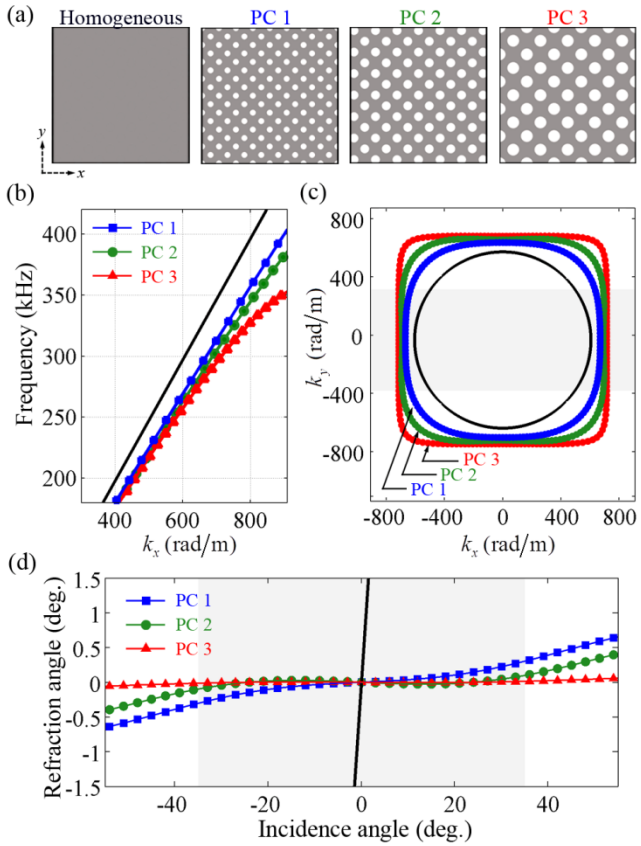

Figure 4.3 (a) Schematics of considered phononoic crystals having different lattice parameters. (b) The dispersion curves, (c) EFC's at 300 kHz, and (d) the refraction angle profile for phononic crystals.

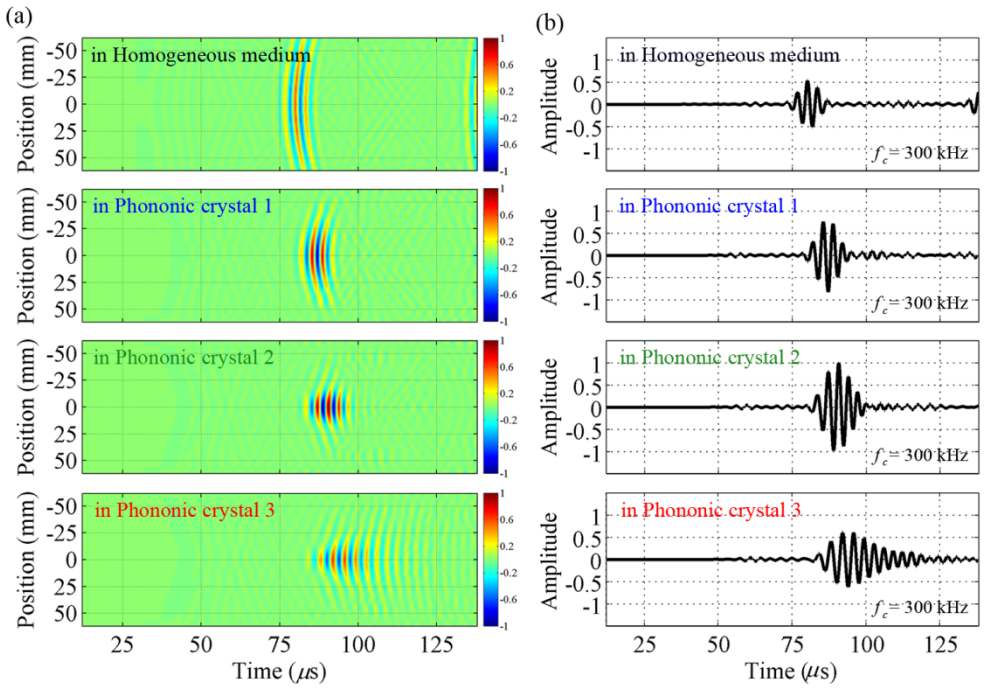

Figure 4.4 (a) The spatiotemporal distributions of the *y* displacement that calculated by numerical time-transient analysis in a homogeneous medium and three different phononic crystals. (b) The corresponding time signals measured at $y = 0$ mm .

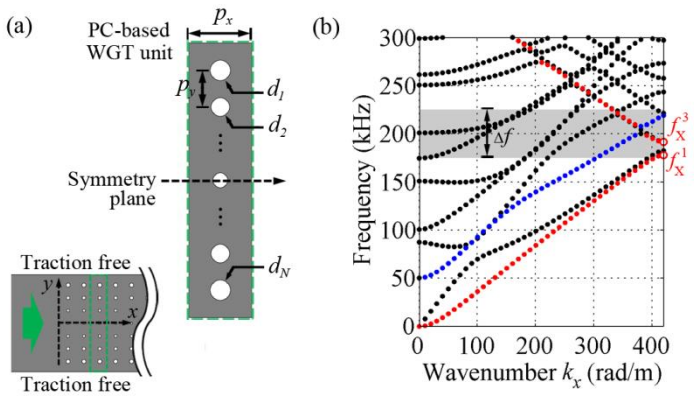

Figure 4.5 (a) Illustration of a considered phononic crystal based waveguide. The inclusion sizes d_i and a periodicity p_x of the phononic crystal based waveguide unit are engineered through the design procedures. (b) The dispersion curves of a nominal phononic crystal waveguide in the first Brillouin zone. The shading denotes the considered frequency range at which the phononic crystal-based waveguide transducer operates.

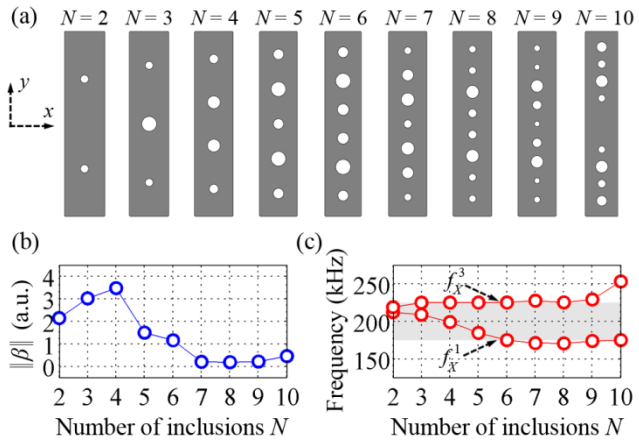

Figure 4.6 (a) The designed phononic crystal waveguide units having different number of inclusions in the *y* direction. (b) The square norms of group velocity dispersion parameters in the target frequency range. (c) The 1st and 3rd frequencies at the edge of the first Brillouin zone corresponding to the designed waveguide units.

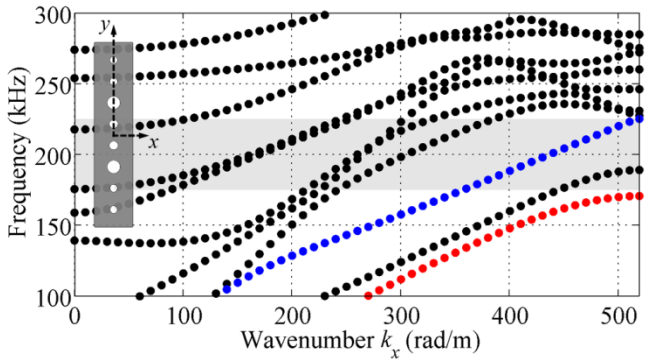

Figure 4.7 The dispersion curve in the first Brillouin zone of the unit structure of the optimally-engineered phononic crystal waveguide structure ($N = 8$).

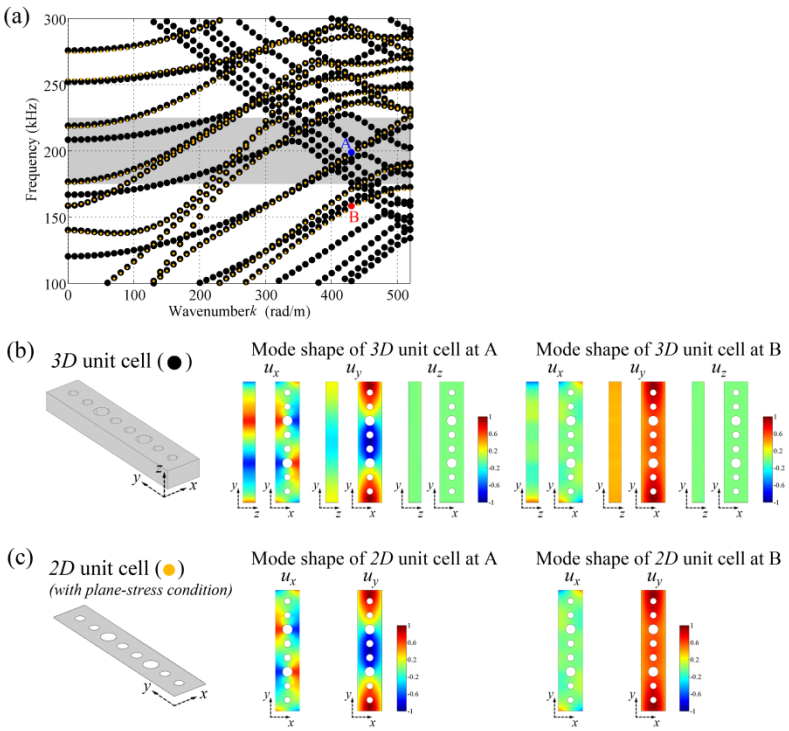

Figure 4.8 (a) Dispersion relations of the phononic crystal waveguide calculated by two- (yellow) and three-dimenaional (black) units. (b) The modal distributions of displacements at Points A and B in Fig. 4.9(a).

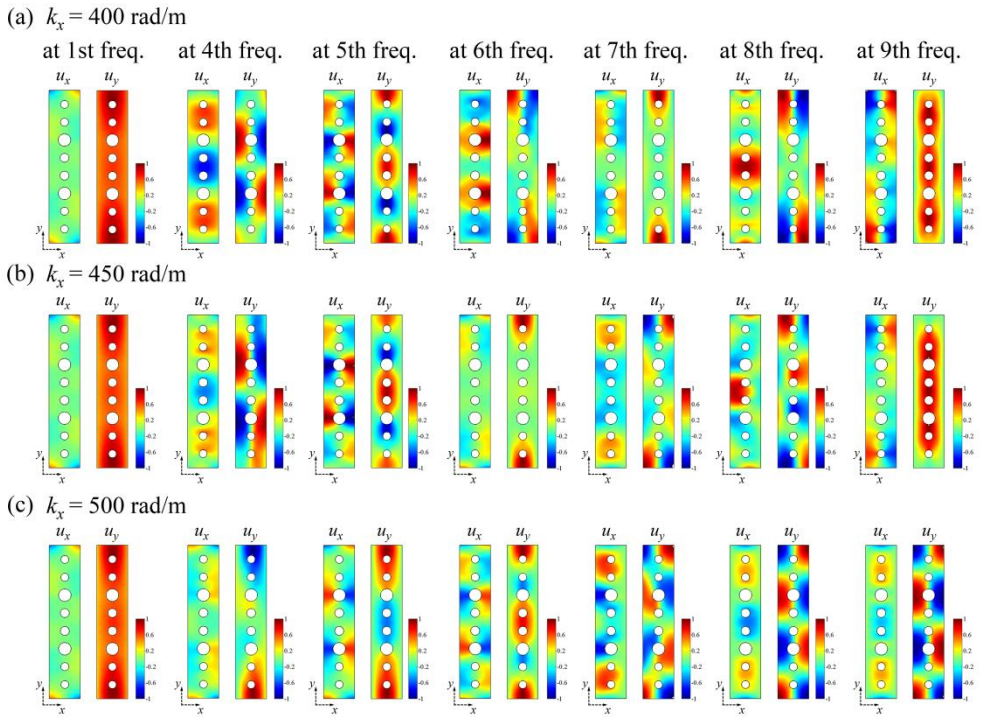

Figure 4.9 The distributions of the *x*- and *y*-displacement components of the eigenmodes of different branches at (a) $k_x = 400$, (b) 450, (c) $500\,\mathrm{rad/m}$, respectively.

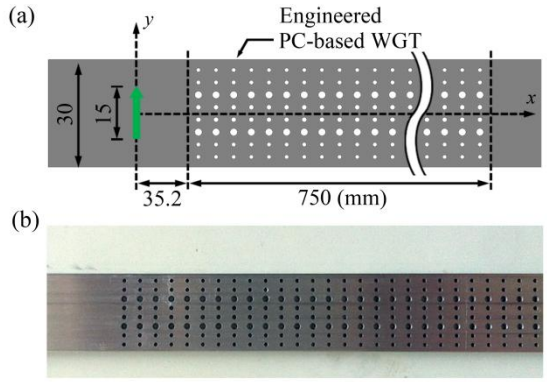

Figure 4.10 (a) Schematic of the engineered phononic crystal waveguide in numerical study. The green arrows represent the shear wave source. (b) Photo of the fabricated phononic crystal waveguide.

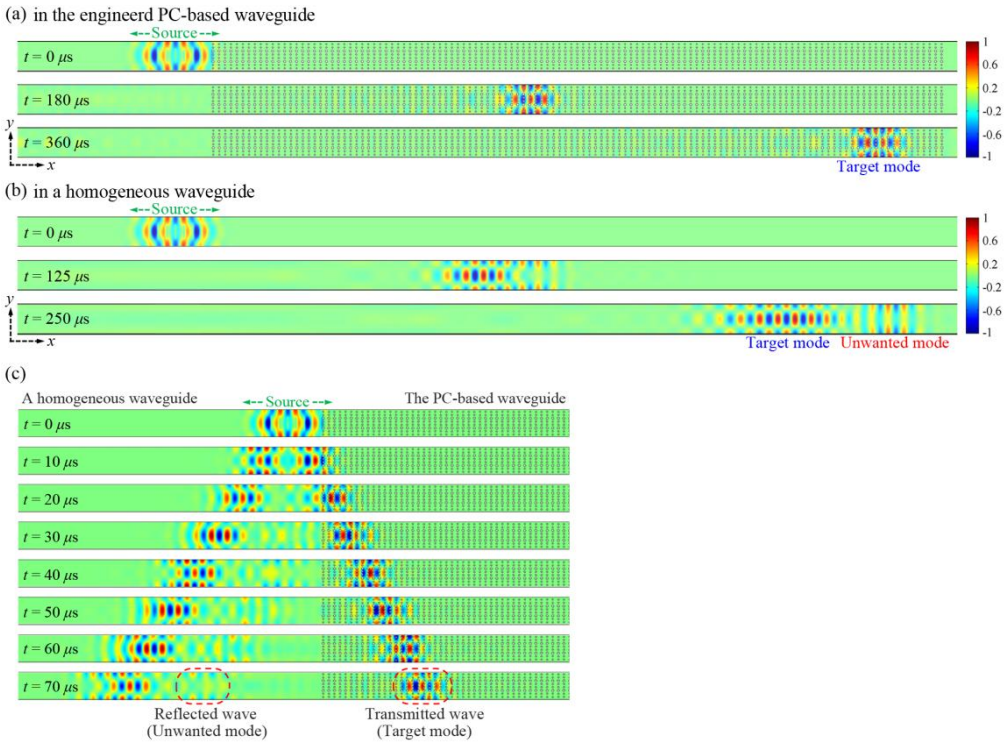

Figure 4.11 The *y*-displacement fields at different time steps in numerical simulations (a) in the engineered phononic crystal based waveguide and (b) in a homogeneous waveguide. (c) The *y*-displacement fields at initial time steps in the phononic crystal waveguide.

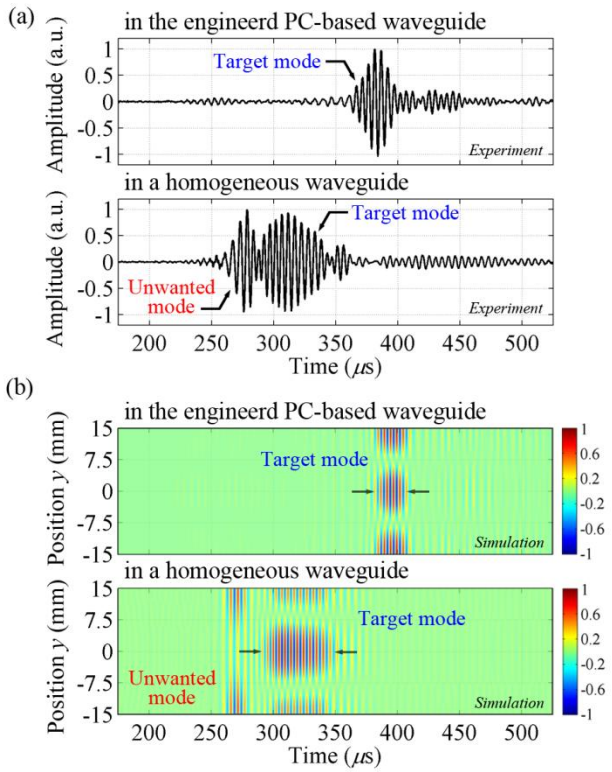

Figure 4.12 (a) The time signals measured experimentally in the engineered phononic crystal based waveguide (upper panel) and in a homogeneous waveguide (lower panel), respectively. (b) The spatiotemporal distributions of the *y*-displacement that calculated by numerical time-transient analysis.

CHAPTER 5

DISPERSION ENGINEERING BY ANISOTROPIC METAMATERIALS

5.1 Overview

The objective of this chapter is to tailor the dispersion relation of a waveguide by employing an elastic anisotropic metamaterial. Compared to the dispersion engineering by phononic crystals, a use of elastic metamaterials brings two dominant benefits: (1) the subwavelength scale and (2) the broadband frequency range. Based on these advantages, ultra-thin lenses are realized by electromagnetic [110, 111] and acoustic metamaterials [112, 113]. Also, the operating frequency range of acoustic cloaking devices can be widened by employing the subwavelength metamaterials [114, 115]. In this chapter, our focus is on the group velocity dispersion of elastic guided waves. We will present that the subwavelength-sized elastic metamaterial can achieve the dispersion engineering of an elastic waveguide. The purpose of the dispersion engineering is the same with Chapter 4, however, a region where the metamaterial layer is occupied is reduced by a factor of 3 and the target frequency range is doubled compared to the phononic crystals. To suppress the dispersion effect of the target guided mode, elastic metamaterials are designed through the following two phases. At the first design phase, we search a proper material property itself by proposed optimization methods. In this phase, general

anisotropic material is considered with some constraints which are related to its realization. Then, at the second design phase, the microstructure of anisotropic metamaterials is designed to have the same wave properties with the material determined at the first design phase.

In earlier studies, the main efforts are devoted to calculate effective material properties of acoustic metamaterials of the given structure. Its inverse process, a realization of the structure for the prescribed effective property, is not extensively investigated so far. The simplest approach is to find the structures by interpolating from the pre-calculated structures. By doing so, the phononic crystal-based devices which is made of multiple phononic crystal structures can be constructed to bend or focus acoustic waves [116-118]. For acoustic metamaterials, arrays of cylindrical inclusions exhibiting an anisotropic mass density in the long wavelength limit [119] was used to realize a transformation-based lens [120]. However, a realization for anisotropic metamaterial which is required to suppress the dispersion effect of elastic guided waves has not been investigated.

In this chapter, we propose the design method for the elastic anisotropic metamaterials by employing topology optimization method. In this method, the material distribution of a design domain is considered as a design variable so that one can obtain a proper material distribution without in the relatively broad solution space. Previously, the topology optimization method has been applied to maximize the band gap frequency of phononic and photonic crystals [121-124]. Recently, this method has been extended to design the resonant metamaterials for electromagnetic and acoustic waves [125-127]. For the broadband metamaterials which is focused

on in this chapter, there is a study for inverse design of an isotropic acoustic metamaterial [128]. In Ref. [128], they used the topology optimization method to reduce the frequency dependence and a difference in the impedance for the metamaterial lens. In the case of this chapter, the anisotropic elastic material is required to minimize the dispersion effect of the guided waves; the wave properties are different along the propagating direction and there are two elastic wave modes, quasi-longitudinal and quasi-transverse waves, to be considered. In this regard, the inverse design of the anisotropic elastic metamaterials is challenging.

In the following section, the dispersion effect of the target guided mode is suppressed by the anisotropic metamaterial. As mentioned above, we employ the optimization method to determine the material properties of metamaterial layers. It will be shown that the group velocity dispersion is effectively reduced depending on the strength of anisotropy. Next, we will discuss the topology design of anisotropic metamaterials; detailed formulation will be given with design examples. Finally, numerical demonstrations are carried out for the realized metamaterial-based waveguide.

5.2 Dispersion engineering by anisotropic metamaterials

5.2.1 Design formulation of metamaterial-based waveguide

The aim of study is to suppress the group velocity dispersion in a waveguide by an anisotropic metamaterial. As a target mode to be engineered, the 2nd order shear dominant wave in a waveguide is considered. Figure 5.1(a) shows the proposed waveguide which anisotropic metamaterial layers are attached on edge of a homogeneous waveguide. In Figure 5.1(b), the dispersion relation is presented when the metamaterial layers have the same material properties with the host material. Note that we assume the plane-strain condition along the out-of-plane direction for an infinite waveguide. The group velocity dispersion appears for the target mode as in Chapter 4; see the broadened output pulse of target mode in Figure 4.1(c). To reduce the dispersion effect, the phononic crystal was applied to tailor the dispersion relation of a waveguide in Chapter 4. At this time, the subwavelength-scaled metamaterial layers are manipulated to suppress the group velocity dispersion. Here, we apply that the metamaterial layers which have the arbitrary anisotropic elastic constants [129] as follows.

$$\mathbb{C}_{MM} = \mathbf{T}(\theta)\begin{bmatrix} c_{11} & c_{12} & c_{12} & 0 & 0 & 0 \\ c_{12} & c_{11} & c_{12} & 0 & 0 & 0 \\ c_{12} & c_{12} & c_{11} & 0 & 0 & 0 \\ 0 & 0 & 0 & c_{44} & 0 & 0 \\ 0 & 0 & 0 & 0 & c_{44} & 0 \\ 0 & 0 & 0 & 0 & 0 & c_{44} \end{bmatrix}\mathbf{T}(\theta)^T \ , \tag{5.1}$$

where $\mathbf{T}(\theta)$ is the transformation matrix for the rotation by an angle θ about the out of plane direction, the superscript T denotes transpose operator. The transformation matrix $\mathbf{T}(\theta)$ is given by

$$\mathbf{T}(\theta)=\begin{bmatrix} \cos^2\theta & \sin^2\theta & 0 & 0 & 0 & \sin 2\theta \\ \sin^2\theta & \cos^2\theta & 0 & 0 & 0 & -\sin 2\theta \\ 0 & 0 & 1 & 0 & 0 & 0 \\ 0 & 0 & 0 & \cos\theta & -\sin\theta & 0 \\ 0 & 0 & 0 & \sin\theta & \cos\theta & 0 \\ -\sin\theta\cos\theta & \sin\theta\cos\theta & 0 & 0 & 0 & \cos 2\theta \end{bmatrix}. \tag{5.2}$$

The material property has the cubic symmetry whose stiffness constants c_{11}, c_{12}, c_{44} are defined as follows:

$$c_{11}=\frac{E_{MM}(1-\nu)}{(1+\nu)(1-2\nu)},$$

$$c_{44}=\frac{E_{MM}}{2(1+\nu)},$$

$$c_{12}=c_{11}-\frac{2}{\gamma}c_{44} \tag{5.3}$$

where E_{MM} is Young's modulus, ν is Poisson's ratio, and γ is anisotropy factor. The rotation angle θ of the cubic material is called the symmetry direction in this study. Since the stiffness constants of the metamaterial are characterized by E_{MM}, γ, θ, these parameters are considered as design variables in the dispersion engineering of a waveguide problem. Also, the density of the metamaterial layer ρ_{MM} is assumed to be changed.

To manipulate the dispersion relation of a waveguide, we try to change the material properties of metamaterial: $\mathbb{C}_{MM}(E_{MM}, \gamma, \theta)$ and ρ_{MM}. As mentioned earlier, the guided waves are originated from the successive reflection of the elastic waves at the traction free boundaries of waveguide. At the free boundary, the quasi-longitudinal and the quasi-transverse waves are reflected and these waves are

developed to the guided waves. Based on this mechanism, we can manipulate the dispersion relation of the guided waves by the phononic crystals in which have the wavelength-scaled scatterers. Here, we use the anisotropic metamaterial to achieve the similar dispersion tailoring. When the anisotropic metamaterial layers are inserted to the waveguide, they scatter the waves at the interface between the metamaterial and host material and at the free boundaries. Since these wave scatterings are different depending on the material properties, we can control the dispersion relation of the guided waves by tailoring material properties of the metamaterial layers.

The objective of this study is to minimize the group velocity dispersion of the 2nd order shear dominant wave mode in a waveguide. To find the material properties of metamaterial for this objective, the optimization method is applied. As in Chapter 4, the following objective function is defined:

$$\begin{aligned} &\min_{E,\gamma,\theta,\rho_{MM}} \|\beta\| \text{ in } \Delta f \\ &\text{subject to} \\ &\quad 0 < E_{MM} < \bar{E}, \\ &\quad \underline{\gamma} < \gamma < \bar{\gamma}, \\ &\quad 0 < \theta < \bar{\theta}, \\ &\quad 0 < \rho_{MM} < \bar{\rho}. \end{aligned} \tag{5.4}$$

where $\beta \equiv \partial^2 k_x / \partial \omega^2$ is the group velocity parameter [103-105], Δf is the target frequency range, the parameter with the superbar (underbar) is the upper (lower) bound of the parameter. For the metamaterial-based waveguide of specific $\mathbb{C}_{MM}(E_{MM}, \gamma, \theta)$ and ρ_{MM}, the dispersion relation is calculated by using FEM. Although the waveguide is not periodic in the propagating direction, a thin unit cell

of the waveguide is considered to apply the formulation of FEM in the dispersion analysis. By this artificial periodicity, there are the folded branches in the dispersion relation of a waveguide. Here, the thickness of a unit cell in the *x* direction is sufficiently thin, so that we can focus on the frequency range below where the folded branch appears. To calculate the wavenumber *k* along the unit vector $\mathbf{l} = l_x\hat{\mathbf{x}} + l_x\hat{\mathbf{y}} + l_z\hat{\mathbf{z}}$ at a specific frequency ω, the element stiffness matrix in (2.35) becomes

$$\bar{\mathbf{k}}_e = k^2\mathbf{P}_e + k\mathbf{Q}_e + \mathbf{R}_e \tag{5.5}$$

where

$$\mathbf{P}_e = \int_\Omega (j\mathbf{lN})^* \mathbb{C}_e (j\mathbf{lN}) dV \tag{5.6}$$

$$\mathbf{Q}_e = \int_\Omega \left\{ \mathbf{B}\mathbb{C}_e (j\mathbf{lN}) + (j\mathbf{lN})^* \mathbb{C}_e \mathbf{B} \right\} dV \tag{5.7}$$

$$\mathbf{R}_e = \int_\Omega \mathbf{B}\mathbb{C}_e \mathbf{B}\, dV. \tag{5.8}$$

Substituting (5.5) into (2.34), it gives

$$k^2\mathbf{P}_e\bar{\mathbf{U}}_e + k\mathbf{Q}_e\bar{\mathbf{U}}_e + (\mathbf{R}_e - \omega^2\mathbf{M}_e)\bar{\mathbf{U}}_e = 0. \tag{5.9}$$

Depending on the material properties of the element, the element matrices in (5.9) can be obtained. The polynomial eigenvalue solver can be used to calculate the wavenumbers *k*'s for different frequencies. It contains the real wavenumber (propagating) as well as the complex value wavenumber (evanescent). By choosing real wavenumbers, one can obtain the dispersion relation of a metamaterial-based waveguide.

The objective function of the optimization procedure is defined as a square norm of the group velocity dispersion parameter β. To calculate the β which is defined

by the second order derivative of the wavenumber, the numerical derivative is used in this study. Then, the sensitivity of the design variables can be obtained from the first derivative of a wavenumber k with respect to the particular material property, say ϕ. By applying the adjoint variable method [130], the derivative of a wavenumber is given by

$$\frac{\partial k}{\partial \phi} = \frac{-\left\{ k^2 \bar{\mathbf{U}}_g \frac{\partial \mathbf{P}_g}{\partial \phi} \bar{\mathbf{U}}_g + k \bar{\mathbf{U}}_g \frac{\partial \mathbf{Q}_g}{\partial \phi} \bar{\mathbf{U}}_g + \bar{\mathbf{U}}_g \frac{\partial (\mathbf{R}_g - \omega^2 \mathbf{M}_g)}{\partial \phi} \bar{\mathbf{U}}_g \right\}}{\left\{ 2k \bar{\mathbf{U}}_g \mathbf{P}_g \bar{\mathbf{U}}_g + \bar{\mathbf{U}}_g \mathbf{Q}_g \bar{\mathbf{U}}_g \right\}}. \quad (5.10)$$

The matrices with subscript *g* are the global system matrices. The derivatives of the global matrices with respect to the material property can be assembled by using (5.1)-(5.3).

5.2.2 Design of metamaterial-based waveguide

In this subsection, we discuss results of the proposed optimization method in (5.4). The aluminum waveguide having metamaterial layers of 5 mm is considered as shown in Figure 5.1. Two metamaterial layers share the material properties of metamaterial (E_{MM}, γ, ρ_{MM}) except for θ. Since the target wave mode is symmetric about the $y = 0$ plane as shown in the inset of Figure 4.1(b), the symmetry angle θ of the upper layer is set to $-\theta$. By the gradient-based optimization method, these variables are updated to minimize the square norm of the dispersion parameter β over the target frequency range of $150 < f < 250\,\text{kHz}$. In the optimization procedure, the design variables (E_{MM}, γ, θ, ρ_{MM}) are updated from initial values until a convergence criteria is satisfied. We use the material

properties of aluminum as initial values of the metamaterial layer to have the same material properties with the host materials.

Prior to conducting the optimization, the bound for the design variables should be determined. The bounded values of the metamaterial depend on a constituent material of a microstructure and an operating frequency of metamaterials. Recently the range of the material properties are expanded to the near zero density or even to negative density and stiffness constants by employing metamaterials. In most cases, however, these extreme material properties are come from the resonant mechanism so that they exhibit the strong frequency dependency. Since we focus on a wave propagation in the relatively broad frequency range, the material whose properties are constant in the target frequency range is needed. In this regard, the non-resonant metamaterial which exhibits the broadband properties is considered in this study. Although the material properties of this type of metamaterial are not extreme as the resonant metamaterials, a use of the non-resonant metamaterial is sufficient for the case of this study. The detailed results of the realization of the non-resonant elastic metamaterial are given in Section 5.3.

In this section, the aluminum in which the air-filled inclusions are arranged periodically is considered as the elastic anisotropic metamaterial. For this configuration, Young's modulus and density are reduced by the air-filled inclusions so that the upper bounds of their material properties are set to those for the aluminum: $\bar{E} = 67.78\text{GPa}$, $\bar{\rho} = 2631.4\text{kg}/\text{m}^3$. And the symmetry angle θ is constrained to have the value between 0 and $\pi/2$ because stiffness constants of the metamaterial have the cubic symmetry as (5.1).

As an example, the optimization for the upper bound of the anisotropy factor, $\bar{\gamma}$, of 4.0 is examined. In Figure 5.2(a), we present the iteration history of the objective function which is decreased as the optimization progressed. Since the objective function can be understood by the curvature of the dispersion curve of the target wave mode, the dispersion curve become straight as the objective function is minimized. This fact can be checked in the dispersion curves shown in Figure 5.2(b). The dispersion relations of the metamaterial-based waveguide in the progress of the optimization are given for iteration numbers of 1, 11, 51, and 109, respectively. The corresponding slowness curve of the anisotropic metamaterial are presented for the same iteration number in Figure 5.2(c). The converged values of the design variables are as follows: $\rho_{MM} = 2631.4\,\mathrm{kg/m^3}$, $E_{MM} = 28.45\,\mathrm{GPa}$, $\theta = 36.58^{\circ}$, $\gamma = 4.0$. With this metamaterials, the objective function is 0.2023 from its intial value of 1.0. The optimization results for the different upper bound values of the anisotropy factor, $\bar{\gamma}$, are also presented in Figure 5.3. Note that converged values of the design variables for different upper bound $\bar{\gamma}$ are summarized in Table 5.1. The corresponding dispersion curve and the slowness curves for the metamaterial are given in Figure 5.3 (a) and (b), respectively. It is shown that the the anisotropy factor are converged to their upper bounds and the metamaterial-based waveguide has the smaller objective function value as $\bar{\gamma}$ is increased.

To demonstrate the effect of the anisotropic metamaterial on the group velocity dispersion in a waveguide, a time-transient simulation is conducted by the commercial finite element software COMSOL multiphysics. The analysis domain is given in Figure 5.4(a) for metamaterial-based waveguide. The aluminum waveguide

of 400 mm in the *x* direction is covered by the anisotropic metamaterial layers of $5\,\text{mm}$ in thickness. For the metamaterials, the material properties of the case for $\bar{\gamma} = 4.0$ are used. To generate a target wave mode in the waveguide, the *y* displacement of 15-mm source is excited. The Gaussian pulse of 200 kHz in the form of $\exp(-t^2/2\sigma^2)\cos(2\pi f_c t)$ is inputted to the source. Figure 5.4(a) shows the snapshots of numerical simulations in the metamaterial-based waveguide; the shear energy density ($-\dot{u}_y^*\sigma_{xy}/2$, the superscript * denotes the complex conjugate) is focused on. For the comparison, we conduct the same simulation for the homogeneous aluminum waveguide of 30 mm in thickness as shown in Figure 5.4(b). Among two wave pulses in a homogeneous waveguide, a slow pulse corresponds to the target wave mode. It is shown that the target wave mode propagates non-dispersively in the metamaterial-based waveguide compared with that in the homogenous waveguide. The group velocities of a homogeneous waveguide and are summarized in Table 5.2; one can find that a difference in group velocities of the target wave range is sufficiently reduced.

In this section, we show that the anisotropic elastic metamaterial can be employed to tailor the dispersion relation of a waveguide. In particular, the group velocity dispersion is suppressed by the metamaterial layers attached on the edge of the waveguide. On the other hand, there is another issue in the use of the anisotropic elastic metamaterial: realization of the anisotropic metamaterial. In the following section, we suggest the formulation to make the anisotropic metamaterial exhibit the desired wave characteristics.

5.3 Realization of anisotropic metamaterial by topology optimization

In the preceding section, the anisotropic material properties are designed to suppress the dispersion effect in a waveguide. But it is hard to find the material which exhibits the required properties in nature. Now, we realize the elastic metamaterial by designing the microstructure to have the desired wave properties. In a realization of anisotropic metamaterials, the following conditions should be satisfied: (1) the wave properties of realized metamaterials are as similar as possible with the required metamaterial; (2) these properties are constant at least over the target frequency range of $150 < f < 250\,\mathrm{kHz}$; (3) the properties can be exhibit in the subwavelength scale. As shown in Chapter 3, we can obtain the anisotropic wave properties by applying the phononic crystals. However, since their properties are strongly dependent on the frequency, the subwavelength-scale metamaterials are considered for broadband anisotropic properties in this study.

Here, we considered the periodic structures whose lattice parameter a is quite small compared with the wavelength λ ($a < \lambda/10$). Then, to find the metamaterial which satisfy Conditions (1)-(3), the topology of inclusions in a unit structure is designed by optimization procedures. Through this process, we can obtain the material whose wave properties are the same with the required material. In the following subsection, we discuss detailed design process and show a validity of the designed metamaterial for the dispersion engineering.

5.3.1 Formulation of topology design for anisotropic metamaterials

To design the microstructure of the metamaterial, we employ the topology optimization method. In the topology optimization method, the design domain is divided into a number of subdomains, then it is determined whether or not there is a material in each subdomain. By choosing a different combination of a material status in subdomain, it is possible to produce an infinite number of designs. For example, if a material exist in a subdomain or not (void), there are 2^N design cases for the total domain consist of N subdomains. Based on the broad solution space of this method, it is possible to find the optimal design in earlier works [131].

In Chapter 4, we designed the unit cell which contains the traction free boundaries of a waveguide. Here, on the contrary, a unit cell of an infinite metamaterial medium is considered as a design domain. The effects of traction free boundaries and the interfaces between the metamaterial layer and a host material on the wave scattering are already reflected the design process in Section 5.2. Therefore, it is sufficient to find the proper unit cell satisfying Condition (1)-(3) as a bulk property in this process. We consider an aluminum-based metamaterial in which a void of arbitrary topology is formed. A unit cell of the metamaterial is arranged with the rectangular lattice a and the material distribution in a unit cell is designed by the topology optimization method. In general, a parameter χ_i is introduced to express whether the material exist or not in i^{th} subdomain; for example, the subdomain is filled with aluminum when $\chi_i = 1$, or with nothing when $\chi_i = 0$. For the intermediate value of χ, we apply Solid Isotropic Material with Penalization

approach (SIMP) to interpolate the material properties [131]. This model assumes that the material for $0<\chi<1$ have the intermediate property between the aluminum and void as follows:

$$\begin{aligned} E(\chi) &= \chi^3 E_{Al} + \left(1-\chi^3\right) E_{LIM}, \\ \rho(\chi) &= \chi\ \rho_{Al} + (1-\chi)\rho_{LIM} \end{aligned}, \tag{5.11}$$

where, E and ρ represent Young's modulus and density, the material properties with subscript *Al* is for aluminum, and those with subscript *LIM* is for the low impedance material. The chosen material properties are as follows: $E_{Al} = 67.78\,\text{GPa}$ and $\rho_{Al} = 2631.4\ \text{kg/m}^3$ for aluminum, $E_{LIM} = 10\,\text{MPa}$ and $\rho_{LIM} = 0.001\ \text{kg/m}^3$ for the low impedance material, respectively. Note that the low impedance material is used to prevent the singularity. For the intermediate density, the element stiffness and mass matrices in (5.6)-(5.8) and (2.31) can be obtained depending on its 'density' χ as follows:

$$\mathbf{P}_e = \chi^3 \int_\Omega (j\mathbf{lN})^* \mathbb{C}_{Al} (j\mathbf{lN}) dV + \left(1-\chi^3\right) \int_\Omega (j\mathbf{lN})^* \mathbb{C}_{LIM} (j\mathbf{lN}) dV, \tag{5.12}$$

$$\begin{aligned} \mathbf{Q}_e = {} & \chi^3 \int_\Omega \left\{ \mathbf{B}\mathbb{C}_{Al} (j\mathbf{lN}) + (j\mathbf{lN})^* \mathbb{C}_{Al} \mathbf{B} \right\} dV \\ & + \left(1-\chi^3\right) \int_\Omega \left\{ \mathbf{B}\mathbb{C}_{LIM} (j\mathbf{lN}) + (j\mathbf{lN})^* \mathbb{C}_{LIM} \mathbf{B} \right\} dV, \end{aligned} \tag{5.13}$$

$$\mathbf{R}_e = \chi^3 \int_\Omega \mathbf{B}\mathbb{C}_{Al}\mathbf{B}\, dV + \left(1-\chi^3\right) \int_\Omega \mathbf{B}\mathbb{C}_{LIM}\mathbf{B}\, dV, \tag{5.14}$$

$$\mathbf{M}_e = \left\{ \chi\rho_{Al} + (1-\chi)\rho_{LIM} \right\} \int_\Omega \mathbf{N}^T \mathbf{N} dV \tag{5.15}$$

where $\mathbb{C}$ and ρ denote the stiffness constants and density, respectively. Then, the assembled global matrix is solved by the wavenumber k along a unit vector of $\mathbf{k} = k_x \hat{\mathbf{x}} + k_x \hat{\mathbf{y}} + k_z \hat{\mathbf{z}}$.

To find the structure of unit cell, we employ the gradient-based optimization scheme for χ's. Figure 5.5(a) shows a schematic of the topology optimization problem dealt in this section. The parameters χ's are considered as the design variable in the topology optimization problem and updated by the optimizer. To find the unit cell of anisotropic metamaterial which has the same properties with the required material, the following objective and constraint functions are defined:

$$\min_{\chi_i} \sum_i \chi_i (1-\chi_i) \tag{5.16}$$

$$\begin{aligned} &\text{subject to } \sum_j \left(e_j^{ql}\right)^2 < \varepsilon^{ql}, \\ &\qquad\qquad \sum_j \left(e_j^{qt}\right)^2 < \varepsilon^{qt} \end{aligned} \tag{5.17}$$

with

$$\begin{aligned} e^{ql} &= \left(1/\bar{V}_p^{ql}\right) - \left(1/V_p^{ql}\right), \\ e^{qt} &= \left(1/\bar{V}_p^{qt}\right) - \left(1/V_p^{qt}\right). \end{aligned} \tag{5.18}$$

where e^{ql} and e^{qt} are differences between the slownesses of the required material $\left(1/\bar{V}_p\right)$ and a metamaterial in the design process $\left(1/V_p\right)$ for the quasi-longitudinal and the quasi-transverse wave modes. First, the objective function measures a degree of the convergence for χ's. As the parameter χ was introduced for the intermediate status in design process, it should be converged to 'real' material (aluminum or void). To do this, the objective function is minimized, leading to the clear material unit cell which consists of aluminum or void. Next, in (5.17), the difference in slownesses between the required material and the designed unit cell is constrained to have the small value. In Figure 5.5(b), the slowness curves for the required material are given by black lines, while those for the designed

metamaterial, by red (the quasi-longitudinal) and blue (the quasi-transverse) lines. By decreasing differences in the slowness curves, e^{ql} and e^{qt}, we can design the microstructure of metamaterial which have desired wave properties as the required materieal. To have a constant property over the target frequency range, we evaluate the slowness curve at the lower and upper bound of the target frequency range, $\underline{f} = 150$ and $\bar{f} = 250\,\text{kHz}$, respectively. At these frequencies, the constraint functions of (5.17) are defined. Lastly, the lattice parameter *a* of a unit cell is set to be relatively smaller than the wavelength λ, 15.6 mm for the transverse wave at 200 kHz.

To evaluate the e^{ql} and e^{qt} in constraint functions of (5.17), the slownesses for the required material and the metamaterial are calculated. From its definition, the slowness is the wavenumber k divided by angular frequency ω. In this study, we evaluated the wavenumbers for the selected direction from $-\pi/2$ to $\pi/2$, which is contains the minimum and maximum slowness of the required material. Although a sufficient number of evaluation points may assure a good performance of designed metamaterial, the numerical cost is also linearly increased with the evaluation points. Here, we evaluate the wavenumber along eight different directions.

For the specific direction of wavenumber, the sensitivity of the objective function is given as follows:

$$\frac{\partial\left(\sum_i \chi_i(1-\chi_i)\right)}{\partial \chi_j} = (1-2\chi_j). \tag{5.19}$$

Also, the sensitivity of the constraint function can be obtained by using (5.10). In the topology optimization, the sensitivity of global matrices with respect to the 'density' of i^{th} element (χ_i) depends on its element matrices. Therefore, (5.10) becomes

$$\frac{\partial k}{\partial \chi_i} = -\left\{ k^2 \bar{\mathbf{U}}_e \frac{\partial \mathbf{P}_e}{\partial \chi_i} \bar{\mathbf{U}}_e + k \bar{\mathbf{U}}_e \frac{\partial \mathbf{Q}_e}{\partial \chi_i} \bar{\mathbf{U}}_e + \bar{\mathbf{U}}_e \frac{\partial \mathbf{R}_e}{\partial \chi_i} \bar{\mathbf{U}}_e - \omega^2 \bar{\mathbf{U}}_e \frac{\partial \mathbf{M}_e}{\partial \chi_i} \bar{\mathbf{U}}_e \right\} \Big/ \left\{ 2k \bar{\mathbf{U}}_g \mathbf{P}_g \bar{\mathbf{U}}_g + \bar{\mathbf{U}}_g \mathbf{Q}_g \bar{\mathbf{U}}_g \right\}. \tag{5.20}$$

Note that the matrices and vector in a numerator are for the i^{th} element of χ_i. Up to now, we suggest the design formulation for anisotropic metamaterials by the topology optimization method; the objective, constraint functions, and their sensitivity are given. In the following section, microstructures of the anisotropic metamaterial are designed by the proposed formulation.

5.3.2 Design examples of elastic metamaterial

In the topology design of anisotropic metamaterial, the objectives are (1) to have the same slowness curves with the required material in the target frequency range of Δf and (2) to be converged to two distinct materials, aluminum or void in this study. To do this, the objective and constraint functions are defined as (5.16) and (5.17). In Section 5.2, we determine the material properties(E_{MM}, γ, θ, ρ_{MM}) to suppress the dispersion effect of the target wave mode in a waveguide. Depending on the upper bound of anisotropy factor $\bar{\gamma}$, different material properties were obtained; their slowness curves are given in the lower panel of Figure 5.3. When the

$\bar{\gamma}$ is increased, it is shown that the dispersion effect of metmaterial-based waveguide is decreased as shown in the upper panel of Figure 5.3. We call these material *target materials* in this section. The stiffness constants $\mathbb{C}_{MM}(E_{MM}, \gamma, \theta)$ and density ρ_{MM} of the target materials are as follows:

for the case of $\bar{\gamma} = 2.0$,

$$\mathbb{C}_{MM} = \begin{bmatrix} 36.298 & 19.952 & 24.038 & 0 & 0 & 0.026 \\ 19.952 & 36.298 & 24.038 & 0 & 0 & -0.026 \\ 24.038 & 24.038 & 32.212 & 0 & 0 & 0 \\ 0 & 0 & 0 & 8.173 & 0 & 0 \\ 0 & 0 & 0 & 0 & 8.173 & 0 \\ 0.026 & -0.026 & 0 & 0 & 0 & 4.087 \end{bmatrix} \text{GPa}, \quad (5.21)$$

$$\rho_{MM} = 2631.4\,\text{kg}/\text{m}^3;$$

for the case of $\bar{\gamma} = 3.0$,

$$\mathbb{C}_{MM} = \begin{bmatrix} 40.984 & 23.519 & 29.272 & 0 & 0 & 1.092 \\ 23.519 & 40.984 & 29.272 & 0 & 0 & -1.092 \\ 29.272 & 29.272 & 35.232 & 0 & 0 & 0 \\ 0 & 0 & 0 & 8.939 & 0 & 0 \\ 0 & 0 & 0 & 0 & 8.939 & 0 \\ 1.092 & -1.092 & 0 & 0 & 0 & 3.187 \end{bmatrix} \text{GPa}, \quad (5.22)$$

$$\rho_{MM} = 2631.4\,\text{kg}/\text{m}^3;$$

for the case of $\bar{\gamma} = 4.0$,

$$\mathbb{C}_{MM} = \begin{bmatrix} 49.506 & 29.459 & 36.808 & 0 & 0 & 2.224 \\ 29.459 & 49.506 & 36.808 & 0 & 0 & -2.224 \\ 36.808 & 36.808 & 42.157 & 0 & 0 & 0 \\ 0 & 0 & 0 & 10.697 & 0 & 0 \\ 0 & 0 & 0 & 0 & 10.697 & 0 \\ 2.224 & -2.224 & 0 & 0 & 0 & 3.347 \end{bmatrix} \text{GPa}, \quad (5.23)$$

$$\rho_{MM} = 2631.4\,\text{kg}/\text{m}^3;$$

for the case of $\bar{\gamma} = 5.0$,

$$\mathbb{C}_{MM} = \begin{bmatrix} 57.567 & 34.885 & 43.755 & 0 & 0 & 3.001 \\ 34.885 & 57.567 & 43.755 & 0 & 0 & -3.001 \\ 43.755 & 43.755 & 48.697 & 0 & 0 & 0 \\ 0 & 0 & 0 & 12.356 & 0 & 0 \\ 0 & 0 & 0 & 0 & 12.356 & 0 \\ 3.001 & -3.001 & 0 & 0 & 0 & 3.486 \end{bmatrix} \text{GPa}, \quad (5.24)$$

$\rho_{MM} = 2631.4\,\text{kg}/\text{m}^3$.

Let us give results of the topology design for the case of $\bar{\gamma} = 4.0$. As mentioned earlier, the elastic metamaterial having a rectangular lattice is considered. The unit cell of the metamaterial is discretized by 2500 finite elements. As an initial topology, we consider a unit cell of $\chi = 0.5$ except for 4 void elements at the center of a unit cell. From the initial topology, the 'density' of each element is updated by a gradient-based optimization schemes until the convergence criteria is satisfied. In Figure 5.6(a), iteration histories of the topology and the slowness curves are presented for $a = 1.0$ mm. As optimization proceeds, the slowness curves of the designed metamaterial (red: the quasi-longitudinal, blue: the quasi-transverse mode) are closed to those of the target material for that case of $\bar{\gamma} = 4.0$. The slowness curves at 150 kHz are represented by dotted line, while that at 250 kHz, solid line, respectively. They are agreed well with the target contours at the last step of an optimization procedure. To confirm that the designed metamaterial exhibit the constant properties in the target frequency range, the dispersion relation of the metamaterial structure is calculated in the frequency domain; it is shown that the its dispersion curves are linear and no resonance gap appears in Δf. Also, the

objective function, convergence of the density χ, is reduced to 0.044 from its initial value of 1.00 as shown in Figure 5.6(b). This fact can be checked with the topology changes in the optimization procedure shown in the upper part of Figure 5.6(a): from an initial topology in which most elements have the density χ of 0.5 to a final topology in which there are two material phases of aluminum (black) and void (white region). Note that the converged topology has the symmetry even though no additional constraint on the densities is used.

Also, an effect of the lattice parameter *a* of the metamaterial unit on results of the proposed topology optimization is checked. We carry out the same topology optimization as in Figure 5.6 but for the different values of *a* in this time. Figure 5.7(a) and (b) show converged values of the differences in the slowness curves and the topologies at the final stage for some lattice parameters. It is shown that the cases of $a < 2.0\,\text{mm}$ have almost the same topology in their unit cells but the optimization cases of larger *a* values than 2.0 mm did not converged to the clear topology. This fact is confirmed by comparing the EFC's of the target materials at 250 kHz and the corresponding 1st Brillouin zones of the different sizes of metamaterial unit. Due to the periodicity of the metamaterials, dispersion relation in the 1st Brillouin zone is repeated in the wavenumber domain. As shown in Figure 5.7(c), the cases of $a > 2.0\,\text{mm}$ have the smaller irreducible Brillouin zone compared with the target EFC's; the metamaterial units of large *a* values cannot have the required EFC's for the target frequency range. From this reason, a lattice parameter of 1 mm is used for the metamaterial design.

We also design anisotropic metamaterials for the cases of different $\bar{\gamma}$ values. Depending on the target material of each case, different topology is obtained. Designed metamaterial units after thresholding and corresponding slowness curves are presented in Figure 5.8. As the $\bar{\gamma}$ is increased, the discrepancies in slowness curves are increased. Although the metamaterial-based waveguide of $\bar{\gamma} = 5.0$ outperforms that of the smaller $\bar{\gamma}$, the metamaterial which exhibit the same material properties cannot be found by the chosen configuration (void in an aluminum matrix). On the contrary, for $\bar{\gamma} = 2.0$, 3.0, and 4.0, we can realize anisotropic metamaterials by tailor the unit structures thorugh the topology optimization. In the following subsection, the designed microstructure is actually inserted into a waveguide and its effect on the dispersion relation of guided waves is investigated.

5.3.3 Numerical analysis of metamaterial-based waveguide

Here, the performance of the designed metamaterial is confirmed by numerical demonstration. To do this, we inserted the engineered microstructure in a waveguide, then the dispersion analysis of the realized metamaterial-based waveguide is conducted. The lower metamaterial layer of 5 mm is filled with five unit cells of the metamaterial structure of $\bar{\gamma} = 4.0$ in Figure 5.8(c). The upper layer is constructed of the same structure but flipped about $y = 0$ plane as shown in the inset of Figure 5.9(a). To obtain the dispersion relation in the frequency domain, the finite element software COMSOL is used. The periodic boundary conditions are applied between boundaries of a waveguide unit as explained in Chapter 2. We calculate the frequency of the Bloch waves in the realized metamaterila-based waveguide for

different number of wavenumber k_x.

Figure 5.9(a) shows the dispersion curves for the realized waveguide- it has the similar curves compared with that for the target waveguide in Figure 5.9(b). Although there are discrepancies near the cut off frequency of higher branches, the lower order branches including the target wave mode show a close correspondence to those of the target waveguide. To compare their dispersion curves quantitatively, the group velocities of the target wave mode are evaluated as shown in Figure 5.10. The miminum and maximum group velocities for the realized waveguide are 2607.00 and 2773.16 m/s, while they are 2513.92 and 2687.42 m/s for the target waveguide over $150 < f < 250\,\mathrm{kHz}$. Compared with the difference in the group velocity of a homogeneous waveguide, which has no metamaterial layers, it is expected that the dispersion effect is sufficiently reduced by the realized metamaterial waveguide.

Next, the modal distributions of the realized metamaterial waveguide are compared with those of a waveguide having target material layers. Figure 5.11 shows modal distribution of *x* and *y* displacements which are obtained along the thickness direction (the *y* direction) at 200 kHz. Note that the modal displacements are normalized by maximum value of each wavenumber. In Figure 5.11(a), the mode shapes of the realized waveguide are given. They are agreed with those of the target waveguide shown in Figure 5.11(b). In particular, the u_y field for the realized waveguide is almost constant distribution in a region of the host material, $-10 < y < 10\,\mathrm{mm}$, as for a target waveguide. From these mode shapes, it is shown

that the designed microstructures of metamaterial have the same effective properties with the target material. It confirms the fact that the anisotropic elastic metamaterial can be realized by matching their slowness curves.

5.4 Concluding remarks

In this chapter, the dispersion engineering by the anisotropic metamaterial was presented. In particular, the group velocity dispersion was considered to be overcome by using elastic metamaterials. To do this, two design phase were suggested for designing metamaterial-based waveguide. First, we searched for the material property itself to suppress the dispersion effect in a waveguide. The material anisotropy factor and its symmetry direction were determined by the proposed optimization method. Second, the microstructure of metamaterial unit was designed to have the same wave properties with those of the target material. We employed the topology optimization method to realize the anisotropic metamaterial. Through this process, the metamaterial can be obtained and it was demonstrated that the realized anisotropic metamaterials can prevent the group velocity effect of a guided wave. Finally, we expect that the proposed method for anisotropic metamaterials can provide opportunities to improve various wave control system.

Table 5.1 Material properties of the anisotropic metamaterials, Young's modulus E_{MM}, anisotropy factor γ, symmetry direction θ, density ρ_{MM}, for different upper bound values of the anisotropy factor $\bar{\gamma}$.

$\bar{\gamma}$	E_{MM} (GPa)	γ (a.u.)	θ (degrees)	ρ_{MM} ($\mathrm{kg/m^3}$)
2.0	21.89	2.0	45.47	2631.4
3.0	23.73	3.0	39.52	2631.4
4.0	28.42	4.0	36.59	2631.4
5.0	32.86	5.0	35.64	2631.4

Table 5.2 The group velocities of the target wave mode at different frequencies in the metamaterial-based waveguide and in the homogeneous waveguide.

frequency (kHz)	Metamaterial-based (m/s)	Homogeneous (m/s)
150	2513.92	2171.59
175	2637.65	2285.65
200	2686.41	2503.29
225	2667.60	2666.71
250	2596.26	2781.01

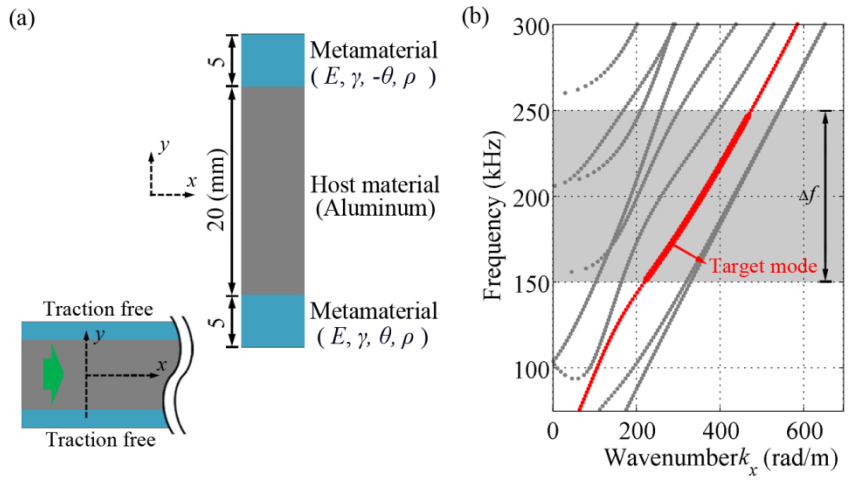

Figure 5.1 (a) Schematics of the metamaterial-based waveguide. The material properties of anisotropic metamaterial layers of 5 mm are adjusted through the proposed optimization. (b) The dispersion curves of the metamaterial-based waveguide. The shading denotes the target frequency range to be considered.

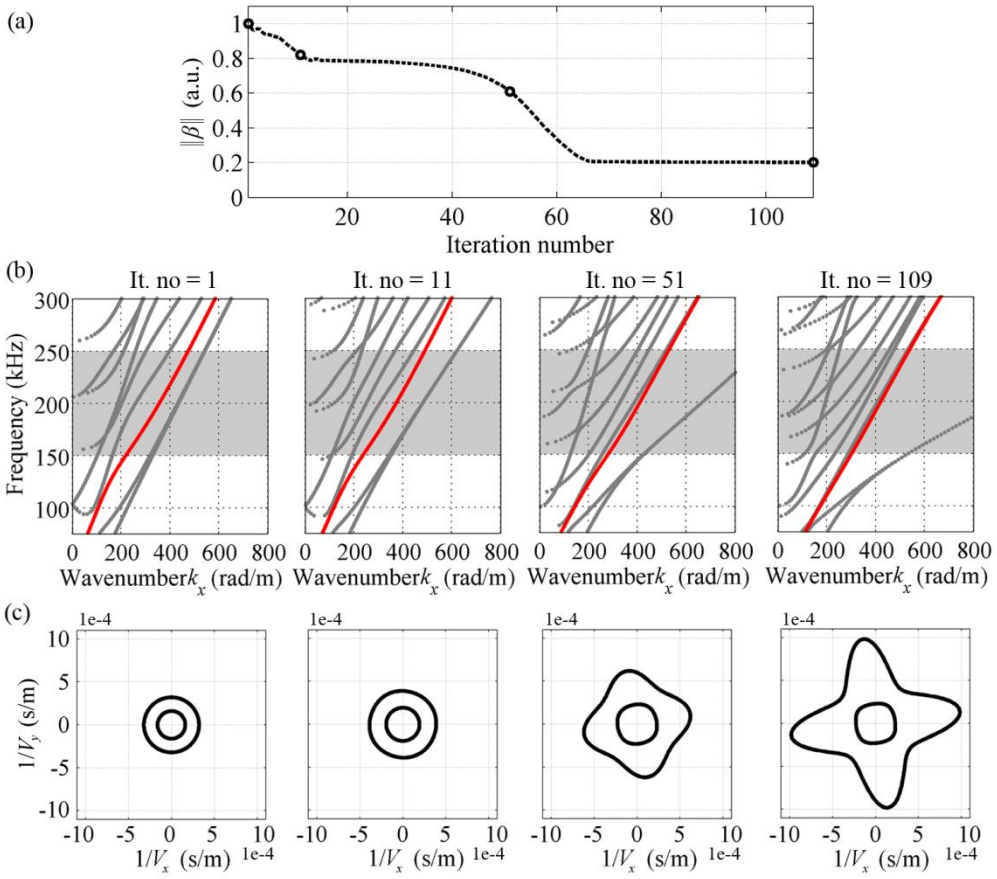

Figure 5.2 (a) Iteration history of the objective function in the proposed dispersion engineering. (b) The dispersion relation of the metamaterial-based waveguide for iteration numbers of 1, 11, 51, and 109. (c) The corresponding slowness curves of anisotropic metamaterials at 200 kHz, respectively.

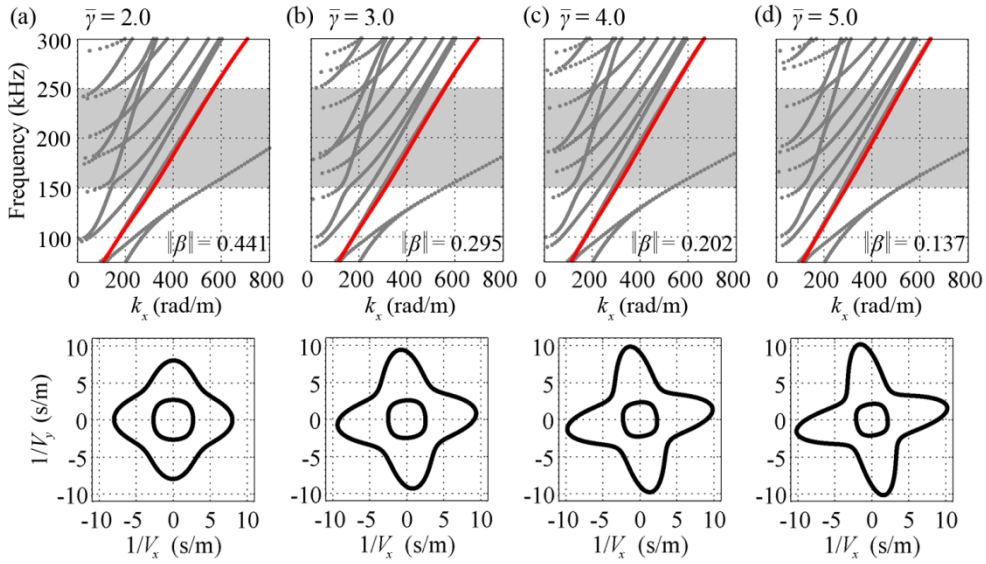

Figure 5.3 Dispersion curves of the engineered metamaterial-based waveguide and the slowness curves of the anisotropic metamaterial (a) for the upper bound of anisotropy factor $\bar{\gamma} = 2.0$, (b) 3.0, (c) 4.0, and (d) 5.0, respectively.

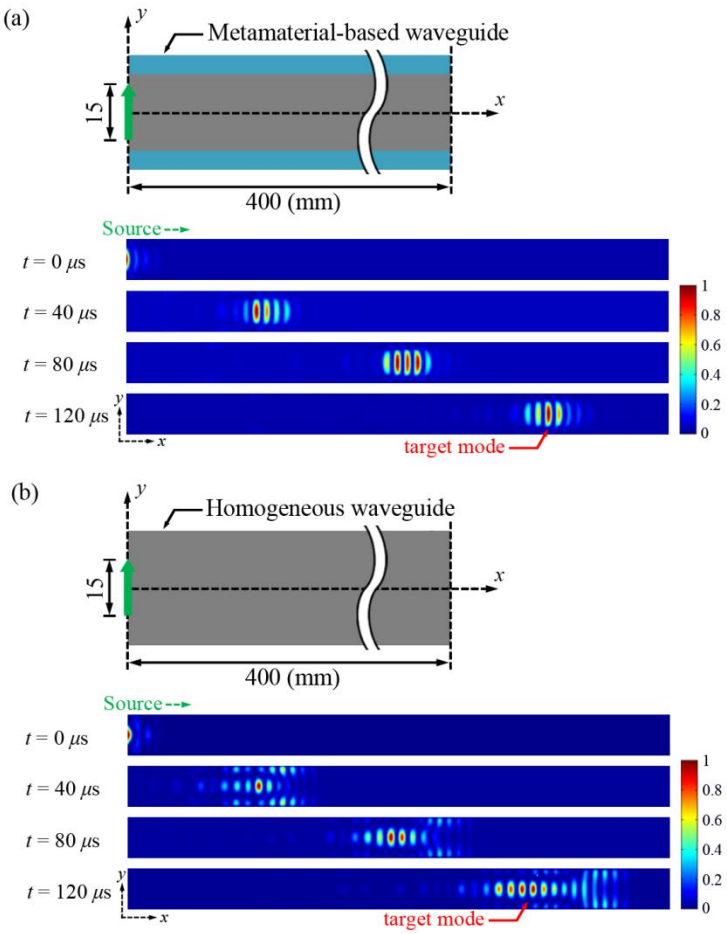

Figure 5.4 Schematic of the waveguide model in time-transient simulations. Snapshots of distribution of shear-energy density (a) in the metamaterial-based waveguide and (b) in a homogeneous waveguide.

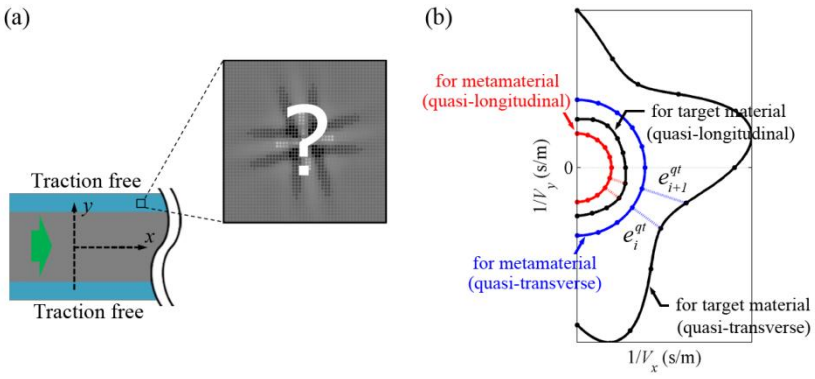

Figure 5.5 (a) Illustration of the proposed topology optimization for anisotropic metamaterials in dispersion engineering of a waveguide. (b) Slowness curves of the target material (black) and the metamaterial in design process (red and blue) Differences in slowness curves, e^{ql} and e^{qt}, are minimized to realize the anisotropic elastic metamaterial.

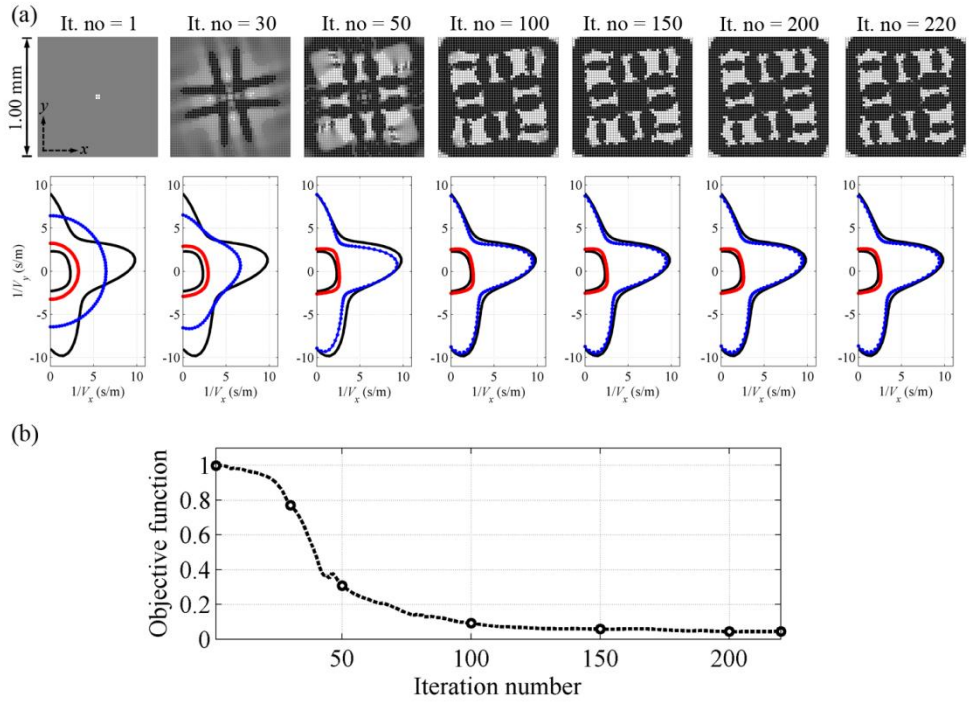

Figure 5.6 (a) Topologies of a metamaterial unit and the corresponding slowness curves for intermediate stages. (b) Iteration history of the objective function in the topology optimization for anisotropic metamaterials.

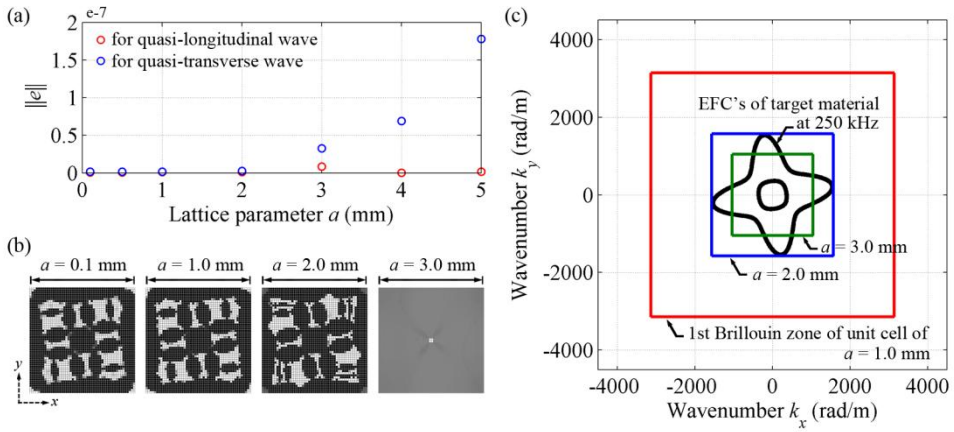

Figure 5.7 (a) The square norms of the difference in slowness curves *e* as a function of lattice parameter *a* of metamaterial unit. (b) Topologies of different unit sizes at the last iteration stage. (c) EFC's of the target material at 250 kHz (black) and the irreducible Brillouin zones of the different sizes of metamaterial units for *a* = 1.0 (red), 2.0 (blue), and 3.0 mm (green), respectively.

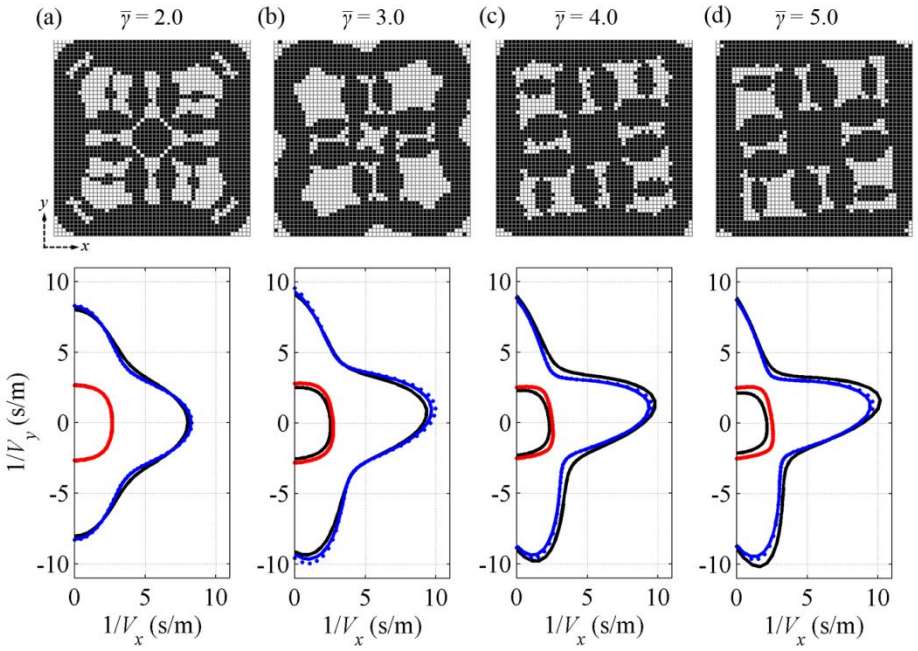

Figure 5.8 The microstructures of realized anisotropic metamaterial and the corresponding slowness curves (a) for the upper bound of anisotropy factor $\bar{\gamma} = 2.0$, (b) 3.0, (c) 4.0, and (d) 5.0, respectively.

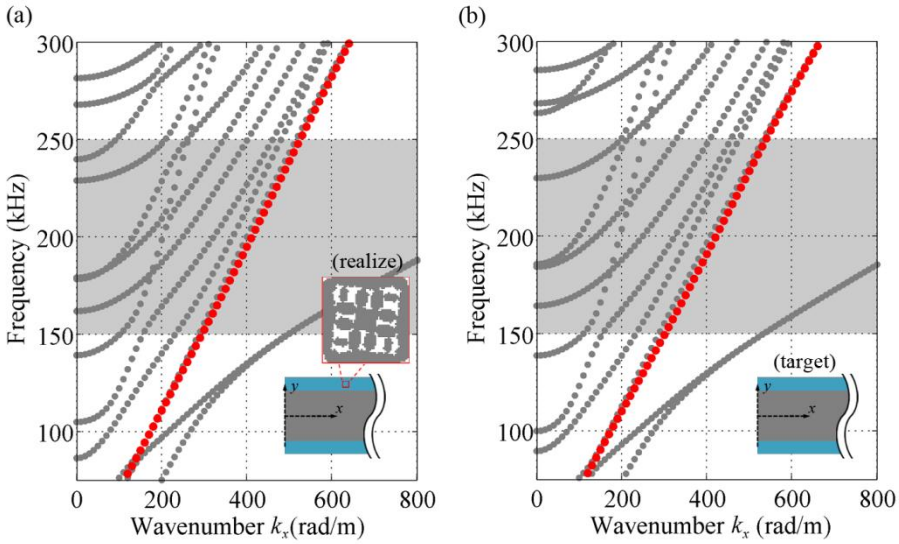

Figure 5.9 Dispersion curves of the metamaterial-based waveguide consisting of (a) the realized elastic metamaterial and (b) the target material.

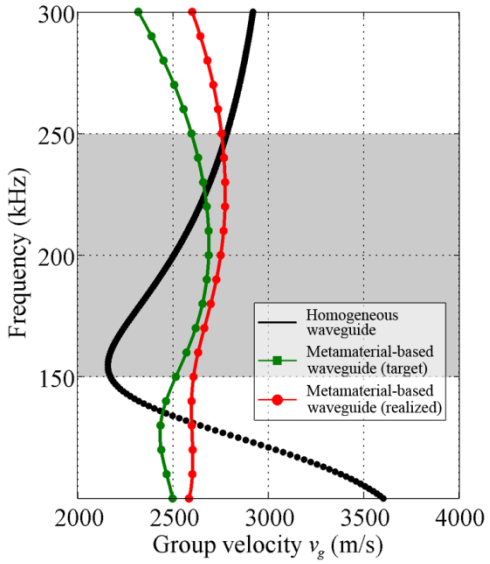

Figure 5.10 The group velocity profiles of the target guided mode. The profile marked by square represents that for the realized metamaterial waveguide and that marked by circle, the target waveguide, respectively.

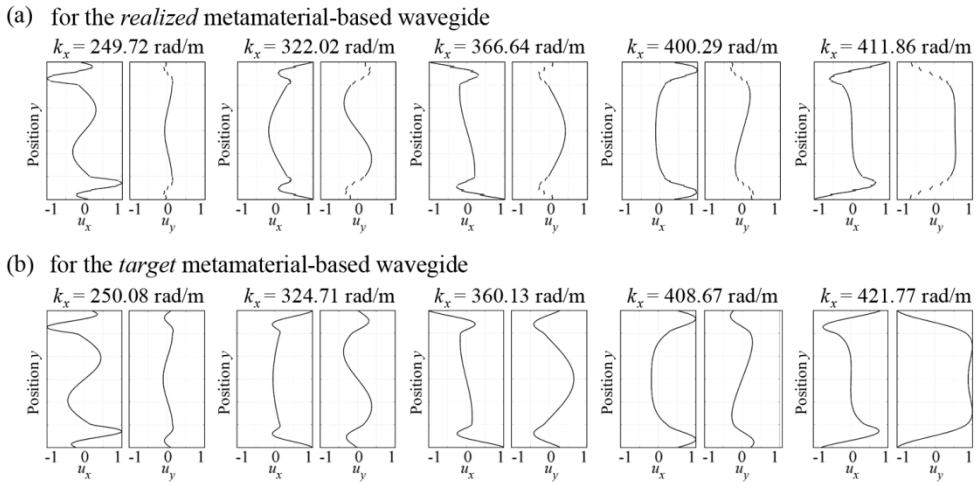

Figure 5.11 The distributions of the *x*- and *y*-displacement components of the eigenmodes at 200 kHz for (a) the realized metamaterial-based waveguide and (b) the target waveguide.

CHAPTER 6

CONCLUSIONS

In this study, phononic crystals and elastic metamaterials are engineered to tailor the dispersion relation of an elastic waveguide. The main focus is on multiple guided modes which exhibit a strongly dispersive behavior. To achieve the control of wave modes in an elastic waveguide, we employ the extraordinary phenomena of phononic crystals and elastic metamaterials including the band gap, the self-collimation phenomena, and the dispersion tailoring. Since these abnormal phenomena are attributed to the unit structure of phononic crystals and elastic metamaterials, we engineer their structure to exhibit the desired wave properties for multiple guided waves and demonstrate performances of designed structures by numerical simulation and ultrasonic experiment in each research topic.

Throughout this investigation, it was shown that guided wave modes can be spatially separated by exploiting anisotropic characteristics of phononic crystals. Also, we presented that the undesired wave mode can be removed by opening the band gap. And the group velocity dispersion of the target guided mode was successfully suppressed by anisotropic elastic metamaterials. In doing so, the systematic approach was employed to find the proper unit structures. Since multiple wave modes are involved in an elastic waveguide, it is essential to find the unit structures which satisfy multiple requirements for each guided mode. In this study,

the lattice parameters of phononic crystals such as a periodicity and a filling factor of inclusions or the topology of elastic metamaterial were obtained through the proposed optimization methods. The size optimization method was suggested to design the phononic crystal-based waveguide transducer and the shape optimization method was formulated for the self-collimating phononic crystals. The topology optimization method was also applied to realize anisotropic elastic metamaterials.

Also, we experimentally studied the guided wave propagation in the engineered phononic crystals. Although the strong dispersive nature and complexity of guided waves make it difficult to demonstrate the guided wave propagation by experiments, here, guided modes of interest were excited selectively and its beam pattern can be controlled by adjusting transducers. The shear-horizontal modes in an aluminum plate can be measured separately at the exit side of phononic crystals. And we can demonstrate the suppression of the wave distortion in the tailored phononic crystal by ultrasonic experiments. In experimental demonstration, the fundamental wave phenomena including the refraction at an interface of phononic crystals and the dispersion effect in space and time were also investigated for elastic guided waves.

The dispersion engineering presented in this study can provide evidence of the possibility of a multiple mode control for guided waves. An excitation of long-wavelength wave mode should be avoided to achieve the high-resolution inspection by guided elastic waves; separate measurements of multiple scattered waves from a defect allow us to know precise information about the defect, its shape and size. The approaches presented in this thesis show an effectiveness of phononic crystals and elastic metamaterials to attain these promising functionalities. Finally, we expect

that extraordinary wave devices based on phononic crystals and elastic metamaterials can be realized by the proposed engineering methods.

ACKNOWLEDGEMENTS

This research was supported by the National Research Foundation of Korea (Grant No. 2013035194) funded by the Korean Ministry of Education, Science and Technology (MEST) contracted through Institute of Advanced Machinery and Design at Seoul National University, World Class University (WCU) program (No. R31-2010-000-10083-0) through NRF funded by MEST, which are gratefully acknowledged.

REFERENCES

[1] Sigalas, M. and E. Economou, "Elastic and acoustic wave band structure," *Journal of Sound and Vibration*, 1992. **158**(2): p. 377-382.

[2] Montero de Espinosa, F., E. Jimenez, and M. Torres, "Ultrasonic band gap in a periodic two-dimensional composite," *Physical Review Letters*, 1998. **80**(6): p. 1208.

[3] Vasseur, J., P. Deymier, B. Chenni, B. Djafari-Rouhani, L. Dobrzynski, and D. Prevost, "Experimental and Theoretical Evidence for the Existence of Absolute Acoustic Band Gaps in Two-Dimensional Solid Phononic Crystals," *Physical Review Letters*, 2001. **86**(14): p. 3012-3015.

[4] Sukhovich, A., L. Jing, and J. Page, "Negative refraction and focusing of ultrasound in two-dimensional phononic crystals," *Physical Review B*, 2008. **77**(1): 014301.

[5] Morvan, B., A. Tinel, A.-C. Hladky-Hennion, J.r. Vasseur, and B. Dubus, "Experimental demonstration of the negative refraction of a transverse elastic wave in a two-dimensional solid phononic crystal," *Applied Physics Letters*, 2010. **96**(10): 101905.

[6] Liu, Z., X. Zhang, W. Mao, Y. Zhu, Z. Yang, C. Chan, and P. Sheng, "Locally Resonant Sonic Materials," *Science*, 2000. **289**(5485): p. 1734-1736.

[7] Li, J. and C. Chan, "Double-negative acoustic metamaterial," *Physical Review E*, 2004. **70**(5): 055602.

[8] Fang, N., D. Xi, J. Xu, M. Ambati, W. Srituravanich, C. Sun, and X. Zhang, "Ultrasonic metamaterials with negative modulus," *Nature Materials*, 2006. **5**(6): p. 452-456.

[9] Zhang, S., L. Yin, and N. Fang, "Focusing Ultrasound with an Acoustic Metamaterial Network," *Physical Review Letters*, 2009. **102**(19): 194301.

[10] Lee, S.H., C. M. Park, Y. M. Seo, Z. G. Wang, and C. K. Kim, "Composite

Acoustic Medium with Simultaneously Negative Density and Modulus," *Physical Review Letters*, 2010. **104**(5): 054301.

[11] Xiang, H. J., Z. F. Shi, S. J. Wang, and Y. L. Mo, "Periodic materials-based vibration attenuation in layered foundations: experimental validation," *Smart Materials and Structures*, 2012. **21**(11): 112003.

[12] Shi, Z. and J. Huang, "Feasibility of reducing three-dimensional wave energy by introducing periodic foundations," *Soil Dynamics and Earthquake Engineering*, 2013. **50**: p. 204-212.

[13] Hopkins, P. E., C. M. Reinke, M. F. Su, R. H. Olsson, E. A. Shaner, Z. C. Leseman, J. R. Serrano, L. M. Phinney, and I. El-Kady, "Reduction in the Thermal Conductivity of Single Crystalline Silicon by Phononic Crystal Patterning," *Nano letters*, 2011. **11**(1): p. 107-112.

[14. Schittny, R., M. Kadic, S. Guenneau, and M. Wegener, "Experiments on Transformation Thermodynamics: Molding the Flow of Heat," *Physical Review Letters*, 2013. **110**(19): 195901.

[15] Auld, B. A., Acoustic fields and waves in solids. Vol. 1. 1973: *Wiley New York*.

[16] Rose, J. L. and P. B. Nagy, "Ultrasonic waves in solid media," *The Journal of the Acoustical Society of America*, 2000. **107**: p. 1807.

[17] Bonello, B., C. Charles, and F. Ganot, "Lamb waves in plates covered by a two-dimensional phononic film," *Applied Physics Letters*, 2007. **90**(2): 021909.

[18] Chen, J.-J., B. Bonello, and Z.-L. Hou, "Plate-mode waves in phononic crystal thin slabs: Mode conversion," *Physical Review E*, 2008. **78**(3): 036609.

[19] Lee, M. K., P. S. Ma, I. K. Lee, H. W. Kim, and Y. Y. Kim, "Negative refraction experiments with guided shear-horizontal waves in thin phononic crystal plates," *Applied Physics Letters*, 2011. **98**(1): 011909.

[20] John, S., "Strong localization of photons in certain disordered dielectric superlattices," *Physical Review Letters*, 1987. **58**(23): p. 2486-2489.

[21] Yablonovitch, E., "Inhibited Spontaneous Emission in Solid-State Physics and Electronics," *Physical Review Letters*, 1987. **58**(20): p. 2059-2062.

[22] Ho, K. M., C. T. Chan, and C. M. Soukoulis, "Existence of a photonic gap in periodic dielectric structures," *Physical Review Letters*, 1990. **65**(25): p. 3152-3155.

[23] Zhang, Z. and S. Satpathy, "Electromagnetic wave propagation in periodic structures: Bloch wave solution of Maxwell's equations," *Physical Review Letters*, 1990. **65**(21): p. 2650-2653.

[24] Yablonovitch, E., T. Gmitter, R. Meade, A. Rappe, K. Brommer, and J. Joannopoulos, "Donor and acceptor modes in photonic band structure," *Physical Review Letters*, 1991. **67**(24): p. 3380-3383.

[25] Joannopoulos, J. D., S. G. Johnson, J. N. Winn, and R. D. Meade, Photonic crystals: molding the flow of light. 2011: *Princeton university press*.

[26] Mekis, A., J. C. Chen, I. Kurland, S. Fan, P. R. Villeneuve, and J. D. Joannopoulos, "High transmission through sharp bends in photonic crystal waveguides," *Physical Review Letters*, 1996. **77**(18): p. 3787.

[27] Knight, J. C., J. Broeng, T. A. Birks, and P. St. Russell, "Photonic Band Gap Guidance in Optical Fibers," *Science*, 1998. **282**(5393): p. 1476-1478.

[28] Painter, O., R. K. Lee, A. Scherer, A. Yariv, J. D. O'Brien, P. D. Dapkus, and I. Kim, "Two-Dimensional Photonic Band-Gap Defect Mode Laser," *Science*, 1999. **284**(5421): p. 1819-1821.

[29] Notomi, M., K. Yamada, A. Shinya, J. Takahashi, C. Takahashi, and I. Yokohama, "Extremely Large Group-Velocity Dispersion of Line-Defect Waveguides in Photonic Crystal Slabs," *Physical Review Letters*, 2001. **87**(25): 253902.

[30] Soljacic, M. and J. D. Joannopoulos, "Enhancement of nonlinear effects using photonic crystals," *Nature Materials*, 2004. **3**(4): p. 211-219.

[31] Kosaka, H., T. Kawashima, A. Tomita, M. Notomi, T. Tamamura, T. Sato, and S. Kawakami, "Superprism phenomena in photonic crystals," *Physical Review B*, 1998. **58**(16): R10 96-99.

[32] Kosaka, H., T. Kawashima, A. Tomita, M. Notomi, T. Tamamura, T. Sato, and S. Kawakami, "Self-collimating phenomena in photonic crystals," *Applied Physics Letters*, 1999. **74**(9): p. 1212-1214.

[33] Pendry, J. B., "Negative refraction makes a perfect lens," *Physical Review Letters*, 2000. **85**(18): p. 3966.

[34] Veselago, V. G., "The electrodynamics of substances with simultaneously negative values of ϵ and μ," *Soviet Physics Uspekhi*, 1968. **10**(4): p. 509-514.

[35] Smith, D.R., W. J. Padilla, D. C. Vier, S. C. Nemat-Nasser, and S. Schultz, "Composite medium with simultaneously negative permeability and permittivity," *Physical Review Letters*, 2000. **84**(18): p. 4184.

[36] Smith, D. R., J. B. Pendry, and M. C. K. Wiltshire, "Metamaterials and Negative Refractive Index," *Science*, 2004. **305**(5685): p. 788-792.

[37] Shalaev, V. M., W. Cai, U. K. Chettiar, H.-K. Yuan, A. K. Sarychev, V. P. Drachev, and A. V. Kildishev, "Negative index of refraction in optical metamaterials," *Optics Letters*, 2005. **30**(24): p. 3356-3358.

[38] Dolling, G., C. Enkrich, M. Wegener, C. M. Soukoulis, and S. Linden, "Simultaneous Negative Phase and Group Velocity of Light in a Metamaterial," *Science*, 2006. **312**(5775): p. 892-894.

[39] Salandrino, A. and N. Engheta, "Far-field subdiffraction optical microscopy using metamaterial crystals: Theory and simulations," *Physical Review B*, 2006. **74**(7): 075103.

[40] Xiong, Y., Z. Liu, C. Sun, and X. Zhang, "Two-dimensional imaging by far-field superlens at visible wavelengths," *Nano letters*, 2007. **7**(11): p. 3360-3365.

[41] Notomi, M., "Theory of light propagation in strongly modulated photonic crystals: Refractionlike behavior in the vicinity of the photonic band gap," *Physical Review B*, 2000. **62**(16): p. 10696.

[42] Soukoulis, C. M., S. Linden, and M. Wegener, " Negative Refractive Index at Optical," *Science*, 2007. **1136481**(47): p. 315.

[43] Luo, C., S. G. Johnson, J. D. Joannopoulos, and J. Pendry, "Subwavelength imaging in photonic crystals," *Physical Review B*, 2003. **68**(4): 045115.

[44] Parimi, P. V., W. T. Lu, P. Vodo, and S. Sridhar, " Imaging by flat lens using negative refraction," *Nature*, 2003. **426**(6965): p. 404-404.

[45] Yang, S., J. H. Page, Z. Liu, M. L. Cowan, C. T. Chan, and P. Sheng, "Focusing of Sound in a 3D Phononic Crystal," *Physical Review Letters*, 2004. **93**(2): 024301.

[46] Sukhovich, A., B. Merheb, K. Muralidharan, J. Vasseur, Y. Pennec, P. Deymier, and J. Page, "Experimental and Theoretical Evidence for Subwavelength Imaging in Phononic Crystals," *Physical Review Letters*, 2009. **102**(15): 154301.

[47] Lee, S. H., C. M. Park, Y. M. Seo, Z. G. Wang, and C. K. Kim, "Acoustic metamaterial with negative density," *Physics Letters A*, 2009. **373**(48): p. 4464-4469.

[48] Li, J., L. Fok, X. Yin, G. Bartal, and X. Zhang, "Experimental demonstration of an acoustic magnifying hyperlens," *Nature Materials*, 2009. **8**(12): p. 931-934.

[49] Lee, H. J., H. W. Kim, and Y. Y. Kim, "Far-field subwavelength imaging for ultrasonic elastic waves in a plate using an elastic hyperlens," *Applied Physics Letters*, 2011. **98**(24): 241912.

[50] Farhat, M., S. Guenneau, and S. Enoch, "Ultrabroadband Elastic Cloaking in Thin Plates," *Physical Review Letters*, 2009. **103**(2): 024301.

[51] Stenger, N., M. Wilhelm, and M. Wegener, "Experiments on Elastic Cloaking in Thin Plates," *Physical Review Letters*, 2012. **108**(1): 014301.

[52] Liang, Z. and J. Li, "Extreme Acoustic Metamaterial by Coiling Up Space," *Physical Review Letters*, 2012. **108**(11): 114301.

[53] Liang, Z., T. Feng, S. Lok, F. Liu, K. B. Ng, C. H. Chan, J. Wang, S. Han, S. Lee, and J. Li, "Space-coiling metamaterials with double negativity and conical dispersion," *Scientific Reports*, 2013. **3**: 1614.

[54] Xie, Y., B.-I. Popa, L. Zigoneanu, and S. A. Cummer, "Measurement of a

Broadband Negative Index with Space-Coiling Acoustic Metamaterials," *Physical Review Letters*, 2013. **110**(17): 175501.

[55] Milton, G.W. and A.V. Cherkaev, "Which elasticity tensors are realizable?," *Journal of engineering materials and technology*, 1995. **117**(4): p. 483-493.

[56] Kadic, M., T. Bückmann, N. Stenger, M. Thiel, and M. Wegener, "On the practicability of pentamode mechanical metamaterials," *Applied Physics Letters*, 2012. **100**(19): 191901.

[57] Su, Z., L. Ye, and Y. Lu, "Guided Lamb waves for identification of damage in composite structures: A review," *Journal of Sound and Vibration*, 2006. **295**: p. 753-780.

[58] Rose, J. L., S. P. Pelts, and M. J. Quarry, "A comb transducer model for guided wave NDE," *Ultrasonics*, 1998. **36**(1): p. 163-169.

[59] Li, J. and J. L. Rose, "Implementing guided wave mode control by use of a phased transducer array," *Ultrasonics, Ferroelectrics and Frequency Control, IEEE Transactions on*, 2001. **48**(3): p. 761-768.

[60] Wilcox, P. D., "A rapid signal processing technique to remove the effect of dispersion from guided wave signals," *Ultrasonics, Ferroelectrics and Frequency Control, IEEE Transactions on*, 2003. **50**(4): p. 419-427.

[61] Wooh, S.-C. and Y. Shi, "Synthetic phase tuning of guided waves," *Ultrasonics, Ferroelectrics and Frequency Control, IEEE Transactions on*, 2001. **48**(1): p. 209-223.

[62] Brillouin, L., Wave propagation in periodic structures: electric filters and crystal lattices. 2003: *Dover.*

[63] Kushwaha, M. S., P. Halevi, L. Dobrzynski, and B. Djafari-Rouhani, "Acoustic band structure of periodic elastic composites," *Physical Review Letters*, 1993. **71**(13): p. 2022-2025.

[64] Wilm, M., S. Ballandras, V. Laude, and T. Pastureaud, "A full 3D plane-wave-expansion model for 1-3 piezoelectric composite structures," *The Journal of the Acoustical Society of America*, 2002. **112**(3): p. 943.

[65] Hladky-Hennion, A. C. and J. N. Decarpigny, "Analysis of the scattering of

a plane acoustic wave by a doubly periodic structure using the finite element method: Application to Alberich anechoic coatings," *The Journal of the Acoustical Society of America*, 1991. **90**: p. 3356.

[66] Langlet, P., A. C. Hladky-Hennion, and J. N. Decarpigny, "Analysis of the propagation of plane acoustic waves in passive periodic materials using the finite element method," *The Journal of the Acoustical Society of America*, 1995. **98**: p. 2792.

[67] Hou, Z., X. Fu, and Y. Liu, "Singularity of the Bloch theorem in the fluid/solid phononic crystal," *Physical Review B*, 2006. **73**(2): 024304.

[68]. Hussein, M. I., "Reduced Bloch mode expansion for periodic media band structure calculations," *Proceedings of the Royal Society A: Mathematical, Physical and Engineering Sciences*, 2009. **465**(2109): p. 2825-2848.

[69] Hsu, J.-C. and T.-T. Wu, "Efficient formulation for band-structure calculations of two-dimensional phononic-crystal plates," *Physical Review B*, 2006. **74**(14): 144303.

[70] Hou, Z. and B. M. Assouar, "Modeling of Lamb wave propagation in plate with two-dimensional phononic crystal layer coated on uniform substrate using plane-wave-expansion method," *Physics Letters A*, 2008. **372**(12): p. 2091-2097.

[71] Vasseur, J. O., P. A. Deymier, B. Djafari-Rouhani, Y. Pennec, and A.-C. Hladky-Hennion, "Absolute forbidden bands and waveguiding in two-dimensional phononic crystal plates," *Physical Review B*, 2008. **77**(8): 085415.

[72] Yu, X. and S. Fan, "Bends and splitters for self-collimated beams in photonic crystals," *Applied Physics Letters*, 2003. **83**(16): p. 3251.

[73] Shi, S., A. Sharkawy, C. Chen, D. M. Pustai, and D. W. Prather, "Dispersion-based beam splitter in photonic crystals," *Optics Letters*, 2004. **29**(6): p. 617-619.

[74] Zabelin, V., L. Dunbar, N. Le Thomas, R. Houdré, M. Kotlyar, L. O'Faolain, and T. Krauss, "Self-collimating photonic crystal polarization beam

splitter," *Optics Letters*, 2007. **32**(5): p. 530-532.

[75] Bayindir, M., B. Temelkuran, and E. Ozbay, "Photonic-crystal-based beam splitters," *Applied Physics Letters*, 2000. **77**(24): p. 3902-3904.

[76] Ao, X., L. Liu, L. Wosinski, and S. He, "Polarization beam splitter based on a two-dimensional photonic crystal of pillar type," *Applied Physics Letters*, 2006. **89**(17): 171115.

[77] Momeni, B., J. Huang, M. Soltani, M. Askari, S. Mohammadi, M. Rakhshandehroo, and A. Adibi, "Compact wavelength demultiplexing using focusing negative index photonic crystal superprisms," *Optics Express*, 2006. **14**(6): p. 2413-2422.

[78] Pennec, Y., B. Djafari-Rouhani, J. Vasseur, A. Khelif, and P. Deymier, "Tunable filtering and demultiplexing in phononic crystals with hollow cylinders," *Physical Review E*, 2004. **69**(4): 046608.

[79] Ke, M., Z. Liu, C. Qiu, W. Wang, J. Shi, W. Wen, and P. Sheng, "Negative-refraction imaging with two-dimensional phononic crystals," *Physical Review B*, 2005. **72**(6): 064306.

[80] Lu, M.-H., C. Zhang, L. Feng, J. Zhao, Y.-F. Chen, Y.-W. Mao, J. Zi, Y.-Y. Zhu, S.-N. Zhu, and N.-B. Ming, "Negative birefraction of acoustic waves in a sonic crystal," *Nature Materials*, 2007. **6**(10): p. 744-748.

[81] Lee, J. S., Y. Y. Kim, and S. H. Cho, "Beam-focused shear-horizontal wave generation in a plate by a circular magnetostrictive patch transducer employing a planar solenoid array," *Smart Materials and Structures*, 2009. **18**(1): p. 015009.

[82] Laude, V., Y. Achaoui, S. Benchabane, and A. Khelif, "Evanescent Bloch waves and the complex band structure of phononic crystals," *Physical Review B*, 2009. **80**(9): 092301.

[83] Moiseyenko, R. P. and V. Laude, "Material loss influence on the complex band structure and group velocity in phononic crystals," *Physical Review B*, 2011. **83**(6): 064301.

[84] Svanberg, K., "The method of moving asymptotes—a new method for

structural optimization," *International journal for numerical methods in engineering*, 1987. **24**(2): p. 359-373.

[85] Notomi, M., H. Suzuki, and T. Tamamura, "Directional lasing oscillation of two-dimensional organic photonic crystal lasers at several photonic band gaps," *Applied Physics Letters*, 2001. **78**(10): p. 1325.

[86] Bucay, J., E. Roussel, J. O. Vasseur, P. A. Deymier, A.-C. Hladky-Hennion, Y. Pennec, K. Muralidharan, B. Djafari-Rouhani, and B. Dubus, "Positive, negative, zero refraction, and beam splitting in a solid/air phononic crystal: Theoretical and experimental study," *Physical Review B*, 2009. **79**(21): 214305.

[87] Wu, T.-T., Z.-G. Huang, and S. Lin, "Surface and bulk acoustic waves in two-dimensional phononic crystal consisting of materials with general anisotropy," *Physical Review B*, 2004. **69**(9): 094301.

[88] Sun, J.-H. and T.-T. Wu, "Propagation of acoustic waves in phononic-crystal plates and waveguides using a finite-difference time-domain method," *Physical Review B*, 2007. **76**(10): 104304.

[89] Thompson, R.B., "Generation of horizontally polarized shear waves in ferromagnetic materials using magnetostrictively coupled meander-coil electromagnetic transducers," *Applied Physics Letters*, 1979. **34**(2): p. 175-177.

[90] Ma, P. S., H. W. Kim, J. H. Oh, and Y. Y. Kim, "Mode separation of a single-frequency bi-modal elastic wave pulse by a phononic crystal," *Applied Physics Letters*, 2011. **99**(20): 201906.

[91] Watkins, R. D., M. O. Deighton, A. B. Gillespie, and R. B. Pike, "A proposed method for generating and receiving narrow beams of ultrasound in the fast reactor liquid sodium environment," *Ultrasonics*, 1982. **20**(1): p. 7-12.

[92] Jen, C.-K., J.-G. Legoux, and L. Parent, "Experimental evaluation of clad metallic buffer rods for high temperature ultrasonic measurements," *NDT & E International*, 2000. **33**(3): p. 145-153.

[93] Lynnworth, L. C., Y. Liu, and J.A. Umina, "Extensional bundle waveguide techniques for measuring flow of hot fluids," *Ultrasonics, Ferroelectrics and Frequency Control, IEEE Transactions on*, 2005. **52**(4): p. 538-544.

[94] Puckett, A. D. and M. L. Peterson, "A semi-analytical model for predicting multiple propagating axially symmetric modes in cylindrical waveguides," *Ultrasonics*, 2005. **43**(3): p. 197-207.

[95] Cegla, F. B., P. Cawley, J. Allin, and J. Davies, "High-temperature (> 500 C) wall thickness monitoring using dry-coupled ultrasonic waveguide transducers," *Ultrasonics, Ferroelectrics and Frequency Control, IEEE Transactions on*, 2011. **58**(1): p. 156-167.

[96] Joo, Y.-S., C.-G. Park, J.-H. Lee, J.-B. Kim, and S.-H. Lim, "Development of ultrasonic waveguide sensor for under-sodium inspection in a sodium-cooled fast reactor," *NDT & E International*, 2011. **44**(2): p. 239-246.

[97] Leduc, D., A.-C. Hladky, B. Morvan, J.-L. Izbicki, and P. Pareige, "Propagation of Lamb waves in a plate with a periodic grating: Interpretation by phonon," *The Journal of the Acoustical Society of America*, 2005. **118**(4): p. 2234.

[98] Kundu, T., S. Banerjee, and K.V. Jata, "An experimental investigation of guided wave propagation in corrugated plates showing stop bands and pass bands," *The Journal of the Acoustical Society of America*, 2006. **120**(3): p. 1217.

[99] Morvan, B., A.-C. Hladky-Hennion, D. Leduc, and J.-L. Izbicki, "Ultrasonic guided waves on a periodical grating: Coupled modes in the first Brillouin zone," *Journal of Applied Physics*, 2007. **101**(11): 114906.

[100] Hou, Z. and B. M. Assouar, "Opening a band gap in the free phononic crystal thin plate with or without a mirror plane," *Journal of Physics D: Applied Physics*, 2008. **41**(21): 215102.

[101] Hsu, F.-C., C.-I. Lee, J.-C. Hsu, T.-C. Huang, C.-H. Wang, and P. Chang, "Acoustic band gaps in phononic crystal strip waveguides," *Applied Physics Letters*, 2010. **96**(5): 051902.

[102] Chen, J., Y. Xia, X. Han, and H. Zhang, "Lamb waves in phononic crystal slabs: Truncated plane parallels to the axis of periodicity," *Ultrasonics*, 2012. **52**(7): p. 920-924.

[103] Frandsen, L. H., A. Lavrinenko, J. Fage-Pedersen, and P. I. Borel, "Photonic crystal waveguides with semi-slow light and tailored dispersion properties," *Optics Express*, 2006. **14**(20): p. 9444-9450.

[104] Kubo, S., D. Mori, and T. Baba, "Low-group-velocity and low-dispersion slow light in photonic crystal waveguides," *Optics Letters*, 2007. **32**(20): p. 2981-2983.

[105] Hao, R., E. Cassan, X. Le Roux, D. Gao, V. Do Khanh, L. Vivien, D. Marris-Morini, and X. Zhang, "Improvement of delay-bandwidth product in photonic crystal slow-light waveguides," *Optics Express*, 2010. **18**(16): p. 16309-16319.

[106] Cegla, F. B., "Energy concentration at the center of large aspect ratio rectangular waveguides at high frequencies," *The Journal of the Acoustical Society of America*, 2008. **123**(6): p. 4218.

[107] Huang, Z.-G. and T.-T. Wu, "Temperature effect on the bandgaps of surface and bulk acoustic waves in two-dimensional phononic crystals," *Ultrasonics, Ferroelectrics and Frequency Control, IEEE Transactions on*, 2005. **52**(3): p. 365-370.

[108] Cheng, Y., X.J. Liu, and D.J. Wu, "Temperature effects on the band gaps of Lamb waves in a one-dimensional phononic-crystal plate (L)," *The Journal of the Acoustical Society of America*, 2011. **129**(3): p. 1157.

[109] Ma, P. S., Y. E. Kwon, and Y. Y. Kim, "Wave dispersion tailoring in an elastic waveguide by phononic crystals," *Applied Physics Letters*, 2013. **103**(15): 151901.

[110] Yu, N., P. Genevet, M. A. Kats, F. Aieta, J. P. Tetienne, F. Capasso, and Z. Gaburro, "Light Propagation with Phase Discontinuities: Generalized Laws of Reflection and Refraction," *Science*, 2011. **334**(6054): p. 333-337.

[111] Monticone, F., N. M. Estakhri, and A. Alù, "Full Control of Nanoscale

Optical Transmission with a Composite Metascreen," *Physical Review Letters*, 2013. **110**(20): 203903.

[112] Popa, B.-I. and S. A. Cummer, "Design and characterization of broadband acoustic composite metamaterials," *Physical Review B*, 2009. **80**(17): 174303.

[113] Li, Y., B. Liang, Z.-m. Gu, X.-y. Zou, and J.-c. Cheng, "Reflected wavefront manipulation based on ultrathin planar acoustic metasurfaces," *Scientific Reports*, 2013. **3**: 2546.

[114] Farhat, M., S. Enoch, S. Guenneau, and A. B. Movchan, "Broadband Cylindrical Acoustic Cloak for Linear Surface Waves in a Fluid," *Physical Review Letters*, 2008. **101**(13): 134501.

[115] Zhang, S., C. Xia, and N. Fang, "Broadband Acoustic Cloak for Ultrasound Waves," *Physical Review Letters*, 2011. **106**(2): 024301.

[116] Martin, T. P., M. Nicholas, G. J. Orris, L.-W. Cai, D. Torrent, and J. Sánchez-Dehesa, "Sonic gradient index lens for aqueous applications," *Applied Physics Letters*, 2010. **97**(11): 113503.

[117] Wu, L.-Y. and L.-W. Chen, "An acoustic bending waveguide designed by graded sonic crystals," *Journal of Applied Physics*, 2011. **110**(11): 114507.

[118] Lin, S.-C.S., B. R. Tittmann, and T. J. Huang, "Design of acoustic beam aperture modifier using gradient-index phononic crystals," *Journal of Applied Physics*, 2012. **111**(12): 123510.

[119] Torrent, D. and J. Sánchez-Dehesa, "Anisotropic mass density by two-dimensional acoustic metamaterials," *New Journal of Physics*, 2008. **10**(2): 023004.

[120] Layman, C. N., T. P. Martin, K. M. Moore, D. C. Calvo, and G. J. Orris, "Designing acoustic transformation devices using fluid homogenization of an elastic substructure," *Applied Physics Letters*, 2011. **99**(16): 163503.

[121] Sigmund, O. and J. S. Jensen, "Systematic design of phononic band–gap materials and structures by topology optimization," *Philosophical Transactions of the Royal Society of London. Series A: Mathematical,*

Physical and Engineering Sciences, 2003. **361**(1806): p. 1001-1019.

[122] Preble, S., M. Lipson, and H. Lipson, "Two-dimensional photonic crystals designed by evolutionary algorithms," *Applied Physics Letters*, 2005. **86**(6): 061111.

[123] Halkjær, S., O. Sigmund, and J. S. Jensen, "Maximizing band gaps in plate structures," *Structural and Multidisciplinary Optimization*, 2006. **32**(4): p. 263-275.

[124] Bilal, O. R. and M. I. Hussein, "Ultrawide phononic band gap for combined in-plane and out-of-plane waves," *Physical Review E*, 2011. **84**(6): 065701.

[125] Diaz, A. R. and O. Sigmund, "A topology optimization method for design of negative permeability metamaterials," *Structural and Multidisciplinary Optimization*, 2009. **41**(2): p. 163-177.

[126] Otomori, M., T. Yamada, K. Izui, S. Nishiwaki, and J. Andkjær, "A topology optimization method based on the level set method for the design of negative permeability dielectric metamaterials," *Computer Methods in Applied Mechanics and Engineering*, 2012. **237-240**: p. 192-211.

[127] Lu, L., T. Yamamoto, M. Otomori, T. Yamada, K. Izui, and S. Nishiwaki, "Topology optimization of an acoustic metamaterial with negative bulk modulus using local resonance," *Finite Elements in Analysis and Design*, 2013. **72**: p. 1-12.

[128] Li, D., L. Zigoneanu, B.-I. Popa, and S. A. Cummer, "Design of an acoustic metamaterial lens using genetic algorithms," *The Journal of the Acoustical Society of America*, 2012. **132**: p. 2823.

[129] Nayfeh, A. H., Wave propagation in layered anisotropic media: With application to composites. 1995: *Elsevier*.

[130] Choi, K. K. and N. H. Kim, Structural sensitivity analysis and optimization 1. Vol. 1. 2005: *Springer*.

[131] Bendsoe, M. P., Topology optimization: theory, methods and applications. 2003: *Springer*.

국문 초록

포노닉 크리스털과 메타물질을 이용한 탄성 유도 초음파의 분산 특성 엔지니어링

마 평 식

서울대학교 대학원

기계항공공학부

본 연구에서는 포노닉 크리스털(phononic crystals)과 메타물질(metamaterials)과 같은 인공적인 구조로 이루어진 물질을 이용한 탄성 유도 초음파(elastic guided waves)의 조절을 다룬다. 인공 물질을 이용하여 파동의 성질을 조절하는 연구는 최근 전자기파에 대하여 광범위하게 연구되고 있으며, 그 결과 회절한계(sub-diffraction limit) 이하의 고해상도 렌즈나 클로킹(cloaking) 장치와 같은 흥미로운 결과들이 도출되고 있다. 본 연구는 탄성 유도 초음파 영역에 포노닉 크리스털과 메타물질을 적용하여 다양한 전파 특성을 갖는 것을 보이고자 한다. 특히 유도 초음파의 다양한 모드에 초점을 맞추어 연구를 진행하였다. 실제로 도파체(waveguide)에 입사된 입력 신호는 다양한 모드가 함께 가진 되거나, 각 모드의 분산 특성으로 인하여 왜곡되게 된다. 이로 인하여 유도 초음파를 이용한 도파체의 결함 탐상과 같은 실제적인 적용에 있어 많은 문제들을 야기한다. 본 연구에서는 포노닉 크리스털과 탄성 메타물질을 이용하여 유도 초음파 모드의 분산 특성(dispersion relation)의 조절 기법을 개발하였다.

본 연구에서 유도 초음파의 분산 특성 엔지니어링(dispersion engineering)은 주파수(frequency)와 파수(wavenumber) 영역에서 수행하였다. 주요 내용으로 서로 다른 유도 초음파 모드를 공간적으로 분리하거나 원치 않는 모드의 전파를

방지하고, 원하는 모드의 분산으로 인한 왜곡을 최소화하는데 중점을 두어 연구를 수행하였다. 포노닉 크리스털 평판을 이용한 전단 초음파 분리에서는 각 모드가 서로 다른 전파 방향을 갖도록 파수 영역의 분산 특성을 조절하였으며, 원치 않는 모드의 전파를 방지하기 위해 포노닉 크리스털 밴드갭(band gap)이 원하는 주파수 대역에서 형성되도록 조절하였다. 또한 포노닉 크리스털과 이방성(anisotropic) 메타물질을 적절히 설계하여 원하는 모드가 일정한 주파수 대역에서 군속도(group velocity)가 일정한 값을 갖도록 함으로써 신호의 왜곡을 최소화하였다. 이렇게 유도 초음파 모드가 각기 원하는 전파 특성을 갖도록 하는 것은 도전적인 과정으로, 본 연구에서는 포노닉 크리스털과 탄성 메타물질을 설계하기 위한 다양한 최적화 기법을 제안하였다. 포노닉 크리스털의 다양한 격자 변수들이나 탄성 메타물질의 단위 구조 위상(topology)에 대하여 제시된 설계 기법을 이용하여 설계를 수행하였으며, 이를 통해 얻어진 도파체 내부 유도 초음파 모드들의 파동 특성을 검증하고자 수치 해석과 초음파 실험을 수행하였다. 특히 실험적 검증에 있어 특정 모드를 선택적으로 가진하고 방사 패턴을 조절하기 위하여 초음파 트랜스듀서 또한 적절히 설계하였다. 본 연구를 통하여 포노닉 크리스털과 메타물질을 적절히 설계하여 이용할 경우 탄성 도파체 내부의 유도 초음파 특성을 효과적으로 조절할 수 있는 것을 검증하였다.

주제어: 유도 초음파, 분산 특성, 포노닉 크리스털, 탄성 메타 물질, 최적화 기법
학 번: 2010-30187